AD-A250 100

NUWC-NL Technical Document 10,023
4 March 1992

DTIC
ELECTE
MAY 1 3 1992
S C D

Near-Field and Far-Field Sound Radiation From a Line-Driven Fluid-Loaded Infinite Flat Plate Having Periodic and Non-Periodic Attached Rib Stiffeners

Benjamin A. Cray
Submarine Sonar Department

Naval Undersea Warfare Center Detachment
New London, Connecticut

92-12580

92 5 11 052

PREFACE

This study was prepared as a dissertation for the degree of Doctor of Philosophy in Mechanical Engineering from the North Carolina State University.

Foremost, the author wishes to express his gratitude to Dr. F. John Kingsbury, Mr. Frederick Manganelli, and Dr. Howard Schloemer, of the Naval Undersea Warfare Center Detachment, for the financial support they made available to the author to pursue and complete the dissertation.

Also greatly appreciated is Dr. David Keyes at Yale University who provided early guidance and strong encouragement to continue in graduate school.

Dr. Richard F. Keltie, the Chairman of the Advisory Committee, was a dedicated researcher and great to work with. His professionalism and knowledge made for a pleasant experience at North Carolina State University.

Finally, the author gives a hearty thanks to his wife, Karen, and to his parents for a lifetime of encouragement.

REVIEWED AND APPROVED: 4 March 1992

F. J. Kingsbury

F. J. Kingsbury
Head: Submarine Sonar Department

REPORT DOCUMENTATION PAGE		Form Approved OMB No. 0704-0188

1. AGENCY USE ONLY (Leave blank)	2. REPORT DATE 4 March 1992	3. REPORT TYPE AND DATES COVERED Final

4. TITLE AND SUBTITLE	5. FUNDING NUMBERS
NEAR-FIELD AND FAR-FIELD SOUND RADIATION FROM A LINE-DRIVEN FLUID-LOADED INFINITE FLAT PLATE HAVING PERIODIC AND NON-PERIODIC ATTACHED RIB STIFFENERS	PR C77202

6. AUTHOR(S)

Benjamin A. Cray

7. PERFORMING ORGANIZATION NAME(S) AND ADDRESS(ES) Naval Undersea Warfare Center Detachment New London, Connecticut 06320	8. PERFORMING ORGANIZATION REPORT NUMBER NUWC-NL TD 10,023

9. SPONSORING/MONITORING AGENCY NAME(S) AND ADDRESS(ES)	10. SPONSORING/MONITORING AGENCY REPORT NUMBER

11. SUPPLEMENTARY NOTES

This study was proposed as a dissertation for the degree of Doctor of Philosophy in Mechanical Engineering from the North Carolina State University.

12a. DISTRIBUTION/AVAILABILITY STATEMENT Approved for public release; distribution is unlimited.	12b. DISTRIBUTION CODE

13. ABSTRACT (Maximum 200 words)

The far-field and near-field solutions for the radiated acoustic pressure from a line-driven fluid-loaded, rib-stiffened thin elastic plate have been obtained. The plate has been configured to have two sets of rib-stiffeners, though the formulation given may be extended to include additional rib-stiffener sets. The stiffeners composing a given set are identical and are spaced periodically with distance ℓ. However, one set of stiffeners is shifted by an amount Δ from the other set. In this manner, portions of the plate may be configured with repeating sections having non-periodic rib spacing. The stiffeners exert reactive forces upon the plate, but not angular moments. Fluid loading is included on the upper surface of the plate while the lower surface is unloaded, except for a time harmonic line force applied normal to the lower surface.

Expressions are derived, for the special case of periodic inter-rib spacing, which give the wavenumbers at which the magnitude of the wavenumber response obtains relative maximum and minimum values. For a stiffened plate, it is seen that excitation frequencies below coincidence generate large magnitude supersonic wavenumber components.

14. SUBJECT TERMS		15. NUMBER OF PAGES 120
Far-Field Sound Radiation Fluid-Loaded, Infinite Flat Plate Near-Field Sound Radiation	Rib-Stiffeners Structural-Acoustic Interaction	16. PRICE CODE

17. SECURITY CLASSIFICATION OF REPORT UNCLASSIFIED	18. SECURITY CLASSIFICATION OF THIS PAGE UNCLASSIFIED	19. SECURITY CLASSIFICATION OF ABSTRACT UNCLASSIFIED	20. LIMITATION OF ABSTRACT SAR

13. (Cont'd)

The far-field radiated pressure has been obtained using the method of stationary phase. Numerical integration techniques were necessary to obtain the near-field acoustic pressure. Numerical calculations are presented for the radiated near-field and far-field sound pressure level, at a fixed observation position, for changes in frequency. For the far-field region, the sound pressure level is obtained for changes in offset at a fixed frequency. The directional radiation characteristics of the stiffened plate are also presented.

The near-field variation of acoustic pressure along the horizontal surface of the plate at a fixed frequency is given. At certain frequencies, the investigation revealed that the wavelength of the stiffened plate's near-field acoustic oscillations — due to the propagating flexural wave — was much greater than that given by the unstiffened plate's bending wavelength. The effect may be due to the stiffened plate's flexural response being split into two components that are close together in wavenumber. The wavelength of acoustic oscillation appears to result from taking the difference of the two spectral components.

TABLE OF CONTENTS

Page

LIST OF FIGURES

LIST OF FIGURES (Cont'd)

iv

LIST OF FIGURES (Cont'd)

LIST OF FIGURES (Cont'd)

vi

LIST OF FIGURES (Cont'd)

LIST OF SYMBOLS

D isotropic plate flexural rigidity, $= \dfrac{1}{12} \dfrac{Eh^3}{(1 - v^2)}$

$w(x,y)$ transverse displacement of the plate

m mass per unit area of the plate

m'_1 mass per unit length of the first set of rib-stiffeners

m'_2 mass per unit length of the second set of rib-stiffeners

E elastic modulus of the plate material

v Poisson's ratio for the plate material

ω harmonic angular frequency

$P_e(x)$ external applied pressure on the plate due to harmonic line force

$P_a(x,0)$ acoustic pressure acting on the upper surface of the plate

$P_1(x)$ total pressure exerted by first set of rib-stiffeners

$P_2(x)$ total pressure exerted by second set of rib-stiffeners

$\sim$ denotes an expression that has been Fourier transformed into the wavenumber domain

k, k_x wavenumber in the direction along the plate's surface perpendicular to the rib-stiffeners

k_y wavenumber in the direction along the plate's surface parallel to the rib-stiffeners

k_b free wavenumber of the plate *in vacuo* , $= \left(\dfrac{m\omega^2}{D} \right)^{1/4}$

k_{fl} fluid-loaded rib-stiffened free wavenumber

k_r stiffener wavenumber *in vacuo*, $= \left(\dfrac{(m'/\ell)\omega^2}{D} \right)^{1/4}$

k_0 acoustic wavenumber, $= \dfrac{\omega}{c_0}$

LIST OF SYMBOLS (Cont'd)

e   base of the Napierian logarithm, $= 2.718 \ldots$

x_0 point of application of line force

x_0, y_0 point of application of point force

F_0 magnitude of applied line force

$\delta(x)$ Dirac delta function

c_0 acoustic phase velocity in the fluid medium

x,y,z cartesian coordinates defined by Figure 1.1

R,θ,ϕ polar coordinates defined by sketch on page 119

$A_1(k)$
$A_2(k)$
$A_3(k)$
$A_4(k)$ differential equation wavenumber-dependent coefficients

i   positive square root of -1

t   time

$u(x)$ physical transverse displacement of rib-stiffeners

ℓ periodic inter rib spacing between any given set of rib-stiffeners

Δ offset of one set of rib-stiffeners to another set

ζ temporary transform variable for manipulating $w(n\ell)$ and $w(n\ell+\Delta)$

π circumference of circle divided by its diameter, $= 3.14\ldots$

$\wedge$ denotes expression which has been Fourier transformed with respect to the transform variable ζ

K_1 dynamic structural mass, $= \dfrac{m_1' \omega^2}{\ell}$, of first set of rib-stiffeners

K_2 dynamic structural mass, $= \dfrac{m_2' \omega^2}{\ell}$, of second set of rib-stiffeners

k_ℓ wavenumber associated with periodic rib spacing, $= \dfrac{2\pi}{\ell}$

LIST OF SYMBOLS (Cont'd)

h   thickness of the plate

$\Gamma(x)$ Gamma function

!   factorial

~   asymptotically equal to

$f(k)$
$\Psi(k)$ wavenumber expressions defined by equation (3.1a,b)

$\bar{k}$ wavenumber stationary phase value

$S(k)$
$F(k)$
$Y(k)$ simplifying wavenumber expressions defined on page 26

$F_p(k)$
$Y_p(k)$
$W_p(k)$ infinite summatations as defined on page 28

ρ_o mass density of acoustic fluid

ρ_s mass density of plate and rib-stiffeners

ε convergence criteria, 10^{-8}

η Young's modulus loss factor

1. INTRODUCTORY DISCUSSION

1.1   INTRODUCTION

This dissertation examines structural radiation from a rib-stiffened plate of infinite extent. Fluid loading is included on the upper surface of the plate while the lower surface is unloaded, except for a time harmonic line force applied normal to the lower surface. Both far-field and near-field solutions for the radiated acoustic pressure are presented.

Previous investigations of rib-stiffened structures have been limited to periodic inter-rib spacing of either an infinite set of attached rib stiffeners or to a small finite set of attached frames. Note, here and commonly throughout the literature, the terms beams, frames, or simply ribs, are interchangeable with the term rib stiffeners. The formulation presented here allows for one infinite set of periodically spaced stiffeners to be offset from another infinite set of periodically spaced rib-stiffeners. The method can be extended to many sets of ribs, all which have a different offset from one another. Hence, composite sections of the plate may be designed, over any length scale, to possess non-periodic frame spacing.

The motivation for investigating the structural radiation characteristics from a sectionally non-periodic rib-stiffened flat plate was to determine whether the sound radiated can be reduced, at selected frequencies, by judicious selection of the size of, and the attachment location of, the rib-stiffeners. An application is in submarine hull design, where a concern exists for reducing the near-field radiated noise created from a ribbed hull and sensed by passive sonar listening devices.

1.2 REVIEW OF LITERATURE

1.2.1 Periodic Structures

Acoustic radiation from stiffened plates has been investigated over the past thirty years with a primary focus on far-field solutions of the radiated acoustic pressure from periodically stiffened structures. Many authors' work has been based upon the concept of propagation constants with the use of supports to model the effect of the attached rib-stiffeners. Other approaches have used Fourier transforms and the construction of suitable Green functions. A few papers have described the concept of normal mode localization for plates that have randomly positioned rib-stiffeners.

The following pages will briefly outline some of the work that has been performed in analyzing the effects of rib-stiffeners on sound radiation. The section has been included to illuminate the type of mathematical analysis used to analyze stiffened structures. Though each technique is described in short, the following section should provide a means for contrasting previous investigations with the work presented in Chapter 2.

Romanov (1971) calculated the radiated power from an infinite plate due to a field of random line forces driving the plate between two frames spaced a distance 2ℓ apart and symmetric about the origin. Both sides of the plate were fluid loaded. Green's functions, which determined the acoustic radiation from a plate driven by a single unit harmonic point force, were obtained. The Green function was convolved with a spatial correlation function of random forces to yield the far-field sound pressure at a given far-field observation point. The acoustic power was obtained, in the usual manner, by integrating the squared pressure divided by acoustic impedance over the half-cylindrical integration space.

Romanov' paper discusses the effect of the plate's structural damping factor on the level of the radiated power. Small structural loss factors will increase the contributions of the frames to the radiated power, while large structural damping reduces the effect of the frames. This effect has also been discussed by Gorman (1974); it is stated in his work that increasing the structural damping in the plate reduces the rib contributions. Intuitively, the

increased loss in vibrational energy, due to the plate's increased structural damping, implies fewer rib-stiffeners will participate significantly to the radiation field, since ribs far away from the applied force will not be excited by flexural energy.

In typical engineering applications, the structural loss factor cannot be substantially changed, so although the effect is noted it is unlikely that it can be exploited.

Using an approach similar to one taken here, Evseev (1973), determined the far-field radiation from an infinite thin plate with attached frames periodically spaced at a distance ℓ. The fluid-loaded plate was driven by a harmonic point force. The effect of the attached frames was modeled as an unknown reaction force applied at each attachment location. Newton's law related the forces produced by the beams to the plate's displacement. The beams were allowed to have mass and bending stiffness properties, but not rotational stiffness.

The forces acting on the plate were assembled into the differential equation governing the stiffened plate's motion. Fourier transforms were then employed and the plate's response in the transformed domain, with the aid of Poisson's summation formula, was obtained. The algebraic manipulations required to explicitly solve for the wavenumber response were later adapted by Mace (1980a) and expanded upon here in the present analysis.

Asymptotic analysis was used—specifically, the method of stationary phase—to approximate the far-field radiated pressure. The numerical results given by Evseev (1973), as Garrelick (1975) states, were in error, though the formulation appears correct.

Evseev notes that the frames can generate large magnitude wavenumber components at certain wavenumbers which are less, in absolute value, than the acoustic wavenumber. The propagation velocity of these components is greater than the acoustic velocity in the fluid. Hence, these large wavenumber components become efficient radiators of sound.

Solutions for the free and forced vibration of a periodic rib-stiffened infinite plate are presented by Rummerman (1975). The paper does not include fluid-loading effects.

The frames were allowed to exert both line forces and line moments onto the plate. A plane wave excitation is applied to the plate, that is, an external pressure is applied which is time and spatially harmonic in the plane of the plate. Fourier transforms are employed to solve, term by term, for the spectral response of the ribbed plate. By introducing the Poisson summation formula, an explicit equation for the spectral velocity response is obtained. The physical velocity was found by analytical evaluation of the Fourier inversion integral.

Garrelick (1975) showed that Evseev's spectral expressions involving infinite summations could be simplified if fluid-loading effects were neglected. That is, the infinite summations given by Evseev converged and were expressable in terms of trigonometric functions.

Results are given by Garrelick which show the far-field radiated pressure for a plate stiffened by an infinite set of periodic frames over a wide band of frequencies. Also shown, for comparison, are results obtain in an earlier paper by Garrelick (1974), which considered only two and four attached frames equally separated and symmetric about the excitation force.

Garrelick illustrates that the radiated far-field pressure from a two-framed, a four-framed, and the plate that has an infinite set of frames, are comparable. That is, nulls and peaks in the radiated acoustic pressure, and the slopes between these values, only differ slightly from the finite framed configurations and the infinitely framed configuration. The latter has, as one might expect, very well defined maxima and minima.

However, caution is advised in assuming the finite framed plate, as presented by Garrelick, has radiation characteristics uniformly similiar to the infinitely periodic stiffened plate. The results presented in the paper are for a single observation point in the acoustic far-field directly above the applied point force. The variation of acoustic pressure

horizontally along the surface of the plate, in the far-field, and certainly in the near-field, may differ considerably for a small finite number of rib-stiffeners and an infinite set.

The first numerical calculations of the near-field acoustic radiation, found by this author, from a fluid-loaded infinite plate having a finite number of attached periodic frames, appear to be from Romanov's (1977) paper. The formulation cited allows the attached beams to exert both forces and moments on the plate but, the numerical calculations given were simplified for line force reactions only.

The inverse Fourier transform was obtained by a combination of the method of steepest descents and numerical integration along additional contours arising from the contour integral approach. The calculations were compared with results obtained by strictly numerically integrating the inverse transform integral.

Romanov averaged the near-field radiated pressure over a large frequency interval for each horizontal observation point along the surface of the plate. The interval was such that the influence of any "resonance frequencies," due to the spacing between the attached frames, was averaged into the non-resonance frequencies. In this manner, Romanov obtained a broad band spatial distribution of the sound pressure along the plate's surface.

The spatial distribution of the frequency-averaged acoustic pressure along the plate's surface showed well-defined and distinct peaks occurring above each rib-stiffener and rolling off away from the point of excitation.

Mace (1980a) considered the far-field radiated pressure from an infinite fluid-loaded plate having two sets of rib stiffeners, one set spaced an integer multiple of the periodic spacing of the other set. A harmonic point force excitation was applied to the unloaded surface of the plate and the far-field pressure was obtained by the method of stationary phase. The frames did not exert moment reactions on the plate.

Mace's formulation parallels that of Esveev (1973) with the additional effect of bulkhead frames placed at an integer multiple of the intermediate frame's periodic spacing.

The solution for the plate's spectral wavenumber response—that is, an explicit expression for the plate's response in the transformed domain—requires clever algebraic manipulations of some finite and infinite summations. The finite summations arise from the finite number of intermediate frames between bulkheads and the infinite summations arise from considering all of the rib stiffeners.

The numerical results given by Mace have been used to verify, for the special case of periodic rib spacing, the far-field radiation formula, equation (3.4), developed in Chapter 3. Figure 3.1 and Figure 3.2, which are thoroughly discussed in Chapter 3, compare both formulations and it is seen that there is exact agreement between the methods.

The results shown by Mace indicate that the far-field radiated pressure varies considerably, depending upon the point of application of the point force. This dependence was similarly seen by the author. Hence, to simplify the investigation, throughout the analysis presented here, the applied line force remains fixed at the origin of the plate.

Later in the same year, Mace (1980b) and Mace (1980c) tackled the problem of an infinite plate stiffened periodically by line supports, which could exert both force and moment reactions, on a plate subjected to, respectively, a convected harmonic pressure and a harmonic point or line force. The formulation presented in this series of detailed papers differs considerably from that of Mace (1980a). The concept of propagation constant is used, which has been employed by many authors, notably Mead (1970), and this type of formulation will be discussed shortly.

Burroughs (1984) extended the formulation given by Mace (1980a) to analyze the far-field radiation from a fluid-loaded infinite cylindrical shell having periodic and identical circular intermediate ring supports and bulkhead supports. The equations of motion for the cylindrical shell were based on Kennard theory, as were the ring supports, which were modeled as stubby cylinders. The ring supports could impart reaction forces in the radial direction only. The applied excitation was a point force and the far-field pressure

was obtained asymptotically by the method of stationary phase. Numerical results presented compared favorably with previous experimental measurements.

Eatwell (1982) gives a thorough development of the vibration of and the sound radiation from an infinite fluid-loaded plate having a finite or infinite set of periodically spaced attached rib-stiffeners. The stiffeners were allowed to exert moments; however, the numerical results given are for force reactions only.

A Green's function integral is developed by Eatwell which gives the displacement of any point on the stiffened plate's surface in terms of an unknown Green's function and the known bending and rotational impedances of the attached beams.

A Fourier transform is then taken of the Green's function integral, and the force and moment reactions of the frames are written in terms of their spectral impedances. The unknown Green function is obtained by combining these spectral impedances with the known transformed unribbed plate Green's function.

The far-field radiated pressure was obtained using the method of stationary phase for both point force and line force excitation. In addition, using contour integration, expressions were also derived for the plate's structural far-field.

The concept of propagation constants for the analysis of wave propagation in stiffened beams and plates was introduced many years ago in a series of papers by Heckl (1961), Ungar (1961), and Lamb (1961). The general formulation has been extended considerably by others, notably Mead (1970, 1978, 1990), Maidanik (1976), and Crighton (1981), to investigate flexural wave propagation and sound radiation from periodically stiffened structures.

It is well understood that flexural waves can be attenuated, at certain frequencies, by a frame impeding its motion as it travels along a stiffened plate. In Heckl's early analysis, the frames could bend and rotate. The problem of determining the effect of a frame or beam on a traveling flexural wave reduced to determining transmission and reflection coefficients, which varied with frequency, at the junctions between the frame and

the plate. Heckl recognized that the physical velocity anywhere on the plate's surface could be determined by considering only the velocity between two adjacent supports, or within a "bay" separated by the supports. Heckl reached this conclusion by assuming the change in the phase and the rate of decay in the plate's velocity—from one bay to an adjacent one, in either direction—could be related, for a fixed frequency, to a constant. This constant was called the propagation constant.

The analysis showed that certain flexural wavenumbers could not propagate across the frame-plate interface, and the frequency regions where this occurred were called *stop bands*. Similarly, other bending wavenumbers would pass unattenuated, and these regions were *pass bands*.

Ungar (1961) obtained the expressions for the reflection and transmission coefficients at a beam-plate interface using classical elasticity theory. Continuity of displacement of the plate and beam at the interface coupled the governing equations of motion of the plate and beam. A traveling flexural wave on the plate was assumed to impinge on the beam at the interface and the resulting deformation of the plate due to the interaction was then obtained.

An infinite beam on equally spaced supports, which could be rigid or flexible, was investigated by Mead (1970). This investigation determined that rigidly supported systems are characterized by a single propagation constant while flexible supports generate two propagation constants. The beam was not fluid-loaded.

Classical equations for the transverse displacement of a finite beam and the prescribed boundary conditions at each support were used to obtain the displacement between two adjacent supports. Propagation constants were then used to yield the displacement anywhere along the supported plate's surface.

Mead noted that a convected pressure field, which travels at a subsonic velocity, may generate waves which travel along the stiffened plate at supersonic velocites. He

further notes that these supersonic traveling waves couple efficiently with an acoustic medium and radiate sound.

Maidanik (1976) investigated the influence that fluid loading, and also a compliant coating, have on the transmission and reflection coefficients determined earlier by Ungar. Maidanik's analysis showed that certain flexural wavenumbers, which are heavily attenuated in the absence of fluid loading, may be transmitted across the frame interface when fluid loading is present.

Crighton (1981) continued to investigate the effect fluid loading has on flexural wave transmission across a single rib stiffener. The analysis determined that the fluid provided a mechanism which was able to "mend" a structural discontinuity presented to a traveling flexural wave by a rib interface. Over certain frequency bands this mending would be complete and, unlike the unloaded case where the impedance was infinite, the flexural wave would pass unimpeded.

The method of space harmonics was used by Mead (1978) to determine an approximate expression for the sound power radiated by an infinite plate which is periodically supported and excited by a uniform convected pressure field. Mead showed the fluid loaded plate's displacement can be determined by expanding the displacement within a single bay by an infinite summation of space harmonics.

In a set of papers, Mace (1980b and 1980c) continued the work of Mead (1978) and considered far-field radiation from periodically supported fluid-loaded plates which were excited, respectively, by a convected pressure field and a point or line force. The approach in both papers was an infinite plate with supports that introduced both force and moment boundary conditions.

Mace (1980c) shows that when fluid loading is neglected, the periodically stiffened plate's displacement, due to line force excitation, may be explicitly obtained using contour integration. For an applied point force, or with the inclusion of fluid loading, numerical integration is necessary.

Mace presents an interesting rule-of-thumb formula for determining the frequency range for which a periodically stiffened plate can be modeled as an orthotropic plate. Mace (1980c, p.497) states, "whenever the stiffener separation is less than one-third of the plate's bending wavelength, then the ribbed plate can be modeled as an orthtropic plate." For typical plate configurations, this formula implies low frequency regions.

In a recent paper, Mead (1990) obtains the sound power radiated, due to a uniform convected pressure field, from a plate which has periodically spaced rib-stiffeners in two orthogonal directions. The formulation is developed with and without fluid loading and employs two-dimensional space harmonics, as earlier introduced by Mead (1971).

Mead concludes that acoustic radiation is fundamentally determined by the periodic geometry of a stiffened plate. This conclusion is supported by the research in Chapter 2 and Chapter 3 of this study. The structural mass and the bending and rotational stiffness properties of the attached rib-stiffeners alter the overall magnitude of the radiated acoustic pressure. It is the inter-rib spacing which determines the frequencies where the stiffened plate radiates strongly and weakly.

1.2.2 Non-Periodic Structures

The first departure from the analysis of wave propagation and of sound radiation from plates having strictly periodic spacing of stiffeners, either as attached frames or supports, appears in the work of Bansal (1979).

Bansal considered an infinite beam, which was unloaded and composed of identical finite beam segments. Each segment rested on non-periodic, though identical, supports. Within a given segment, the mean of the different lengths between supports was obtained. The averaged length was then used to assume periodic stiffening within the beam section and, using analysis similar to Mead (1970), the free flexural wave motion over the entire plate was determined.

This work differs considerably from the formulation given in Chapter 2. Specifically, the rib-stiffener positions are precisely specified and no averaging of the inter-frame spacing occurs. Secondly, one set of rib-stiffeners, in the analysis presented by the author, may differ from the other set of rib-stiffeners. These differences are significant. As will be shown, the wavenumber response of a true non-periodic rib stiffened plate cannot be easily approximated using a pseudo-periodic spacing.

Bansal (1979, p.48) states, "The sound power radiated from a disordered beam (or plate) is thus expected to be higher (than from a periodic plate)." Although the applied excitation in Bansal differs from the line force used in Chapter 2, the conclusion that sound radiation from a disordered beam is higher than that from a periodic beam is not supported by the present investigation. For the simple case of two sets of rib-stiffeners, one set offset from the other set, at certain frequencies the disordered system radiates less sound, both in the far-field and near-field, than the periodic ordered system.

Though the problem has not yet been mathematically posed for a fluid-loaded, rib-stiffened plate, some investigation into the vibration of a disordered system has been done by Hodges (1982 and 1983).

These papers discuss the phenomenon of Anderson localization, or the confinement of vibrational energy due to backscattering of traveling flexural waves from irregularly positioned scatters. Hodges (1982) notes that no physical system is ideally periodic and even a small difference in periodic spacing can yield normal mode localization, or vibration confinement, over a scale of significant length. Essentially, normal mode localization may be considered as an additional mechanism for damping the spatial vibration of a stiffened system. Hence, the spatial vibrations of a rib-stiffened structure will decay with distance from the point of excitation due to *both* structural damping and vibrational confinement.

A simple experiment was performed by Hodges (1983) which consisted of small masses positioned on a thin wire such that the spacing between each mass varies by 2% or less. Normal mode localization was illustrated by comparing the experimentally measured

12

mode shapes of the fixed wire with irregularly spaced masses with theoretical predications. Agreement was good, though it was pointed out that the localization phenomenon requires a system to have extended disorder.

1.3 DESCRIPTION OF THE PROBLEM FORMULATION

Figure 1.1 is a conceptual illustration of the fluid-loaded, rib-stiffened infinite flat plate under in /estigation. The plate is fluid-loaded on the upper surface only; the lower surface is *in vacuo*. An external time harmonic line force, of magnitude F_0, is applied perpendicularly to the plate's lower surface.

Two sets of attached rib-stiffeners are shown and both are spaced periodically with a distance denoted ℓ. One set of stiffeners is offset from the other set by a distance denoted as Δ. The stiffeners composing a given set are identical. That is, they have the same cross-sectional areas and material properties. The properties of one set, though, can differ from that of the other set.
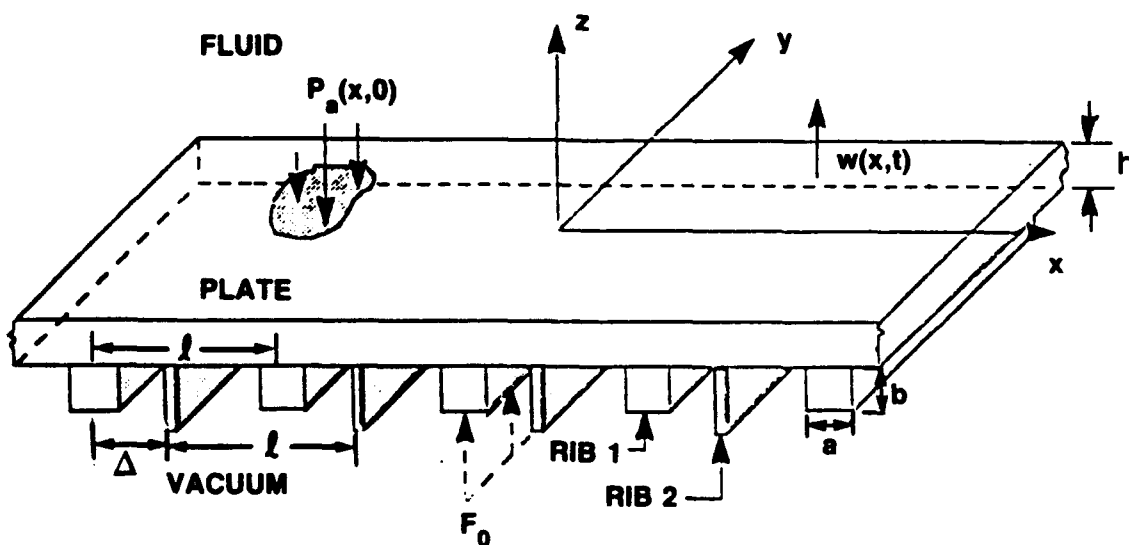
Figure 1.1. Geometry of flat plat showing two sets of rib-stiffeners and the external forces acting on the stiffened plate.

The elastic plate is of uniform thickness, h. It is isotropic, homogenous, and its transverse motion is assumed to be governed by Euler-Bernoulli's equation of motion. Therefore, for the excitation frequencies of interest, it is assumed the flexural wavelengths are greater than the plate's thickness. This implies that rotary inertia and shear deformation effects within the plate can be neglected, as indicated by Mindlin (1951). The rib-stiffeners are modeled similarly, using classical transverse bending of a beam without rotary inertia and shear deformation. The plate has structural damping which has been included by allowing for a complex Young's modulus through use of a loss factor η.

The rib-stiffeners exert reactive forces upon the plate, but not angular moments. Eatwell (1982), Mace (1980b), and others have included angular displacements or rotations of the rib-stiffeners and the extension is not difficult. For simplicity, though, this analysis neglects angular displacements of the stiffeners and the angular moments their displacements produce.

Also, to simplify the formulation the applied excitation is a line force. This forcing precludes any spatial variation of the plate's displacement in the direction parallel to the stiffener, or in the y-direction shown in Figure 1.1. As will become apparent in Chapter 2, the algebraic manipulations of the Fourier-transformed differential equation of motion are likely to appear awkward at first. Retaining spatial variations in the y-direction, by considering an applied point force, would make these calculations appear that much more cumbersome. Once understood, there is no mathematical difficulty in extending the formulation to point force excitation, and the extension is given in the Appendix. For line force excitation, the rib-stiffeners act only as structural masses attached to the plate; to include bending stiffness, an applied point force must be used.

The coordinates are such that the z-direction is normal to the plate's upper surface and the stiffeners lie perpendicular to the x-direction and parallel to the y-direction.

The geometry of the periodic spacing ℓ for each set of rib-stiffeners and the offset of additional sets of stiffeners to other sets is illustrated in Figure 1.2. Four rib-stiffener

sets are shown, three of which have offset Δ_1, Δ_2, and Δ_3. The are no restrictions on the

size of ℓ or on the value of the offset except that any offset must be less than the distance ℓ.

Further, stiffeners can be of any size or of any elastic material. It is apparent that a plate

may be configured to have repeating sections, of length ℓ, which have different and non-

periodic rib spacing.
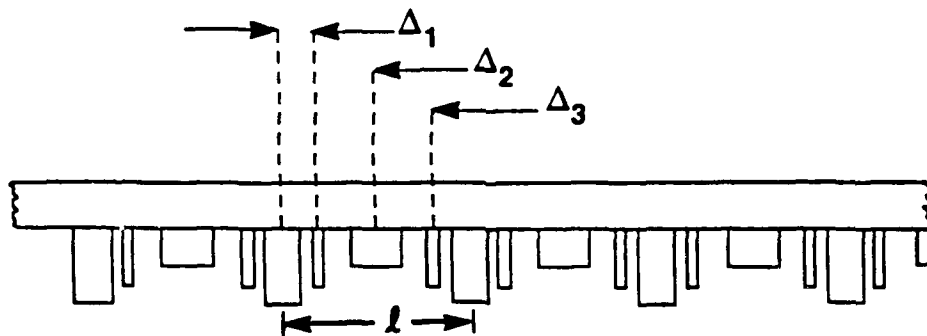
Figure 1.2. General plate configuration showing additional sets of
rib-stiffeners of different size and different offset.

It should be noted here that each additional rib set introduces an additional equation

which must be solved simultaneously with equations involving the other rib sets, in the

transformed wavenumber domain, to obtain an explicit solution for the stiffened plate's

wavenumber response. For a large number of different rib-stiffeners, the algebra would be

cumbersome, and a computational symbolic manipulation program would likely be

necessary.

The geometrical, material, and acoustic fluid properties used for the numerical

calculations presented in Chapter 2, Chapter 3, and Chapter 4 are given in Table 1.1. The

geometrical properties were obtained from unclassified material, Schloemer (1981), relative

to submarine pressure hull design. Two configurations are considered, and are denoted as

the BASELINE design and an ALTERNATE design. Both configurations will be compared

to each other and with an unstiffened plate, which is simply refered to as an UNRIBBED

configuration. Throughout the chapters, as an aid to the reader, the configurations will be capitalized as shown above.

Table 1.1. Geometric, material, and acoustic properties

Geometrical Properties:

Plate Thickness (h)	0.0254 m (1.0 in.)
Periodic Rib Spacing (l)	
Baseline	0.6035 m (24 in.)
Alternate	0.30175 m(12 in.)
Cross-Sectional Rib Area ($a \times b$)	
Baseline	0.004215 m^2 (6.5 in.^{2})
Alternate	0.001935 m^2 (3.0 in.^{2})

Material Properties:

Young's Modulus (Steel, E)	19.5 10^{10} Pa (27.7 10^6 psi)
Modulus Loss Factor (Steel, η)	0.02
Density (Steel, ρ_s)	7.7 10^3 kg/m^3 (475 lbf/ft^3)
Poisson's Ratio (Steel, v)	0.28

Fluid Properties:

Density (Water, ρ_o)	1.0 10^3 kg/m^3 (62 lbf/ft^3)
Sound Speed (Water, c_o)	1.5 10^3 m/s (4921 ft/s)

As Table 1.1 indicates, the ALTERNATE configuration has a periodic rib spacing that is exactly half of the periodic spacing of the BASELINE configuration. The cross-sectional area of the ALTERNATE rib-stiffeners is approximately half that of the BASELINE stiffeners, and both configurations have steel rib-stiffeners.

Unless otherwise stated, the BASELINE and ALTERNATE designs have identical rib-stiffeners which are spaced periodically along the plate. That is, the offset for both designs is one-half the distance l. Hence, these designs simply describe a fluid-loaded infinite plate which has one set of identical rib-stiffeners which are spaced periodically with distance $\Delta = l/2$.

Comparisons are made, in Chapters 2, 3, and 4, for an offset which deviates, by some percentage amount, from the periodic spacing achieved for $\Delta = l/2$. For example, a

"20% shifted" BASELINE configuration implies a 20% change in the offset from the one-half ℓ spacing, such as

$$\Delta = \frac{\ell}{2} + 0.2\frac{\ell}{2} = 1.2\frac{\ell}{2}.$$

Throughout the investigation, the magnitude of the line force is 1kN (224 lbf), and the force is applied directly beneath a rib-stiffener at the plate's origin. The frequencies of excitation, except for swept frequency analysis, were chosen as 250 Hertz, 500 Hertz, 1000 Hertz, and 2000 Hertz. All of these frequencies are below coincidence for the plate investigated.

Light fluid loading (Air) was considered only to verify certain formulas developed in Chapter 2 which are more difficult to validate if fluid loading is included. Unless otherwise stated, all other parameters remain fixed throughout the investigation.

Exponential Fourier transforms have been used to transform the governing differential equation of motion into the wavenumber domain, k. It is assumed the transforms are well-defined and exist over the domain of integration.

The rib-stiffeners are assumed to act over an infinitely narrow region of the plate. Hence, their point of application can be modeled by a Dirac delta function. The harmonic time dependence of the plate's displacement and the radiated acoustic pressure will be suppressed throughout the analysis.

1.4 ORGANIZATION OF CHAPTERS

Chapter 2 develops the equation of motion for the fluid loaded rib-stiffened plate and, after transforming this equation term by term, presents the solution for the plate's wavenumber response, or spectral response, in the transformed domain. A single rib offset is considered in the formulation.

A complete investigation of the periodic rib-stiffened plate's wavenumber response is given. Key wavenumber relationships are developed; they specify wavenumbers that yield maximum and minimum spectral response.

The chapter culminates with a discussion of frequency formulas, which can be obtained from the key wavenumber relationships. These formulas give, for a fixed observation point and for an applied excitation beneath a rib, the excitation frequencies that determine maximum and minimum far-field radiated pressure.

Chapter 2 presents the major contribution this dissertation has to the field of structural acoustics. The manipulations necessary to obtain an explicit expression for the wavenumber response of a rib-stiffened plate, which has stiffeners with arbitrary offset, has not been previously achieved.

A straightforward application of the method of stationary phase, used to obtain the far-field radiated acoustic pressure, is given in Chapter 3. For line force excitation, the stationary phase formulation shows that the far-field pressure is a function of radial stand-off distance, R, and polar angle, θ. The far-field pressure due to a point force is given in the Appendix. The radiated far-field pressure is compared to numerical results given by Mace (1980a) and agreement is exact.

Numerical calculations are presented for the radiated far-field sound pressure level, at a fixed observation position, for changes in frequency and for changes in offset at a fixed frequency. Also shown are the plate's directional radiation characteristics at fixed frequencies of excitation. It is shown that non-periodic rib spacing may produce highly directional unsymmetric radiation patterns.

In Chapter 4, numerical integration has been used to obtain the near-field acoustic pressure radiated from the rib-stiffened plate. A Romberg integration technique was chosen, since it was found to reduce the number of integrand function evaluations necessary for integral convergence. Fairly lengthy computational times were required on a shared IBM 6000 RISC-based computer system to obtain numerical results.

Results are given for the radiated near-field sound pressure level, at a distance of 1/3 meter from the plate's surface, for changes in frequency. Also shown is the variation of acoustic pressure along the horizontal surface of the plate at fixed frequencies. It will be seen that the rib-stiffeners can significantly increase or decrease the near-field radiated sound pressure level.

The chapter concludes with a detailed analysis of the integrand and Fourier inversion integral which yields the radiated acoustic pressure. It is shown that a small change in offset which allows the plate to have non-periodic stiffener spacing may eliminate spectral components that are strong radiators of sound.

Chapter 5 summarizes the significant findings presented in the previous chapters and reiterates the key frequency relationships uncovered during the analysis. A procedure is outlined for reducing, at a fixed frequency, the far-field and near-field radiated pressure. Many recommendations for future investigations and extensions of the formulation are given.

2. SOLUTION AND ANALYSIS OF THE STIFFENED PLATE RESPONSE IN THE TRANSFORMED WAVENUMBER DOMAIN

2.1 THE STIFFENED PLATE EQUATION OF MOTION

The motion of the rib-stiffened fluid loaded plate, as depicted in Figure 1.1, is assumed to be governed by the Euler-Bernoulli differential equation of motion for a thin infinite flat plate and is subjected to external applied pressures as shown below.

$$D\left(\frac{\partial^2}{\partial y^2} + \frac{\partial^2}{\partial x^2}\right)^2 w(x,y) - m\omega^2 w(x,y) = \sum \text{Applied Pressures} \qquad (2.1)$$

where D is the plate's rigidity, $w(x,y)$ is the transverse plate displacement, m is the plate's mass per unit area, ω is the applied excitation frequency.

Since the line force excitation precludes any spatial variation of the plate's displacement in the y-direction, and the applied pressures are specified, equation (2.1) can be rewritten as

$$D\frac{d^4 w(x,y)}{dx^4} - m\omega^2 w(x) = P_e(x) - P_a(x) - \{P_1(x) + P_2(x) + \dots P_N(x)\}. \qquad (2.2)$$

The external pressure due to the applied line force is denoted $P_e(x)$ and the acoustic pressure acting on the upper surface of the plate is $P_a(x,0)$. The total pressure exerted by all of the sets of rib stiffeners are, $P_1(x)$, $P_2(x)$, ... ,$P_N(x)$.

Notice, as mentioned in Chapter 1, terms involving rotary inertia and terms involving shear deformation are not included in equation (2.2). Timoshenko (1955) discusses these terms and their incorporation into the classical equation of motion governing beam and plate vibrations.

The harmonic time dependence, $e^{-i\omega t}$, chosen negative by convention, will be suppressed throughout the analysis.

2.2 FOURIER TRANSFORM OF THE EQUATION OF MOTION

Equation (2.2) is transformed, term by term, using Exponential Fourier transforms, which are defined as

$$\widetilde{w}(k) = \int_{-\infty}^{\infty} w(x)e^{-ikx}\, dx$$

and

$$w(x) = \frac{1}{2\pi} \int_{-\infty}^{\infty} \widetilde{w}(k)e^{ikx}\, dk.$$

The spatial transform variable, k, has physical significance as the wavenumber, and the wavenumber response or spectrum, $\widetilde{w}(k)$, is simply the stiffened plate's response in the wavenumber domain. It is assumed throughout the analysis that both transforms exist over their entire domain of definition.

Equation (2.2) can be immediately transformed and the result is given as

$$(Dk^4 - m\omega^2)\,\widetilde{w}(k) = \widetilde{P}_e(k) - \widetilde{P}_a(k) - \{\widetilde{P}_1(k) + \widetilde{P}_2(k) + \dots \widetilde{P}_N(k)\} \qquad (2.3)$$

where the ~ denotes the transformed expressions.

The transforms of the different applied pressures will be obtained in a sequential fashion in the same order, left to right, as shown above.

The transform of the external pressure due to the applied line force of magnitude F_0, which acts along a line parallel to the rib-stiffeners at some location x_0, is simply

$$\widetilde{P}_e(k) = \int_{-\infty}^{\infty} F_0\, \delta(x-x_0)\, e^{-ikx}\, dx = F_0\, e^{-ikx_0}. \qquad (2.4)$$

The acoustic pressure, $P_a(x,0)$, applied to the plate's upper surface is determined, in the usual manner, through the acoustic wave equation and the condition of continuity of velocity at the interface between the plate and the fluid medium.

The development of the transformed response of the fluid loading pressure will be brief since the coupling of an acoustic fluid with an infinite flat plate is well-documented and understood.

The two-dimensional wave equation is written, assuming harmonic time dependence of the acoustic pressure, as

$$(\frac{\partial^2}{\partial x^2} + \frac{\partial^2}{\partial z^2}) P_a(x,z) = \frac{-\omega^2}{c_0^2} P_a(x,z).$$ (2.5)

The above equation is transformed, with respect to x, treating the z dependence as a parameter. The result of the transform yields second-order differential equations, in the parameter z, defined in two wavenumber regions

$$\frac{d^2\widetilde{P}_a(z;k)}{dz^2} + (k_0^2 - k^2)\, \widetilde{P}_a(z;k) = 0 \quad |k| \leq k_0,$$ (2.6a)

and

$$\frac{d^2\widetilde{P}_a(z;k)}{dz^2} - (k^2 - k_0^2)\, \widetilde{P}_a(z;k) = 0 \quad |k| \geq k_0,$$ (2.6b)

where $k_0 = \frac{\omega}{c_0}$, the acoustic wavenumber.

The general solution to equation (2.6a) and equation (2.6b) is known, and with the condition that the acoustic pressure must be bounded and travels outward yields

$$P_a(z;k) = A_1(k)e^{i\sqrt{k_0^2 - k^2}\, z} \qquad |k| \leq k_0$$ (2.7a)

and

$$P_a(z;k) = A_2(k)e^{-\sqrt{k^2 - k_0^2}\, z} \qquad |k| \geq k_0$$ (2.7b)

where $A_1(k)$ and $A_2(k)$ are unknown wavenumber-dependent coefficients.

22

The unknown coefficients are determined by the boundary condition at the interface of the plate with the acoustic fluid. The fluid is assumed ideal, and the boundary condition is given, after transforming the linearized momentum equation, at the plate's upper surface as

$$\frac{d\widetilde{P}_a(z;k)}{dz}\bigg|_{z=0} = \rho_0\omega^2\widetilde{w}(k). \tag{2.8}$$

Solving for the coefficients $A_1(k)$ and $A_2(k)$ yields the general solution to equations (2.6a,b)

$$\widetilde{P}_a(z,k) = \frac{-i\rho_0\omega^2\ \widetilde{w}(k)}{\sqrt{k_0^2-k^2}}\ e^{i\sqrt{k_0^2-k^2}\ z}\quad |k| \le k_0 \tag{2.9a}$$

and

$$\widetilde{P}_a(z,k) = \frac{-\rho_0\omega^2\ \widetilde{w}(k)}{\sqrt{k^2-k_0^2}}\ e^{-\sqrt{k^2-k_0^2}\ z}\quad |k| \ge k_0. \tag{2.9b}$$

Substituting these values into the inverse transform integral for the physical radiated pressure from the fluid-loaded stiffened plate's surface gives

$$P_a(x,z) = -\frac{i\rho_0\omega^2}{2\pi}\int\limits_{|k|\le k_0}\frac{\widetilde{w}(k)}{\sqrt{k_0^2-k^2}}\ e^{i\sqrt{k_0^2-k^2}\ z}\ e^{ikx}dk. \tag{2.10a}$$

$$P_a(x,z) = -\frac{\rho_0\omega^2}{2\pi}\int\limits_{|k|\ge k_0}\frac{\widetilde{w}(k)}{\sqrt{k^2-k_0^2}}\ e^{-\sqrt{k^2-k_0^2}\ z}\ e^{ikx}dk. \tag{2.10b}$$

The transformed acoustic pressure acting on the surface of the plate is, from equations (2.9a,b),

$$\tilde{P}_a(0,k) = \frac{-i\rho_0\omega^2\tilde{w}(k)}{\sqrt{k_0^2-k^2}} \qquad |k| \le k_0, \qquad (2.11a)$$

and

$$\tilde{P}_a(0,k) = \frac{-\rho_0\omega^2\tilde{w}(k)}{\sqrt{k^2-k_0^2}} \qquad |k| \ge k_0. \qquad (2.11b)$$

Equation (2.2) depicts N-sets of attached rib stiffeners acting on the fluid loaded plate. Without loss in generality, for the formulation here, only two sets of rib stiffeners will be considered. As mentioned in Chapter 1, the rib stiffeners, for line force excitation, act only as structural masses attached to the plate. A point force allows the ribs to have bending stiffness and this extension is given in the Appendix.

The reactive force produced by an idealized single rib-stiffener acting over an infinitely narrow region of the plate is simply equal to the product of the mass and acceleration of the stiffener. It is assumed the rib motion, $u(x)$, varies harmonically with time, and each set of stiffeners produce a total reactive pressure acting beneath the plate

$$P_1(x) = - \sum_{n=-\infty}^{\infty} m_1{}' \, \omega^2 u_1(x) \, \delta(x-n\ell), \qquad (2.12a)$$

and

$$P_2(x) = - \sum_{n=-\infty}^{\infty} m_2{}' \, \omega^2 u_2(x) \, \delta(x-(n\ell+\Delta)), \qquad (2.12b)$$

where $m_1{}'$ and $m_2{}'$ are the mass per unit length of each of the rib stiffener sets. The displacement of each set of rib stiffeners is denoted by $u_1(x)$ and $u_2(x)$.

Both of the above equations are transformed, with respect to x, and, assuming the summations are uniformly convergent, the order of integration may be interchanged with the summations, obtaining the following

24

$$\tilde{P}_1(k) = -m_1' \, \omega^2 \sum_{n=-\infty}^{\infty} w(n\ell) \, e^{-ikn\ell}, \qquad (2.13a)$$

and

$$\tilde{P}_2(k) = -m_2' \, \omega^2 \sum_{n=-\infty}^{\infty} w(n\ell + \Delta) \, e^{-ik(n\ell+\Delta)}. \qquad (2.13b)$$

Notice that the plate's displacement, $w(n\ell)$ and $w(n\ell+\Delta)$, has been substituted for the displacement of the rib's displacement, $u(n\ell)$ and $u(n\ell+D)$, since the plate and ribs are rigidly attached at $x_n = n\ell$ and $x_n = n\ell+\Delta$.

Also notice that equations (2.13a,b) are not in terms of the transformed variable, k, but are in terms of a physical displacement variable, $n\ell$ and $n\ell+\Delta$. By introducing a new transformation domain, denoted the ζ domain, manipulations may be performed to write equations (2.13a,b) in terms of the wavenumber, k.

The manipulation is accomplished by introducing the transform shown below

$$w(n\ell) = \frac{1}{2\pi} \int_{-\infty}^{\infty} \hat{w}(\zeta) e^{i\zeta(n\ell)} d\zeta. \qquad (2.14)$$

Substituting equation (2.14) into equations (2.13a,b) gives

$$\tilde{P}_1(k) = \frac{-m_1'\omega^2}{2\pi} \int_{-\infty}^{\infty} \hat{w}(\zeta) \sum_{n=-\infty}^{\infty} e^{in\ell(\zeta-k)} \, d\zeta, \qquad (2.15a)$$

$$\tilde{P}_2(k) = \frac{-m_2'\omega^2}{2\pi} \int_{-\infty}^{\infty} \hat{w}(\zeta) \sum_{n=-\infty}^{\infty} e^{i(n\ell+\Delta)(\zeta-k)} \, d\zeta, \qquad (2.15b)$$

Poisson's Summation formula, Stakgold (1979), which is an essential relationship required to proceed and is shown in a general form below, is introduced into equations (2.15a,b)

$$\sum_{n=-\infty}^{\infty} e^{in\tau} = 2\pi \sum_{n=-\infty}^{\infty} \delta(\tau - 2\pi n)$$

Using the above relationship, equations (2.15a,b) can be rewritten as

$$\tilde{P}_1(k) = \frac{-m_1'\omega^2}{2\pi} \int\limits_{-\infty}^{\infty} \hat{w}(\zeta) \left\{ \frac{2\pi}{l} \sum_{n=-\infty}^{\infty} \delta\left(\zeta-(k+\frac{2\pi n}{l})\right) \right\} d\zeta, \qquad (2.16a)$$

$$\tilde{P}_2(k) = \frac{-m_2'\omega^2}{2\pi} \int\limits_{-\infty}^{\infty} \hat{w}(\zeta) \left\{ \frac{2\pi}{l} e^{i\Delta(\zeta-k)} \sum_{n=-\infty}^{\infty} \delta\left(\zeta-(k+\frac{2\pi n}{l})\right) \right\} d\zeta, \quad (2.16b)$$

Interchanging the order of the summation and integration, the integrals of equations (2.16a,b) can be evaluated exactly, yielding

$$\tilde{P}_1(k) = \frac{-m_1'\omega^2}{l} \sum_{n=-\infty}^{\infty} \tilde{w}\left(k + \frac{2\pi n}{l}\right) \qquad (2.17a)$$

$$\tilde{P}_2(k) = \frac{-m_2'\omega^2}{l} \sum_{n=-\infty}^{\infty} \tilde{w}\left(k + \frac{2\pi n}{l}\right) e^{i(2\pi n\Delta/l)} \qquad (2.17b)$$

The following quantities are defined to simplify the algebraic manipulations required to explicitly solve for the wavenumber response, $\tilde{w}(k)$, of the stiffened plate. It will also be seen that these quantities are key parameters which describe the behavior of the radiated acoustic pressure.

$$k_l = \frac{2\pi}{l} \qquad\qquad K_1 = -\frac{m_1'\omega^2}{l} \qquad\qquad K_2 = -\frac{m_1'\omega^2}{l}$$

Note that k_l is a constant wavenumber corresponding to the periodic inter-rib spacing, l. The other terms, K_1 and K_2, represent the dynamic mass of the attached rib stiffeners. Equations (2.17a,b) can now be rewritten as

$$\tilde{P}_1(k) = K_1 \sum_{n=-\infty}^{\infty} \tilde{w}(k + k_l n) \qquad (2.18a)$$

$$\tilde{P}_2(k) = K_2 \sum_{n=-\infty}^{\infty} \tilde{w}(k + k_l n)e^{ik_l n\Delta}. \qquad (2.18b)$$

Substituting all of the transformed external pressures, equation (2.4), equations (2.11a,b) and equations (2.18a,b), back into equation (2.3) yields the fluid-loaded stiffened plate's wavenumber response, though not in an explicit form.

$$(Dk^4 - m\omega^2)\,\widetilde{w}(k) = F_0 e^{-ikx_0} + \frac{i\rho_0\omega^2\widetilde{w}(k)}{\sqrt{k_0^2 - k^2}}$$

$$-K_1 \sum_{n=-\infty}^{\infty} \widetilde{w}(k + k_\ell n) - K_2 \sum_{n=-\infty}^{\infty} \widetilde{w}(k + k_\ell n)\, e^{ik_\ell n\Delta} \qquad |k| \le k_0, \quad (2.19a)$$

$$(Dk^4 - m\omega^2)\,\widetilde{w}(k) = F_0 e^{-ikx_0} + \frac{\rho_0\omega^2\widetilde{w}(k)}{\sqrt{k^2 - k_0^2}}$$

$$-K_1 \sum_{n=-\infty}^{\infty} \widetilde{w}(k + k_\ell n) - K_2 \sum_{n=-\infty}^{\infty} \widetilde{w}(k + k_\ell n)\, e^{ik_\ell n\Delta} \qquad |k| \ge k_0. \quad (2.19b)$$

Equations (2.19a,b) may be further simplified by introducing the following expressions

$$S(k) = \begin{cases} D\!\left(k^4 - k_b^4\right) - \dfrac{i\rho_0\omega^2}{\sqrt{k_0^2 - k^2}} & |k| \le k_0, \\[4mm] D\!\left(k^4 - k_b^4\right) - \dfrac{\rho_0\omega^2}{\sqrt{k^2 - k_0^2}} & |k| \ge k_0, \end{cases}$$

$$F(k) = \frac{F_0 e^{-ikx_0}}{S(k)} \qquad\qquad Y(k) = \frac{1}{S(k)}$$

where $k_b^4 = \dfrac{m\omega^2}{D}$, is the free *in vacuo* plate wavenumber.

With the above substitutions, equation (2.19) can be written in an simplfied form as

$$\tilde{w}(k) = F(k) - K_1 Y(k) \sum_{n=-\infty}^{\infty} \tilde{w}(k + nk_{\ell}) - K_2 Y(k) \sum_{n=-\infty}^{\infty} \tilde{w}(k + nk_{\ell}) e^{ik_{\ell} n \Delta}. \quad (2.20)$$

Note that if additional sets of rib stiffeners, of different size and offset, had been retained, equation (2.20) would simply become

$$\tilde{w}(k) = F(k) - Y(k) \left\{ \sum_{n=-\infty}^{\infty} (K_1 + K_2 e^{ink_{\ell}\Delta_1} + \ldots \right.$$

$$\left. + K_N e^{ink_{\ell}\Delta_{N-1}}) w(k + nk_{\ell}) \right\}. \quad (2.21)$$

2.3 EXPLICIT SOLUTION OF THE WAVENUMBER RESPONSE

The difficulty now lies in determining an explicit expression for the plate's wavenumber response, $\tilde{w}(k)$. That is, it is necessary to manipulate equation (2.20) such that the summations which contain the wavenumber response $\tilde{w}(k + k_{\ell} n)$, may be written in terms of known quantities.

The algebraic manipulations presented below perform two functions. First, they correctly solve for the immediate problem of obtaining an explicit wavenumber response for a fluid-loaded plate having two sets of rib stiffeners. More importantly, they show a new technique for solving for the acoustic radiation from a non-periodic, rib-stiffened structure. This new technique represents a significant contribution to the field of structural acoustics.

The manipulations will be performed for two sets of rib stiffeners and it will be seen that the two sets generate two independent equations in two unknowns. The unknowns are summations involving $\tilde{w}(k + k_{\ell} n)$ and $\tilde{w}(k + k_{\ell} n) e^{ik_{\ell} n \Delta}$, which must be solved simultaneously. Nuttall (1992), who became quite interested in the problem,

assisted in expanding the solution so that any number of rib-stiffener sets could be considered, and introduced a simplifying notation which will be adopted here.

The following summation expressions are defined, where the subscript p denotes the integer value in the summation exponent.

$$W_p(k) \equiv \sum_{n=-\infty}^{\infty} \tilde{w}(k + nk_1) \, e^{ik_1 n \Delta p},$$

$$F_p(k) \equiv \sum_{n=-\infty}^{\infty} F(k + nk_1) \, e^{ik_1 n \Delta p},$$

$$Y_p(k) \equiv \sum_{n=-\infty}^{\infty} Y(k + nk_1) \, e^{ik_1 n \Delta p}.$$

Each summation defined above has the following key property:

$$G_p(k + k_1 m) = G_p(k) \, e^{-ik_1 \Delta m p}.$$

This property requires that the summations be infinite and can be understood by considering the $p = 0$ case. For this case, it is readily seen that increasing the argument of the function being summed by an integer does not change the summation since the function is being summed over all integers.

The expression for the summed plate response is substitued into equation (2.20) and yields the following expression

$$\tilde{w}(k) = F(k) - K_1 Y(k) W_0(k) - K_2 Y(k) W_1(k). \tag{2.22}$$

To explicitly solve for $\tilde{w}(k)$ in equation (2.22), let $k = k + k_1 m$, and sum both sides of equation (2.22) over all m, which yields, considering the above relationship,

$$W_0(k) = F_0(k) - K_1 Y_0(k) W_0(k) - K_2 Y_{-1}(k) W_1(k). \tag{2.23}$$

Returning to equation (2.22), both sides are now multiplied by $e^{ik_{\ell}m}$, the substitution $k = k + k_{\ell}m$ is made, and both sides are summed over all integers m, which yields

$$W_1(k) = F_1(k) - K_1 Y_1(k) W_0(k) - K_2 Y_0(k) W_1(k). \tag{2.24}$$

Equation (2.23) and equation (2.24) are solved simultaneously for $W_0(k)$ and $W_1(k)$, which gives

$$W_0(k) = \frac{F_0(k)}{(1+K_1 Y_0(k))} - \frac{K_2 Y_{-1}(k)}{1+K_1 Y_0(k)} *$$

$$\left\{ \frac{F_1(k)+K_1(F_1(k)Y_0(k)-F_0(k)Y_1(k))}{1+(K_1+K_2)Y_0(k)+K_1 K_2(Y_0^2(k)-Y_1(k))Y_{-1}(k)} \right\}. \tag{2.25a}$$

$$W_1(k) = \frac{F_1(k)+K_1(F_1(k)Y_0(k)-F_0(k)Y_1(k))}{1+(K_1+K_2)Y_0(k)+K_1 K_2(Y_0^2(k)-Y_1(k)Y_{-1}(k))}. \tag{2.25b}$$

Substituting equations (2.25a,b) back into equation (2.22) gives the explicit wavenumber response of the fluid-loaded, infinite flat plate having two sets of attached rib stiffeners

$$\tilde{w}(k) = F(k) - Y(k) *$$

$$\left\{ \frac{K_2(1+K_1 Y_0(k))F_1(k)+K_1(1+K_2 Y_0(k))F_0(k)-K_1 K_2(F_0(k)Y_1(k)+F_1(k)Y_{-1}(k))}{1+(K_1+K_2)Y_0(k)+K_1 K_2(Y_0^2(k)-Y_1(k)Y_{-1}(k))} \right\}$$

$$\tag{2.26}$$

It may be easily shown that this result includes previously obtained results for a single set of periodically spaced ribs. For the special case of identical rib stiffeners spaced periodically with distance ℓ, for example $K_2 = 0.0$, equation (2.26) simplifies to

$$\tilde{w}(k) = F(k) - \frac{Y(k)K_1 F_0(k)}{1+K_1 Y_0(k)}. \tag{2.27}$$

Equation (2.27) is identical to that which was obtained by Mace (1980a).

Each additional set of rib stiffeners introduces an additional summation, $W_p(k)$, which must be solved simultaneously with the other summation terms, to obtain the explicit form of the plate's wavenumber response. For example, ten independent rib-stiffener sets, nine of which have different offset, would generate ten equations in ten unknowns, $W_0(k), W_1(k), \ldots, W_9(k)$.

Hence, for a large number of rib sets, the algebra becomes unwieldy, and a symbolic manipulation program, such as MACSYMA or MATHEMATICA, would be needed to obtain an analytical solution for the wavenumber response. A very large number of different rib-stiffener sets may always be solved numerically, as discussed in Nuttall (1991).

The general wavenumber response given by equation (2.26) collapses predictably to equation (2.27) by letting, for example, K_1 or K_2 be zero, or allowing the offset, Δ, to be zero or half the periodic spacing, ℓ. If both K_1 and K_2 are set to zero, then equation (2.26) simply becomes the wavenumber response of a unribbed fluid-loaded, infinite flat plate.

2.4 ANALYSIS OF THE TRANSFORMED WAVENUMBER RESPONSE

Equation (2.26) is an involved expression. To analyze it in general, with the many variables that contribute to the plate's wavenumber response, would be a lengthy and difficult task. Therefore, in order to bound the analysis, certain parameters have been held fixed throughout the investigation. All of the material properties and the fluid properties, except for certain air-loading special cases, remain constant as specified in Table 1.1.

The excitation is applied at the plate's origin, $x_0 = 0.0$, throughout, and four fixed frequencies of excitation are considered — 250 Hertz, 500 Hertz, 1000 Hertz, and 2000 Hertz — though swept frequency analysis is also included.

Holding the above-mentioned parameters fixed, however, still does not ease the difficulty in mathematically evaluating equation (2.26) in detail. Of interest are the wavenumbers at which the wavenumber spectra of the stiffened plate have maxima and minima. It was determined, therefore, to quantitatively investigate equation (2.27), the periodic configuration. Next, equation (2.26) could be qualitatively analyzed by changing the offset by a small prescribed amount. Keeping this in mind, the analysis begins with a three-dimensional perspective view of the UNRIBBED wavenumber response.

2.4.1 Periodic Wavenumber-Frequency Figures

A descriptive presentation of the wavenumber-frequency response of the UNRIBBED, BASELINE, and ALTERNATE stiffened plate configurations is given in this section. The section is meant to provide an overall general description of features seen in the spectral response of a periodically stiffened plate. A detailed discussion and analysis of the features illustrated begins in Section 2.4.3.

Figure 2.1 shows the normalized magnitude of the UNRIBBED plate's wavenumber, or spectral, response within the frequency range 250 Hertz to 5,500 Hertz and with wavenumber range -40 m^{-1} to 40 m^{-1}. The response has been normalized by the maximum modulus in wavenumber for a given frequency.

Displayed in Figure 2.1 is the effect of radiation damping on the plate's response at the acoustic wavenumber, k_0. Also apparent is the dispersive nature of the fluid-loaded flexural wavenumber, k_{fl}, and the large spectral response at this wavenumber. Radiation damping, which is seen as a null in the spectral response and indicated by arrows in Figure 2.1, varies linearly with increasing frequency. Whereas, the peak in the spectral response at the flexural wavenumber is seen to vary non-linearly with increasing frequency.

Eventually (though not shown in Figure 2.1) as frequency increases, the acoustic wavenumber intersects with the plate's flexural wavenumber. The frequency at this intersection is referred to as the coincidence frequency.

Recall that spectral components that have supersonic wavenumbers couple well with the acoustic fluid since the propagating wavenumber is traveling faster than the acoustic wavenumber. These components are strong radiators of sound.

As can be seen in Figure 2.1, no large spectral responses are seen below coincidence in the cone-shaped region defined by the acoustic wavenumbers, $\pm k_0$.
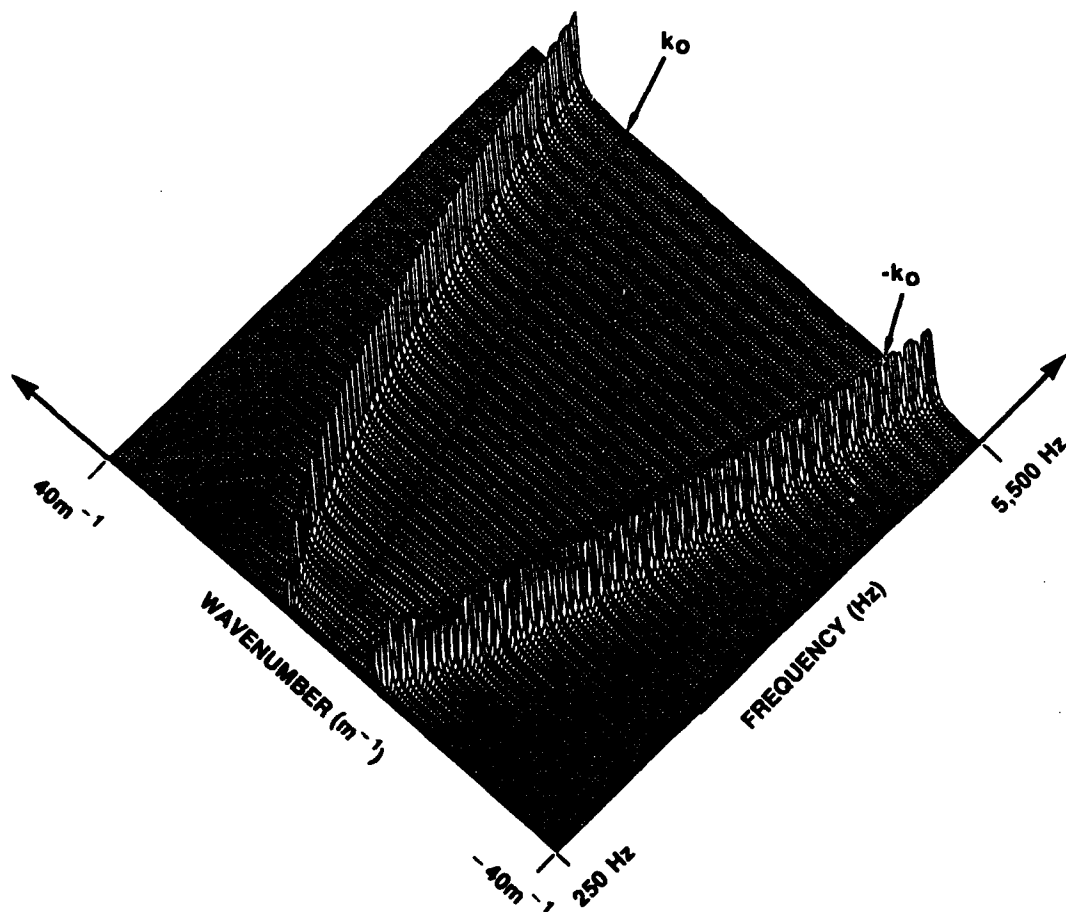
Figure 2.1. Normalized magnitude of the UNRIBBED plate wavenumber response versus frequency and wavenumber.

Figure 2.2 is simply a slice through the normalized wavenumber response given in
Figure 2.1 at a frequency of 500 Hertz and within the wavenumber range of -40 m^{-1} to 40
m^{-1}. The absolute value of the acoustic wavenumber at 500 Hertz is 2.1 m^{-1} and the nulls
produced in the magnitude of the wavenumber response, due to vibrational energy being
transferred away from the plate into the fluid, are shown. The large spectral response at
wavenumber, ± 10 m^{-1}, represents the plate's response at the classical fluid-loaded free
wavenumber, k_{fl}.
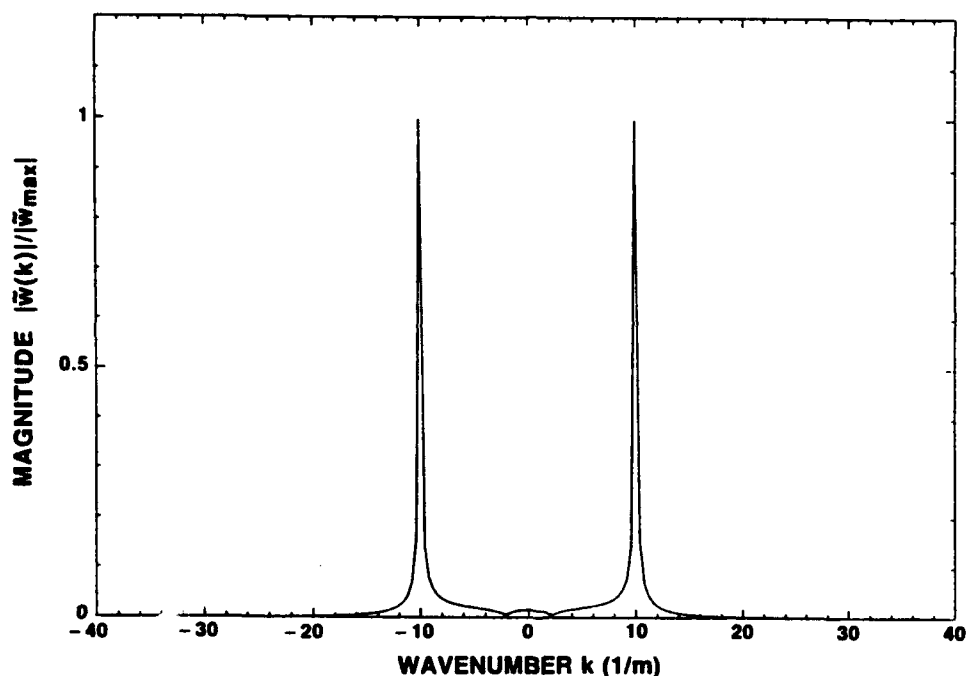
Figure 2.2. Normalized magnitude response of the UNRIBBED plate for a
fixed frequency of 500 Hertz.

The spectral response of the UNRIBBED plate changes in a predictable manner
with increasing excitation frequency. Figure 2.3 shows the normalized magnitude of the
wavenumber response of the UNRIBBED plate at a frequency of 2,000 Hertz. The location

of the nulls due to radiation damping have shifted to ± 8.3 m^{-1} and the peaks in the spectral response have shifted upward to ± 19 m^{-1}.
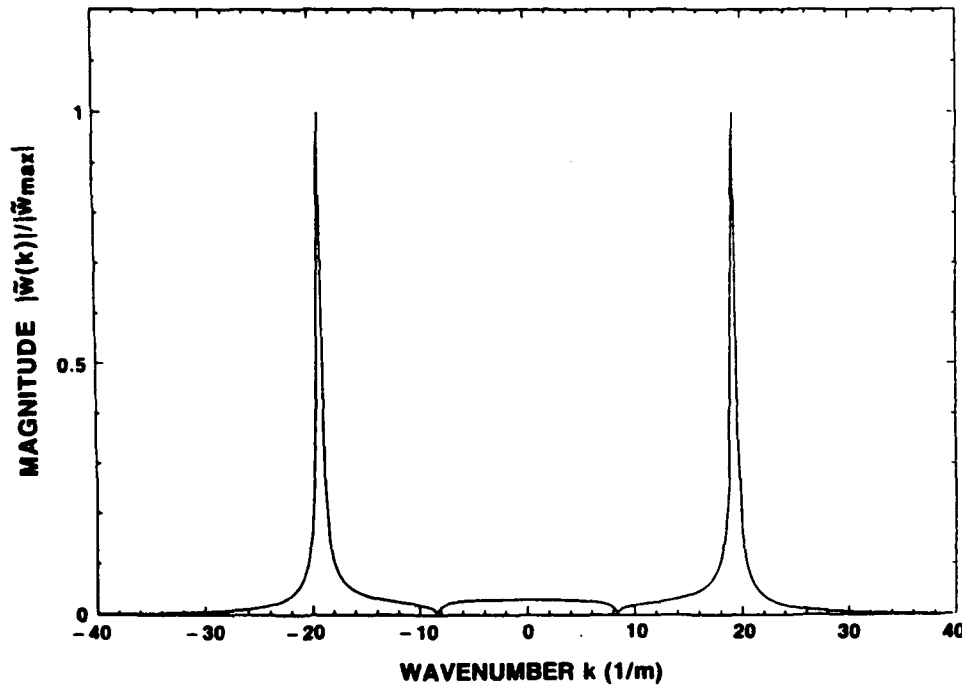
Figure 2.3 . Normalized magnitude response of the UNRIBBED plate for a
fixed frequency of 2000 Hertz.

The periodic BASELINE configuration is shown in Figure 2.4, which again has been normalized by the maximum modulus in wavenumber for a given frequency. The frequency range is between 250 Hertz and 5,500 Hertz and the wavenumber range is -40 m^{-1} to 40 m^{-1}.

The response shown is symmetric about the wavenumber origin and is markedly patterned. The pattern shows curves of constant zero wavenumber response and curves of constant relative maximum response. The curves are evenly spaced in wavenumber from one another, and show the identical dispersive nature as the flexural wavenumber.
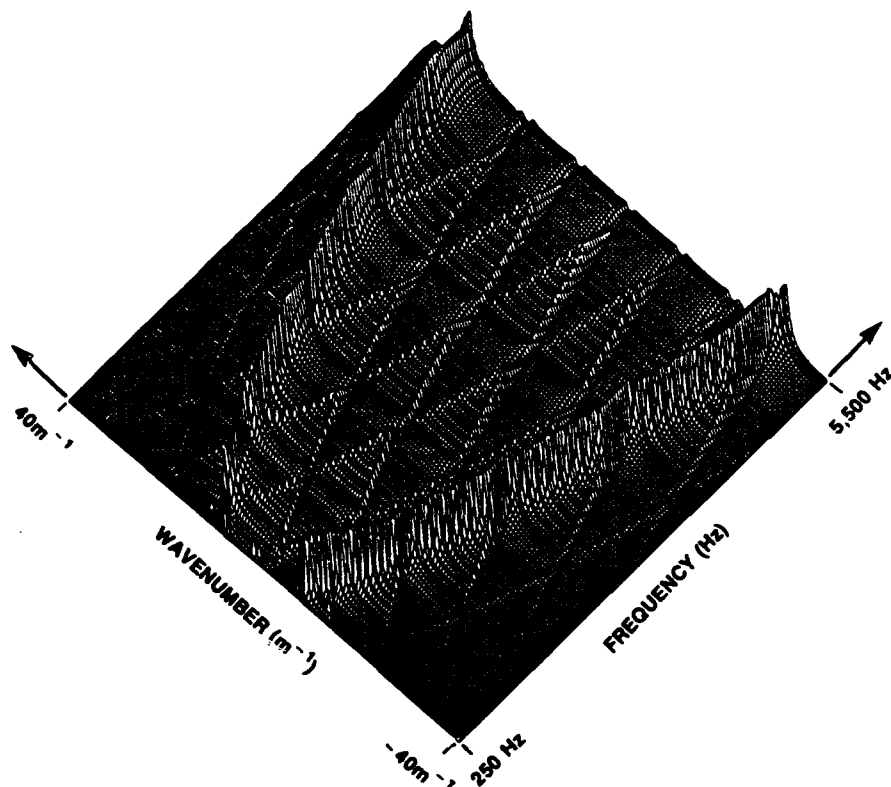
Figure 2.4. Normalized magnitude of the BASELINE plate wavenumber
response versus frequency and wavenumber.

It can be seen from Figure 2.4, that the spectral response decays rapidly for
wavenumbers greater, in absolute value, than the flexural wavenumber. Examining the
term $S(k)$, given in equation (2.27), reveals that the wavenumber response decays, above
the flexural wavenumber, to one over the fourth power in wavenumber. Hence, the region
of interest is spectral components which have wavenumbers less, in absolute value, than
the plate's flexural wavenumber.

Not clearly seen in Figure 2.4, because of the perspective viewing angle used in the
three-dimensional plotting routine, are the nulls in the wavenumber response due to acoustic

damping. These nulls are present and are located in the same position as shown in Figure 2.1. These nulls are entirely independent of the attachment of rib-stiffeners to the plate.

Comparing Figure 2.4, the BASELINE response, with Figure 2.1, the UNRIBBED response, the BASELINE response has large magnitude spectral components within the cone-shaped region demarcated by the acoustic wavenumbers, $\pm k_0$. As mentioned, these components will be efficient radiators of sound into the far-field.

Figure 2.5, Figure 2.6, and Figure 2.7 show a slice through the normalized magnitude of the BASELINE plate's wavenumber response, given in Figure 2.4, at the fixed frequencies, 500 Hertz, 1000 Hertz, and 2000 Hertz, respectively.

In Figure 2.5, notice that nulls—located at wavenumbers $\pm 10.5 \ m^{-1}$—in the magnitude of the spectral response occur near the spectral peaks at the flexural wave-numbers $\pm 10.0 \ m^{-1}$. In Figure 2.6 and Figure 2.7, these nulls have shifted, and since all other variables, besides frequency, are held constant, the location of the nulls in the BASELINE plate's wavenumber response are clearly frequency dependent. The presence of nulls in the wavenumber response which are located near to flexural wavenumbers may have a significant effect on the structural response of the stiffened plate. The effect may lead to two traveling flexural waves, rather than one, that travel away from the point of excitation in a modulated manner. This effect is discussed in more detail in Section 2.4.4.

Shown in Figure 2.7 are relatively large magnitude components of the wavenumber response, at approximate wavenumbers, $\pm 1.0 \ m^{-1}$, which lie within a region less, in magnitude, than the acoustic wavenumber, $k_0 = 8.4 \ m^{-1}$. Hence, these spectral components will likely be strong radiators of acoustical pressure which were not present in the UNRIBBED plate configuration. In section 2.4.3 a simple expression is developed for a periodically stiffened plate which has *light* fluid-loading which gives wavenumbers for a relative maximum spectral response. The expression can be used to predict the frequencies which yield a relatively large spectral response at supersonic wavenumbers.

Figure 2.5. Normalized magnitude response of the BASELINE plate for a
fixed frequency of 500 Hertz.
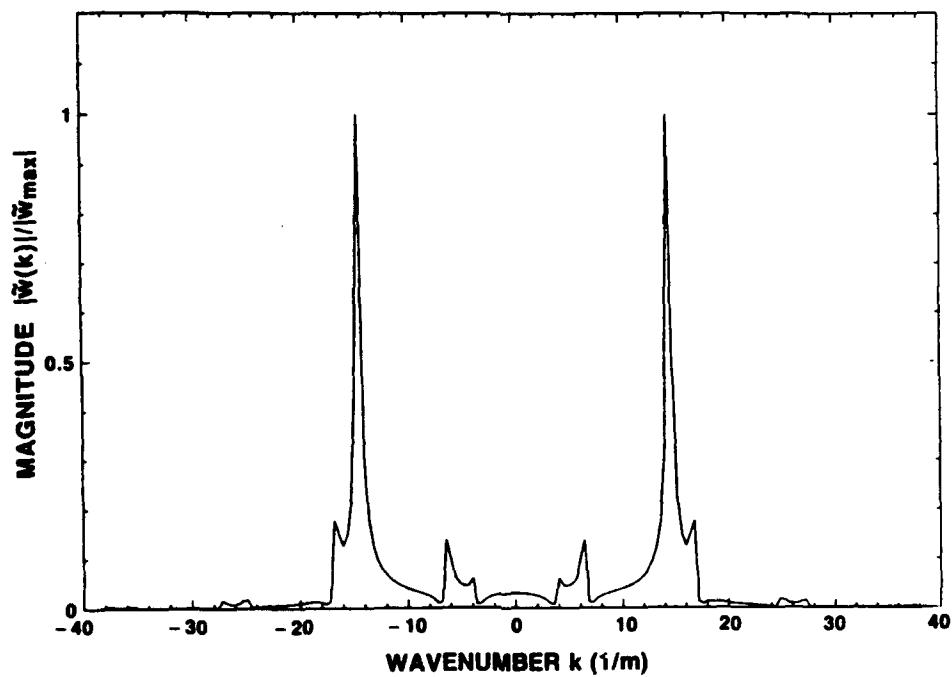
Figure 2.6. Normalized magnitude response of the BASELINE plate for a
fixed frequency of 1000 Hertz.
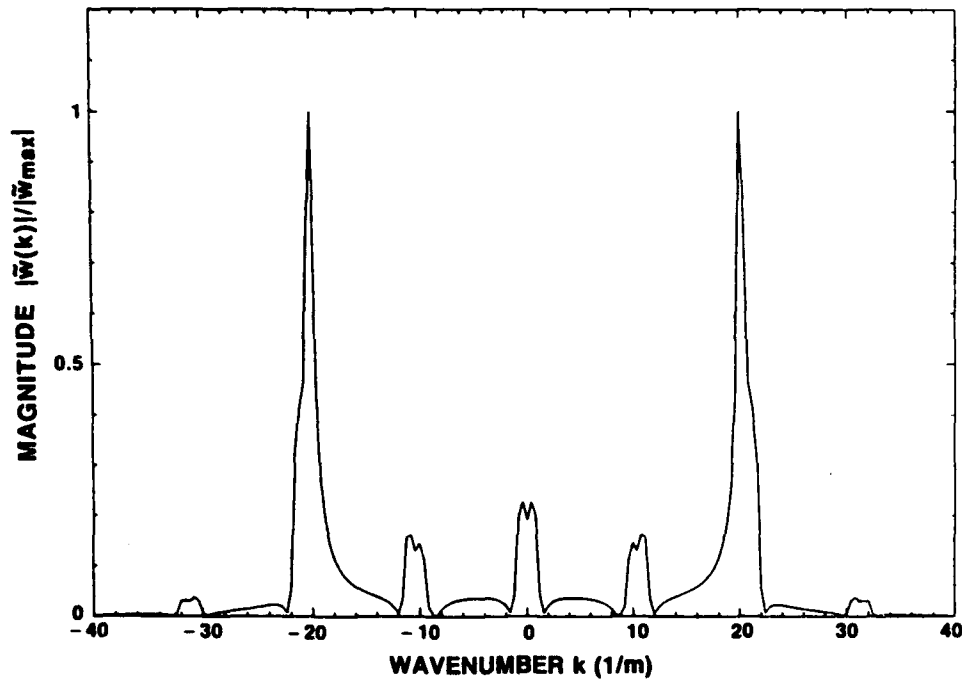
Figure 2.7. Normalized magnitude response of the BASELINE plate for a
fixed frequency of 2000 Hertz.

Figure 2.8 shows the normalized magnitude of the ALTERNATE plate's
wavenumber response versus frequency and wavenumber over the same ranges as Figure
2.1 and Figure 2.4. The overall pattern shown is similiar to that shown in Figure 2.4 for
the BASELINE configuration, though fewer curves of constant zero response are seen in
the ALTERNATE configuration than the BASELINE's configuration. The fewer curves of
constant zero response are due to the change in inter-rib spacing and is examined in detail in
section 2.4.3.

The nulls in the magnitude of the normalized spectral response due to acoustic
damping, unlike Figure 2.4, are clearly seen.
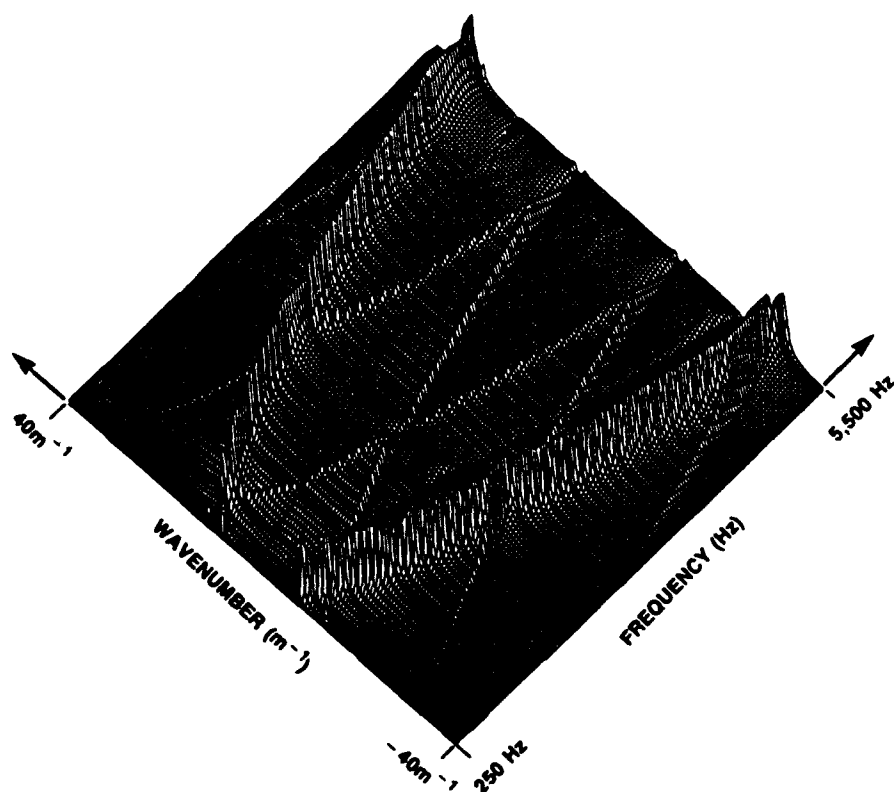
Figure 2.8. Normalized magnitude of the ALTERNATE plate wavenumber
response versus frequency and wavenumber.

Again, Figure 2.9, Figure 2.10, and Figure 2.11 are slices through the magnitude
of the normalized wavenumber response of the ALTERNATE plate given in Figure 2.8, at
excitation frequencies of 500 Hertz, 1000 Hertz, and 2000 Hertz. The location of the
spectral peaks and spectral nulls change with frequency, and not surprisingly, with
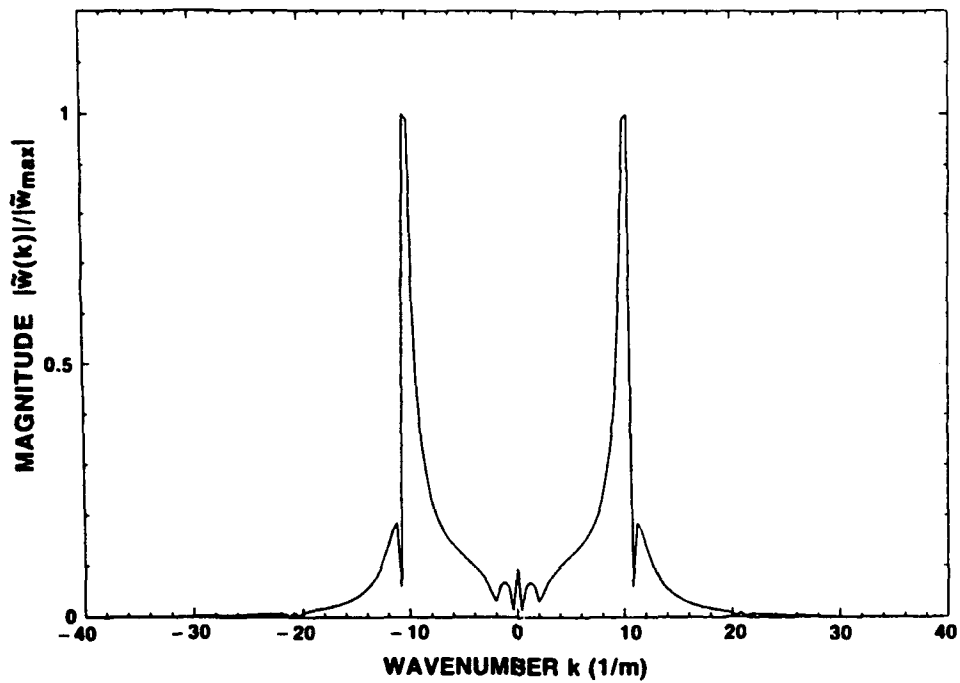stiffener geometry.
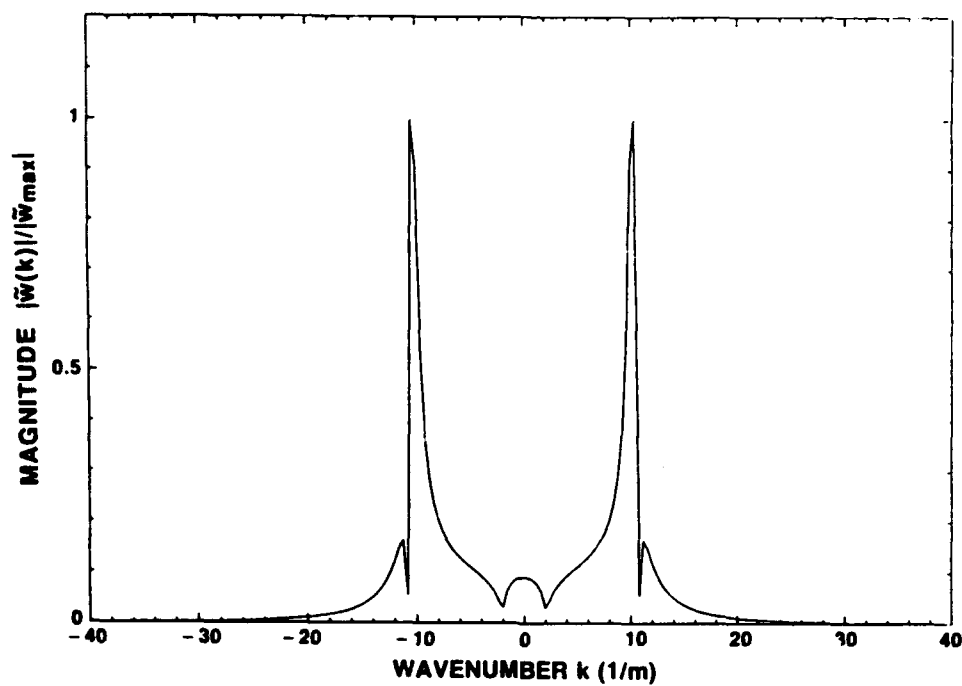
Figure 2.9. Normalized magnitude response of the ALTERNATE plate for a fixed frequency of 500 Hertz.
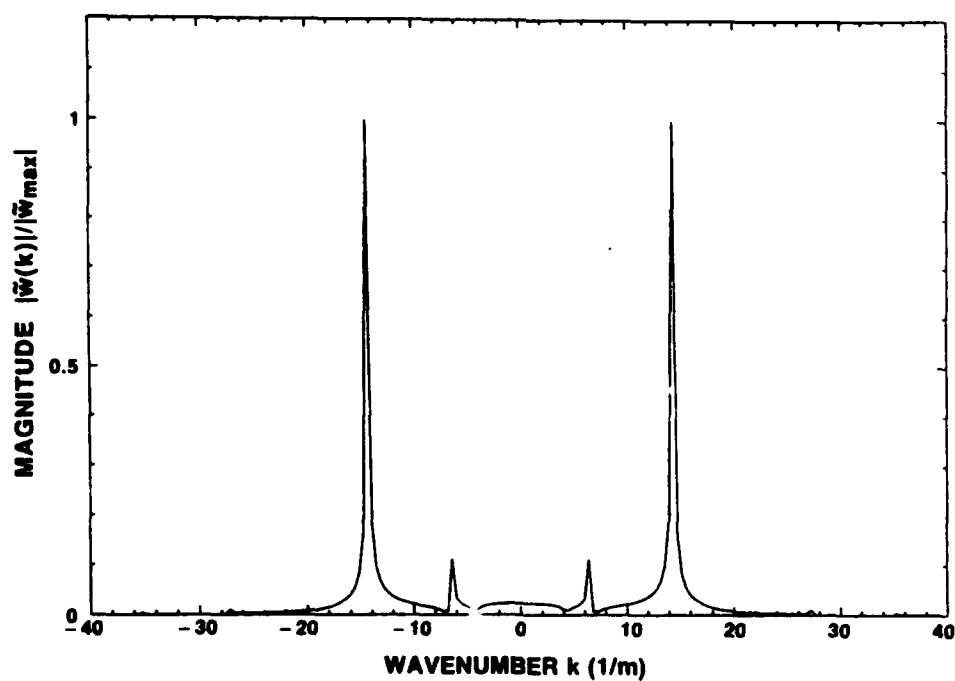
Figure 2.10. Normalized magnitude response of the ALTERNATE plate for a fixed frequency of 1000 Hertz.
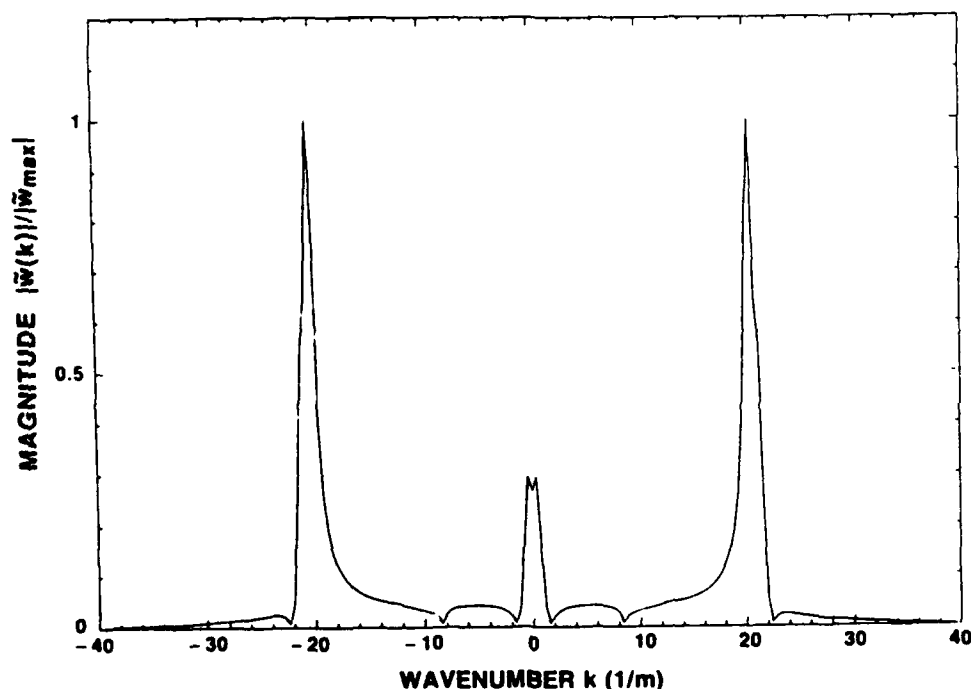
Figure 2.11. Normalized magnitude response of the ALTERNATE plate for a
fixed frequency of 2000 Hertz.

The wavenumber frequency patterns shown in Figure 2.4 and Figure 2.8 are able to

be described by mathematically investigating equation (2.27). The location of the nulls in

the magnitude of the spectral response, as well as the wavenumber location of the relative

maximas shown, can be easily determined.

2.4.2 Effect of Stiffeners on the Flexural Wavenumber

Before discerning the wavenumber frequency pattern, another issue will be briefly

discussed. Figure 2.12 compares the normalized magnitude of the spectral response of the

BASELINE configuration with the UNRIBBED configuration for a *fixed* wavenumber of

6.0 m^{-1} and a swept excitation frequency range between 100 Hertz and 400 Hertz. The

solid line represents the UNRIBBED fluid-loaded magnitude of the wavenumber response

and the dashed line denotes the BASELINE's response.

Not surprisingly, the additional mass of the rib stiffeners causes the unstiffened

free-bending wavenumber to shift downward in frequency, which is shown in Figure

2.12. Hence, two independent effects should be noted that change the flexural wave-
number: First, fluid loading changes the free-bending wavenumber; second, the additional
mass of the rib stiffeners alters the bending wavenumber.
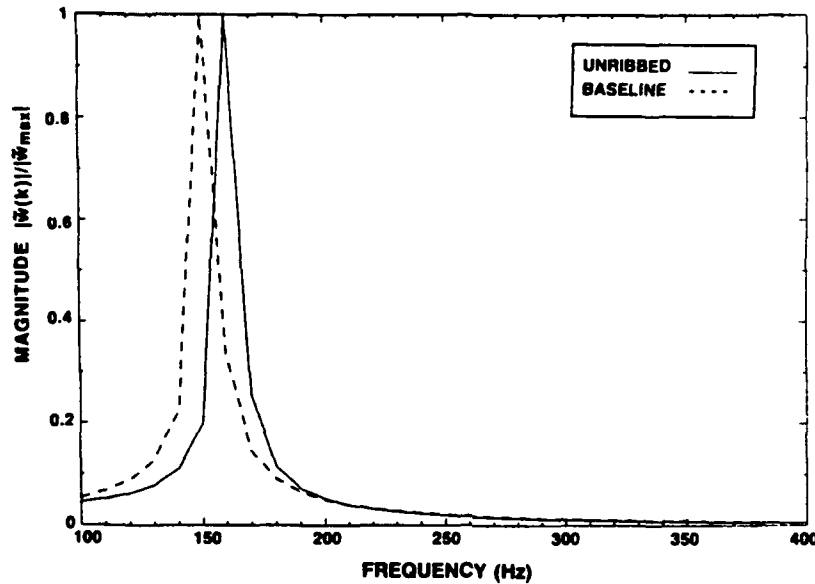
Figure 2.12. Comparison of the normalized magnitude of the BASELINE and the
UNRIBBED plate frequency response for a fixed wavenumber of 6.0 m^{-1}.

The downward shift in frequency can be predicted mathematically by careful

consideration of equation (2.27).This consideration leads to the type of analysis necessary

to explain the curves of constant zero spectral response seen in Figure 2.4 and Figure 2.8.

Recall that the applied line force is acting at the plate's origin, $x_0 = 0$. The following

analysis is only valid for a point of application of the line force such that the exponential

term, e^{-ikx_0}, is unity.

For reference, equation (2.27) is repeated below

$$\tilde{w}(k) = F(k) - \frac{Y(k)K_1F_0(k)}{1+K_1Y_0(k)} . \tag{2.27}$$

From the requirement that the line force acts at the origin of the plate, equation (2.27) simplifies, since $F_0(k) = F_0 Y_0(k)$, as

$$\widetilde{w}(k) = \frac{F_0}{S(k)} \left\{ \frac{1}{1+K_1 Y_0(k)} \right\} . \tag{2.28}$$

Expanding a few terms of the summation $Y_0(k)$, shown above in equation (2.28), about the origin yields

$$\widetilde{w}(k) = \frac{F_0}{S(k)+K_1+K_1 \left\{ ... + \dfrac{S(k)}{S(k-k_l)} + \dfrac{S(k)}{S(k+k_l)} + ... \right\}} . \tag{2.29}$$

The term shown bracketed, which is multiplied by K_1, is much smaller than the other terms in the denominator of equation (2.29) near the zeroth summation value, $n = 0$. The terms $S(k-k_l n)$ and $S(k+k_l n)$ are much greater than $S(k)$, since $S(k)$ is of the order k^4. Hence, their inverse is much smaller and the equation (2.29) will have a maximum when the approximated denominator goes to zero, $S(k) + K_1 \rightarrow 0$.

For simplification, at this point, it will be assumed that the stiffened plate is unloaded and has zero structural damping. For the present geometery and material properties, this simplification does not trivialize the analysis, since the loss factor is small and fluid-loading changes the unloaded flexural wavenumber only slightly.

Substituting the expression for $S(k)$ and K_1 into the above yields

$$D(k^4-k_b^4) - \frac{m'_1 \omega^2}{\mathit{l}} = 0.0. \tag{2.30}$$

Equation (2.30) can be rewritten by substituting in the definition of the *in vacuo* free wavenumber k_b. The resulting equation may then be solved for the wavenumber, denoted k'_b, for which equation (2.30) equals zero.

$$k_b'^4 = \left(m + \frac{m'_1}{\mathit{l}} \right) \frac{\omega^2}{D} . \tag{2.31}$$

44

Hence, for a fixed wavenumber, the mass-per-unit length of a rib-stiffener, m_1', lowers the frequency of the traveling bending wave as given below

$$f_b' = \frac{1}{2\pi} \frac{k_b^2}{\sqrt{\frac{m}{D} + (m_1'/D\ell)}} \qquad (2.32)$$

In the remaining work, the flexural wavenumber, unless otherwise stated, will be written as k_{fl}, where it is understood that this wavenumber refers to the fluid-loaded, rib-stiffened plate's wavenumber.

2.4.3 Analysis of the Periodic Wavenumber-Frequency Curves

The family of curves shown in Figure 2.4 for the normalized magnitude of the wavenumber response of the BASELINE design, and Figure 2.8 for the ALTERNATE design will now be considered.

The curves demarcate a locus of zeros in the magnitude of the wavenumber response, one which follows the trace of the positive flexural wavenumber, and the other which follows the negative flexural wavenumber. Equation (2.27) can be written, neglecting fluid loading, as shown below

$$\tilde{w}(k) = \frac{F_0}{S(k)} (1-T(k)) \qquad (2.33)$$

where

$$T(k) = \frac{K_1 Y_0(k)}{1 + K_1 Y_0(k)},$$

$$Y_0(k) = \sum_{n=-\infty}^{\infty} \frac{1}{D\{(k+k_1 n)^4 - k_b^4\}} .$$

Apparently, the magnitude of the spectral response will be zero for values of $T(k)$ equal to unity. Hence, from the definition of $T(k)$, this occurs for values of wavenumber such that $1 + K_1 Y_0(k) \cong K_1 Y_0(k)$.

The above only can be true if $K_1 Y_0(k)$ is very large. Since K_1 is constant for a given frequency and given plate design, it is worthwhile to consider values of wavenumber for which $Y_0(k)$ is large.

Certainly, any value of wavenumber for which the denominator of $Y_0(k)$ approximately goes to zero will cause $Y_0(k)$ to be large. Hence, the values of interest are wavenumbers for which $D\{(k+k_\ell n)^4 - k_b^4\} \to 0$.

The above can be immediately solved for real wavenumbers, which make $Y_0(k)$ large and hence for which $T(k)$ approximately equals unity,

$$k_n = \pm k_b \pm n k_\ell \quad n = 1,2,3,\dots \tag{2.34}$$

Notice that the index above begins with one, not zero, as a careful review of the previous section indicates that $n = 0$ does not lead to a wavenumber root for which the magnitude of the periodically rib-stiffened spectral response goes to zero.

Remember that wavenumber values which are greater, in absolute value, than the free flexural wavenumber, yield spectral components which rapidly decay with wavenumber. Therefore, of most interest, is a subset of roots given by equation (2.34), namely

$$k_j = k_b - j k_\ell \qquad j = 1,2,3,\dots, J \tag{2.35a}$$

$$k_j = -k_b + j k_\ell \qquad J \leq INT\left\{\frac{|k_b|}{k_\ell}\right\}. \tag{2.35b}$$

Equations (2.35a,b) are significant relationships which may be verified by considering the locus of zeros in the magnitude of the BASELINE response and the ALTERNATE response in Figure 2.4 and Figure 2.8, respectively.

The wavenumber associated with the periodic spacing, k_ℓ, is fixed and depends only on the inter-rib spacing, ℓ. It is independent of frequency. Hence, equations (2.35a,b) are simple translations of the dispersion curve defined by k_b. Equation (2.35a) yields the

wavenumbers that give the curves that proceed from the positive flexural wavenumber; equation (2.35b) gives the curves that lead away from the negative flexural wavenumber.

The ALTERNATE configuration has a periodic rib spacing half the size of the BASELINE configuration, which means the wavenumber associated with the periodic spacing, k_t, of the ALTERNATE design is twice as large as the BASELINE's value. Therefore, as indicated by equations (2.35a,b), the wavenumber distance separating the curves of constant zero spectral response in Figure 2.8, the ALTERNATE design, are twice that of the distance shown in the BASELINE design.

Also seen in Figure 2.4 and Figure 2.8 are local maxima which lie very close to, and follow the shape of, the curves which define zero spectral response. The location of the relative maxima may be predicted by returning to equation (2.27), which for convenience is written below

$$w(k) = \frac{F_0}{S(k)} \left\{ \frac{1}{1 + K_1 Y_0(k)} \right\} . \tag{2.27}$$

Proceeding in the manner just discussed, the wavenumber values of interest, where equation (2.27) will have maxima, are those wavenumbers for which the bracketed denominator goes to zero, $1 + K_1 Y_0(k) \to 0$.

For any given summation index, say $n = m$, a wavenumber may be found which, at that summation index m, produces a relative maximum in equation (2.27). Other values for the summation index will be much smaller than the summation term involving m. Therefore, we can determine, at a fixed index, the approximated wavenumber response which produces a relative maximum

$$\tilde{w}(k) \cong \frac{F_0}{S(k)} \left\{ \frac{S(k - mk_t)}{K_1 + S(k - mk_t)} \right\} . \tag{2.36}$$

near $n = m$.

From the above expression, it is easily shown that the magnitude of the spectral response, $\tilde{w}(k)$, will be large for values of wavenumber such that $S(k-mk_\ell)+K_1 \to 0$.

Substituting in the definition of $S(k)$ and K_1, the following relationship is found

$$(k-mk_\ell)^4 - k_b^4 - k_r^4 = 0 \tag{2.37}$$

where $k_r^4 = \dfrac{(m'/\ell)\omega^2}{D}$ is defined as the *in vacuo* stiffener wavenumber.

Hence, in the wavenumber region of most interest, the wavenumbers at which the magnitude of the periodically rib-stiffened plate's spectral response achieves maxima, are given by

$$k_j = \left(k_b^4 + k_r^4\right)^{1/4} - jk_\ell \qquad j = 1,2,3, ..., J \tag{2.38a}$$

$$k_j = -\left(k_b^4 + k_r^4\right)^{1/4} + jk_\ell \qquad J \le INT\left\{\dfrac{|k_b|}{k_\ell}\right\}. \tag{2.38b}$$

Note, for the particular geometry and material chosen for this investigation, as given in Table 1.1, k_b is much greater than k_r. Therefore, as shown in Figure 2.4 and Figure 2.8, for the BASELINE and ALTERNATE configuration respectively, the relative maximum in the spectral response is located quite near the curve defining minimum response. In other applications, however, the relative maximum and minimum spectral response may be widely separated.

The frequencies at which the wavenumbers given by equation (2.35a) intersect with those of equation (2.35b) are particularly interesting, as are the frequencies where equation (2.38a) and equation (2.38b) intersect. In the latter case, Figure 2.4 and Figure 2.8 show a blending together of two relative maximas into a substantial peak at these intersections.

Consider equation (2.35a) intersecting with equation (2.35b), which means

$$k_b - jk_\ell = -k_b + ik_\ell \qquad \begin{aligned} j &= 1,2,3, ..., J \\ i &= 1,2,3, ..., I. \end{aligned}$$

By substituting in the value for the bending wavenumber, k_b, and squaring both sides, then solving for the angular frequency, the following expression is obtained

$$\omega = \frac{(j+i)^2}{r} \, k_\ell^2 \, \left(\frac{D}{m}\right)^{1/2} . \tag{2.39}$$

Substituting the value for the periodic wavenumber, k_ℓ, and noting $p = i + j$, yields

$$\omega_p = (p\pi)^2 \sqrt{\frac{D}{m \, \ell^4}} \qquad\qquad \begin{array}{l} p = 2,3,4, ..., P \\ P \le J + I. \end{array} \tag{2.40}$$

The summation index, p, begins at 2 simply because the region of wavenumber interest has been restricted to spectral components less than, in absolute value, the flexural wavenumber.

The angular frequency given by equation (2.40) is precisely the classical value for the resonant frequencies of a simply-supported strip plate as given in Mierovitch (1967).

In an identical manner, the frequencies for which equation (2.38a) intersects with equation (2.38b), which produces large spectral peaks within the wavenumber region of interest, are

$$\omega_p = (p\pi)^2 \sqrt{\frac{D}{\ell^4(m+(m_1'/\ell))}} \qquad\qquad \begin{array}{l} p = 2,3,4, ..., P \\ P \le J + I. \end{array} \tag{2.41}$$

Again, the form of the above equation is the same as that given by classical resonant frequency analysis of a simply-supported plate with the additional inclusion of the mass of a single rib stiffener.

2.4.4 Verification of Wavenumber-Frequency Relationships

In the following section, the wavenumber equations just developed, equations (2.35a,b) and equations (2.38a,b), are verified by considering *light* (AIR) fluid loading on the BASELINE configuration at fixed frequencies over the the wavenumber range -40 m^{-1}

to 40 m^{-1}. The first frequency chosen will be that given by equation (2.40) for p = 2 and the remaining frequencies will be between and up to the final frequency given at p = 3.

Figure 2.13 is the normalized magnitude of the wavenumber spectrum, for light fluid-loading, at a frequency of 2,653 Hertz. The reader will recall that this is one of the frequencies at which equation (2.35a) intersects with equation (2.35b). The value of the periodic wavenumber, k$_4$, is 10.4 m^{-1} and the absolute value of the flexural wavenumber, k$_b$, is 20. m^{-1}. Applying equations (2.35a,b), it is seen that the zeros in the magnitude of the wavenumber response are located as predicted. Figure 2.13 illustrates a flat spectral response between wavenumbers -10.0 m^{-1} and 10.0 m^{-1}, except for the well-defined null at zero wavenumber. Reviewing Figure 2.13 through Figure 2.18, it is seen that this even pattern again occurs at the next frequency defined by equation (2.40); that is, p = 3. A careful look at Figure 2.4 suggests this behavior, where it is shown that the spectra are flat and even, except for nulls, at the frequencies at which zero-magnitude curves cross.

Increasing frequency from the initial value, 2,653 Hertz, to 2750 Hertz, as shown in Figure 2.14, causes ridges to develop on either side of a given null boundary. As frequency continues to increase, from 2750 Hertz to 3400 Hertz, as given in Figure 2.15, the ridges increase in height.

At a frequency of 3650 Hertz, shown in Figure 2.16, which is the p = 2 value determined by equation (2.41), the ridges are seen to merge into large, evenly spaced, spectral peaks. Note well that the peaks lying in the region defined by wavenumbers that are less, in absolute value, than the acoustic wavenumber, become strong radiators of sound. At 3,650 Hertz, the acoustic wavenumber is 15.3 m^{-1}; therefore, the spectral peaks at approximately ±5.0 m^{-1} become efficient far-field sound generators.

Figure 2.17 illustrates the magnitude of the wavenumber response at an excitation frequency of 4,000 Hertz. The relative spectral maximas are seen to be significantly reduced from those shown in Figure 2.16. The spectrum is also seen to be evening out to a pattern similiar to that given in Figure 2.13.

Figure 2.13. Normalized magnitude response of the BASELINE plate for
light fluid-loading (AIR) at the fixed frequency of 2653 Hertz.

Figure 2.14. Normalized magnitude response of the BASELINE plate for
light fluid-loading (AIR) at the fixed frequency of 2750 Hertz.

Figure 2.15. Normalized magnitude response of the BASELINE plate for light fluid-loading (AIR) at the fixed frequency of 3400 Hertz.

Figure 2.16. Normalized magnitude response of the BASELINE plate for light fluid-loading (AIR) at the fixed frequency of 3650 Hertz.
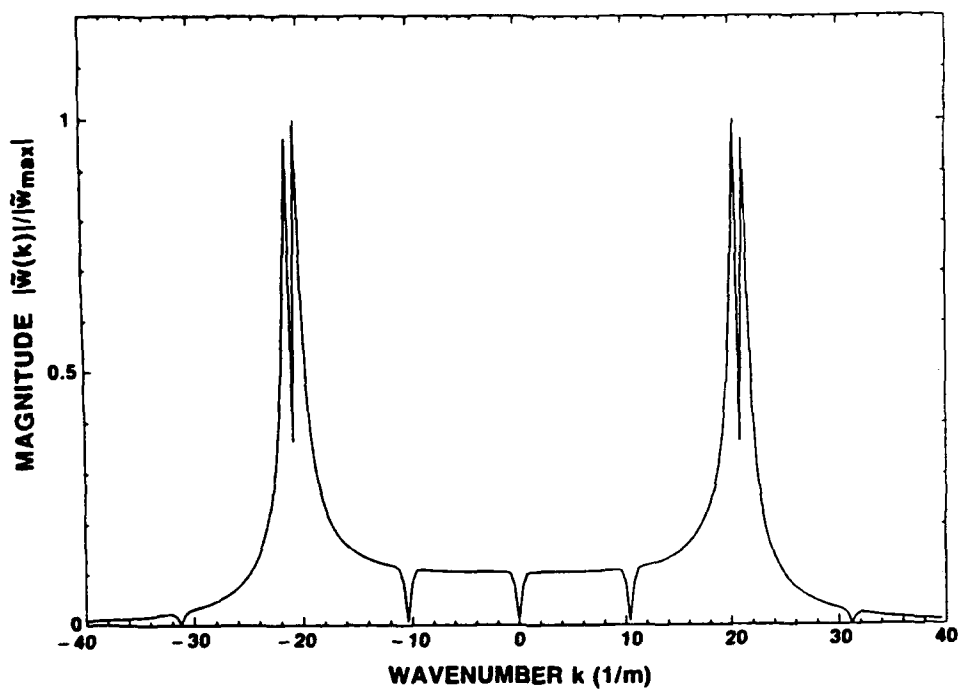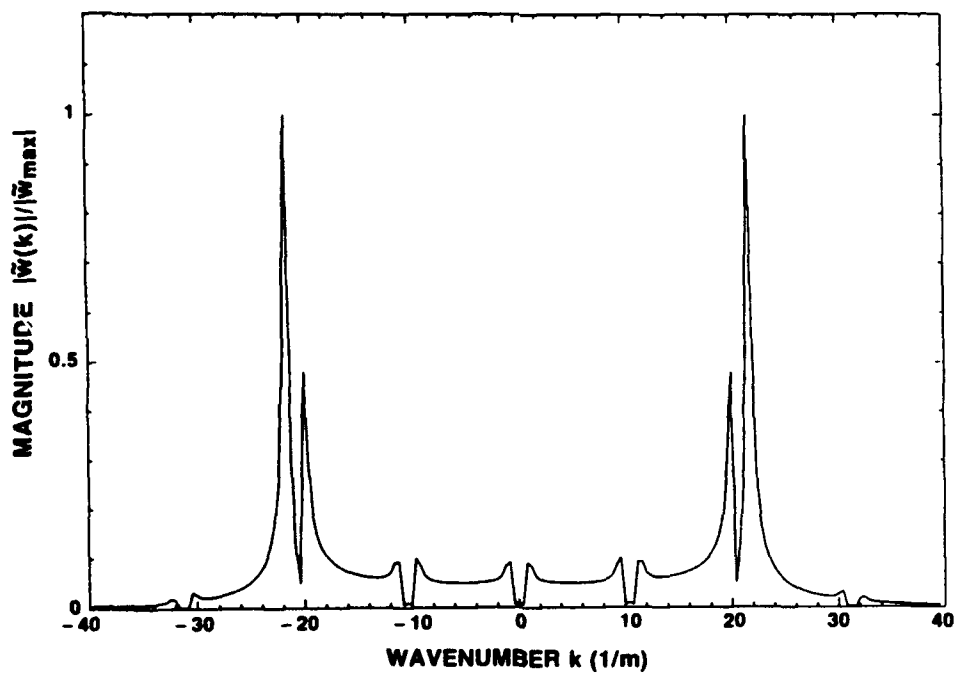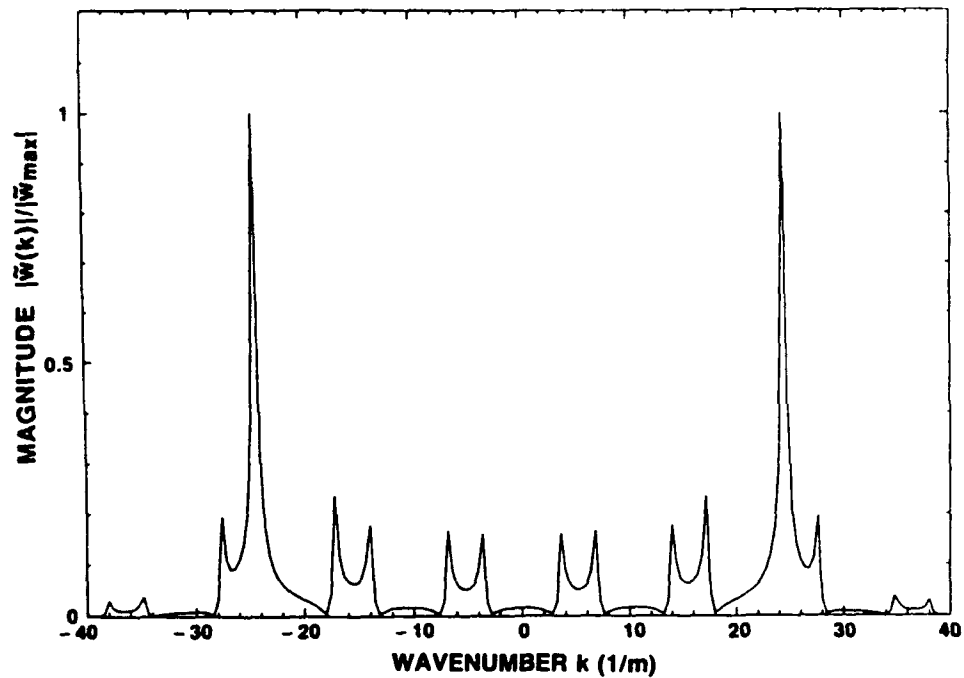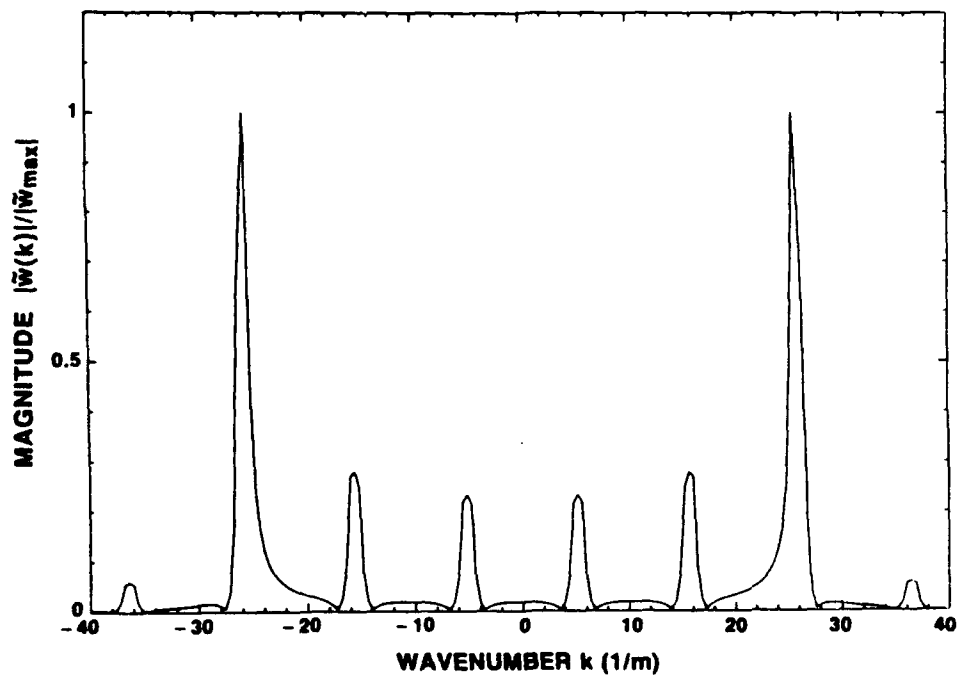
52
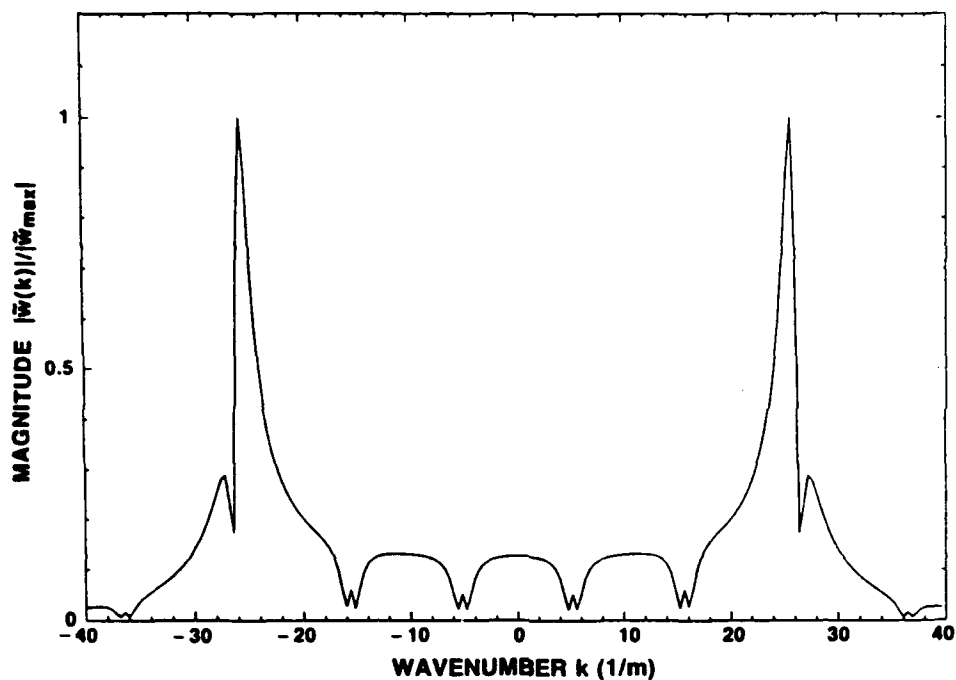
Figure 2.17. Normalized magnitude response of the BASELINE plate for light fluid-loading (AIR) at the fixed frequency of 4000 Hertz.
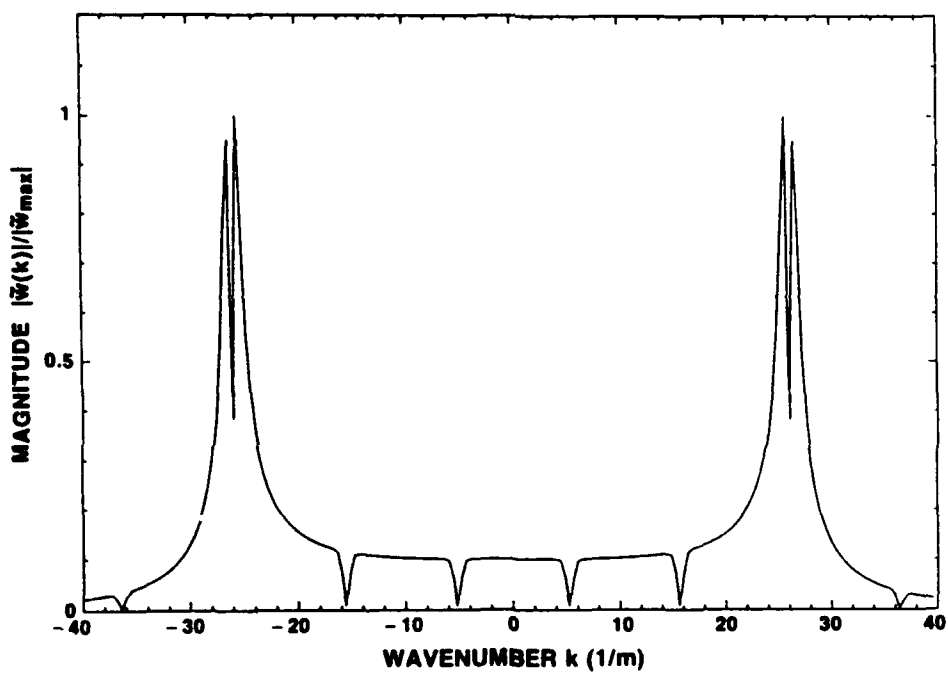
Figure 2.18. Normalized magnitude response of the BASELINE plate for light luid-loading (AIR) at the fixed frequency of 4146 Hertz.

The frequency determined from the value p = 3 by equation (2.40) is 4146 Hertz, and the wavenumber response at this frequency is shown in Figure 2.18. The spectrum shown is similiar to that of Figure 2.13, although an additional null is seen and the location of the nulls has changed since the flexural wavenumber has increased.

Both Figure 2.13 and Figure 2.18 illustrate spectral nulls which happen to be close to the flexural wavenumber. In essence, these nulls appear to split the large spectrum response at the bending wavenumber into two relatively large components which are close together in wavenumber.

This effect suggests that the forced vibration response of a periodically stiffened plate, at certain frequencies, may be governed by two wavenumber components, which are close together, rather than a single component at the flexural wavenumber.

A spatial *beating* phenomenon may therefore be present. The beat wavelength will be the difference of the two wavelengths determined by the two large spectral components. The phenomenon has been discussed jointly with Keltie (1991), and Keltie investigated in detail the effect of the beating phenomenon on the structural response of a finite rib-stiffened flat plate.

2.4.5 Non-Periodic Wavenumber-Frequency Figures

Figure 2.19 and Figure 2.20, which are similar to Figure 2.4 and Figure 2.8 respectively, show the effect of introducing a small change in offset such that periodicity is removed. A 10% shift in the offset has been introduced. Figure 2.19 illustrates the *10% shifted* BASELINE normalized magnitude response, and Figure 2.20 shows the *10% shifted* ALTERNATE configuration's response.

Immediately noticeable is the disruption of the well-defined pattern in the magnitude of the spectral response which was seen in the periodic configurations illustrated in Figure 2.4 and Figure 2.8. The curves that trace out the wavenumbers—defined by equations (2.35a,b) and equations (2.38a,b)—are no longer valid. It is seen in Figure

2.19, for the *10% shifted* BASELINE design, additional curves of zero spectral response are present. Similiarly Figure 2.20, the *10% shifted* ALTERNATE configuration, has additional curves over those shown in Figure 2.8.
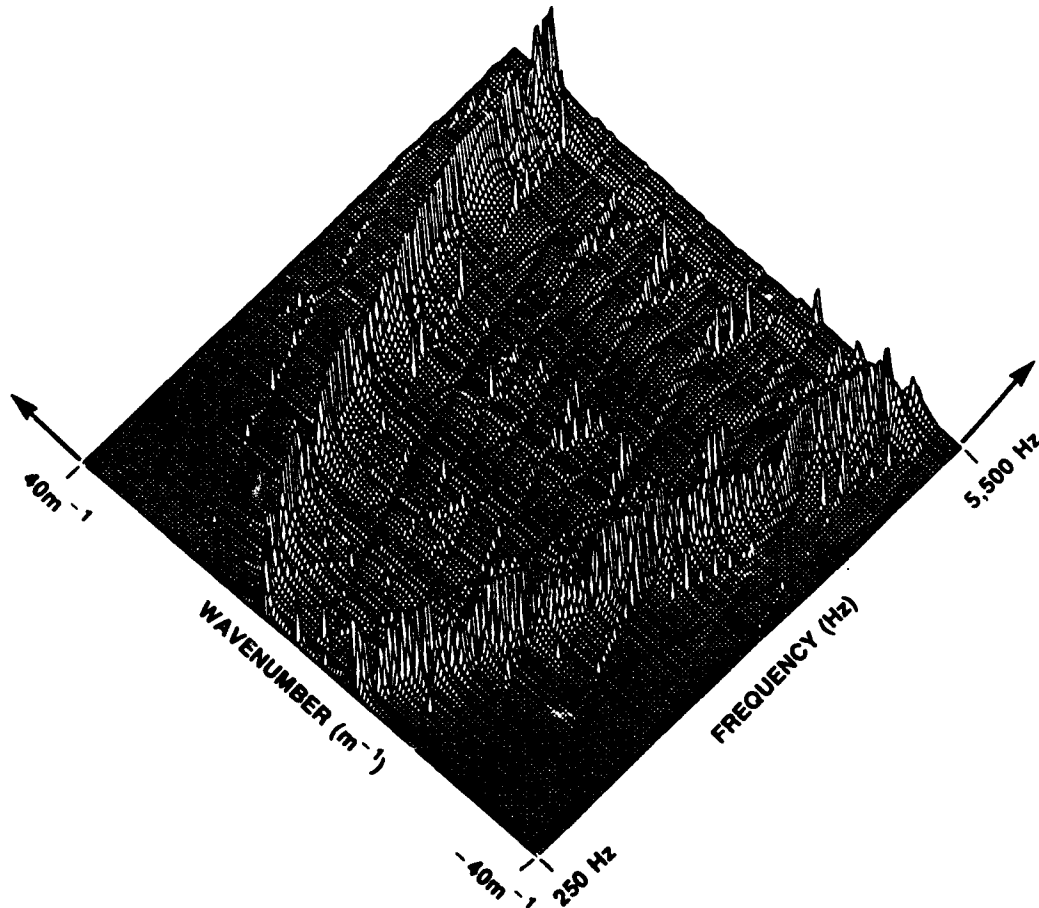
Figure 2.19. Normalized magnitude of the *10% shifted* BASELINE plate
wavenumber response versus frequency and wavenumber.
The offset distance here is $\Delta = 1.1$ $(\ell/2)$.

It is also seen in both figures that many more nulls in the magnitude of the wavenumber response disrupt the flexural wavenumber response.
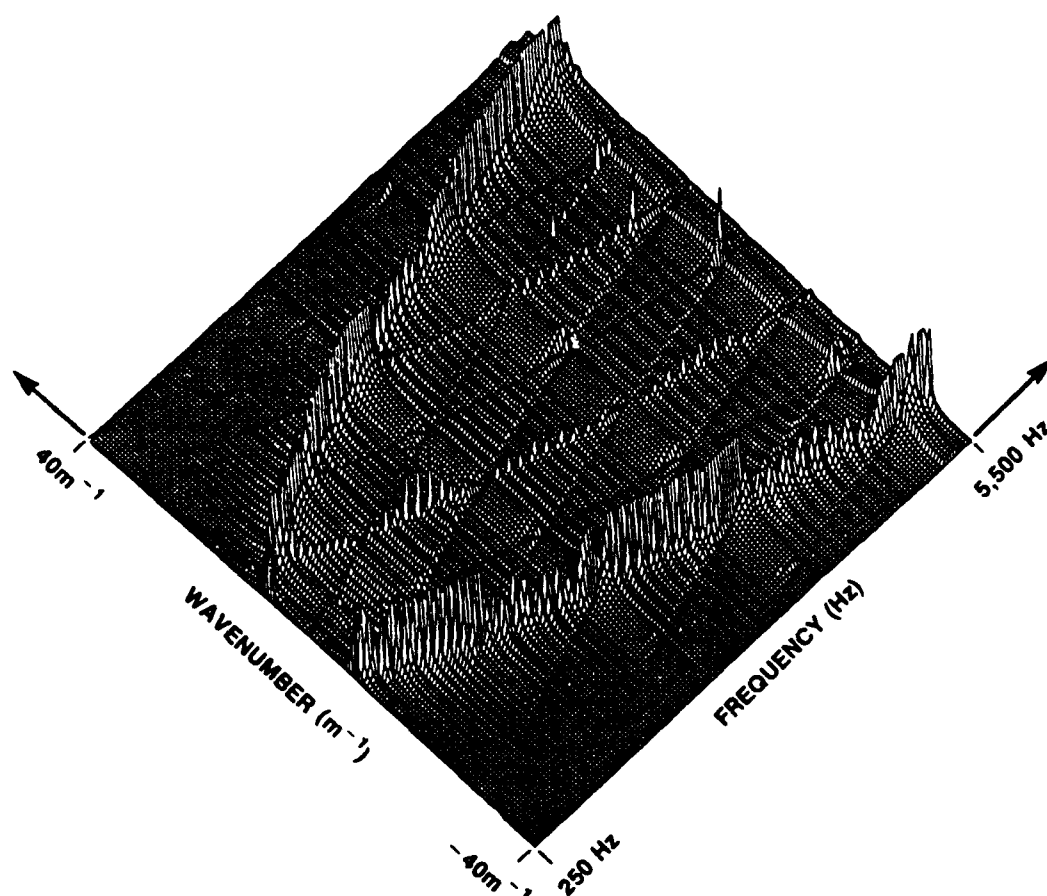
Figure 2.20. Normalized magnitude of the *10% shifted* ALTERNATE plate
wavenumber response versus frequency and wavenumber.

At this point, a caveat needs to be mentioned in the interpretation of the spurious

spikes in magnitude seen throughout the wavenumber-frequency spectrum in both Figure

2.19 and Figure 2.20.

Care was taken in programming equation (2.26), the general wavenumber

response, to ensure the summation terms converged. The summations are complex-valued

functions, and both the real and imaginary parts were required to converge within a

tolerance of $\varepsilon = 10^{-8}$. Further, the convergence was checked for five terms beyond the

initial term which converged. Even with these precautions, for Figure 2.19 and Figure 2.20

only, certain wavenumber-frequency combinations did not converge. The values that did

not converge represented a very small percentage of the thousands of values generated to

produce the three-dimensional illustrations.

Since tightening the convergence tolerance criterion slowed the computational

process considerably and increased the programming complexity, the changes were not

incorporated. Convergence never became a problem in any of the other numerical results

used within this investigation. However, the spurious spikes may be due to numerical

errors.

2.4.6 Qualitative Analysis of the Non-Periodic Wavenumber-Frequency Curves

An interpretation of the additional curves tracing out wavenumbers which give zero

wavenumber response, shown in Figure 2.19 and 2.20, as being definable in terms of the

fundamental spacing variables, such as ℓ, Δ, $\ell-\Delta$, does not seem valid. No equations

similiar to those given by equations (3.35a,b) and equations (3.38a,b) were derived. Recall

that the general wavenumber response, for only two sets of rib stiffeners, equation (2.26),

is considerably less tidy than the periodic response, equation (2.27). Equation (2.26) does

not lend itself well to the type of analysis which was performed on the periodic

wavenumber response, equation (2.27).

The effect of non-periodic spacing between the rib stiffeners may be analyzed

qualitatively, though, and Figures 2.19 through Figure 2.22 are meant to do so.

Figure 2.21 and Figure 2.22 illustrate the normalized magnitude of the wavenumber

response for the *10% shifted* BASELINE configuration which is 'lightly' fluid-loaded at

frequencies of 2653 Hertz and 4000 Hertz respectively. These figures may be compared to

Figure 2.13 and Figure 2.17 to indicate the effect that the change in offset has on the

BASELINE configuration spectral response.

Notice in Figure 2.21 and Figure 2.22 that the spectral response is no longer

symmetric in wavenumber about the origin. In Figure 2.21, the spectral response

associated with the positive flexural wavenumber, k_b, has dramatically been reduced from the new offset, relative to the response seen in the unshifted periodic response. Neither figure shows the behavior seen in the periodic configurations where a null apparently split the flexural wavenumber components.

The additional nulls seen in Figure 2.21 and Figure 2.22 appear to be evenly spaced in wavenumber, though, as mentioned, no simple wavenumber expressions were developed which predicted the location of these nulls.

The lack of symmetry in the wavenumber response is likely due to the corresponding loss of symmetry of the excitation force with respect to the rib-stiffeners. For the periodic configurations, the line force was applied beneath a stiffener at the plate's origin. Hence, the periodic stiffeners were symmetric about the applied excitation. For the non-periodic configurations, the stiffeners are no longer symmetric about the origin of the plate. A greater shift in offset, for example a *30% shifted* BASELINE configuration, may produce even less symmetry than the symmetry which is suggested in Figure 2.21 and Figure 2.22.

For all of the numerical results presented in this chapter, the effect of changing the cross-sectional area of a given rib-stiffener set, and hence their mass, had negligible effect on the location of spectral nulls and peaks.

With increasing rib mass, the stiffened plate's flexural wavenumber shifts slightly lower. Therefore, the nulls, as given by equations (2.35a,b), which depend upon the plate's flexural wavenumber, also shift slightly. Otherwise, the mass of a set of rib stiffeners affects the magnitude of the spectral components more than the wavenumber location of these components.

58
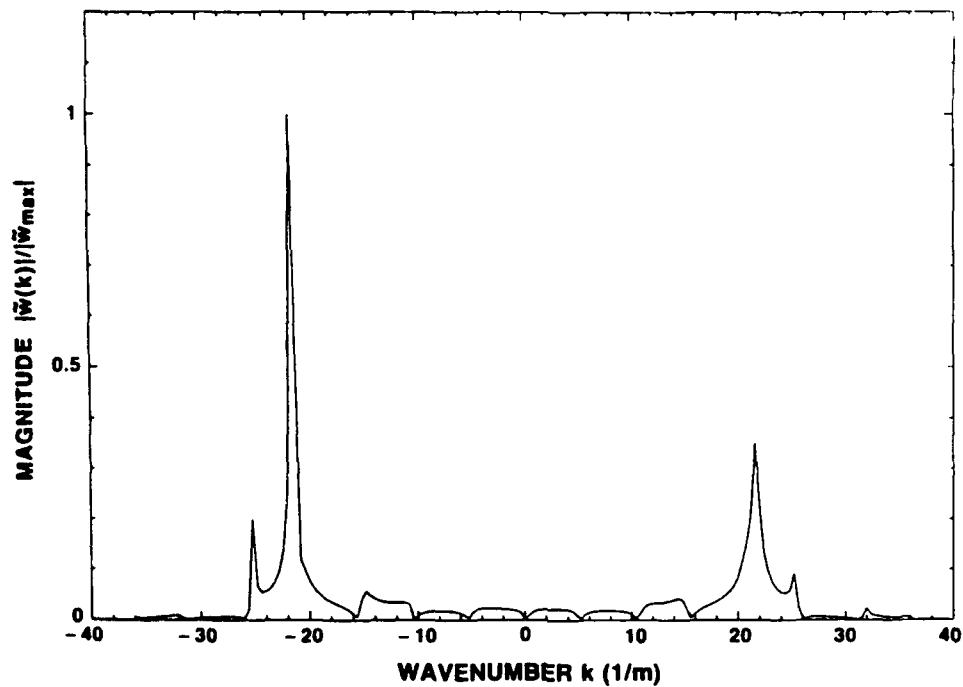
Figure 2.21. Normalized magnitude response of a *10% shifted* BASELINE plate
for a fixed frequency of 2653 Hertz.
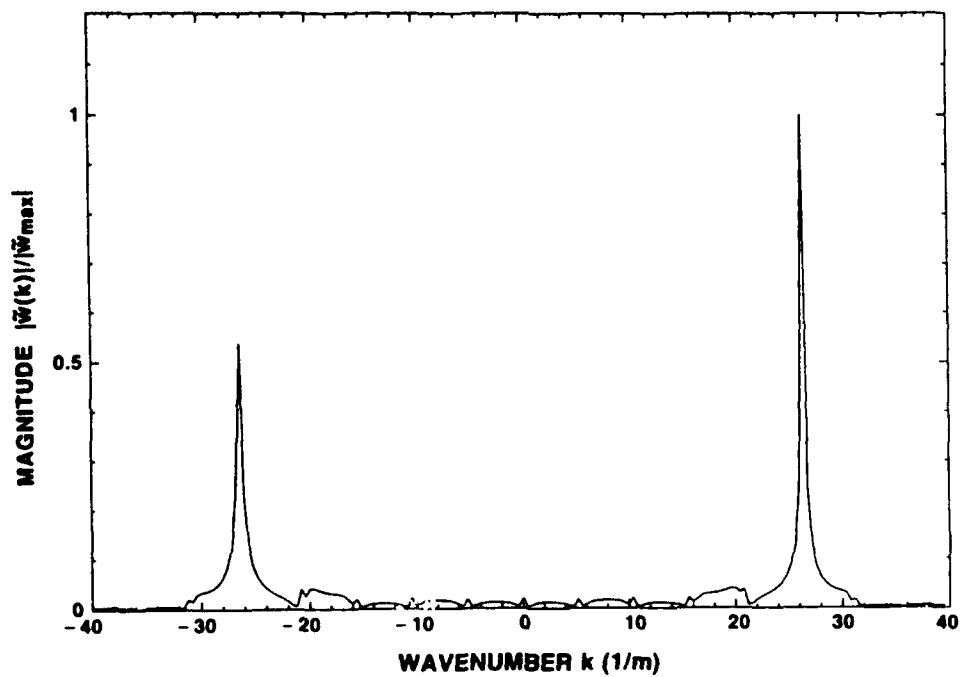
Figure 2.22. Normalized magnitude response of a *10% shifted* BASELINE plate
for a fixed frequency of 4000 Hertz.

3. FAR-FIELD ACOUSTIC RADIATION USING
THE METHOD OF STATIONARY PHASE

The inversion integrals, equations (2.10a,b), which give the radiated pressure

generated by the stiffened plate's surface, may be evaluated in the far-field; that is, for a

large distance away from the surface, using asymptotic expansion techniques. Introducing

a change of variables, from Cartesian into Cylindrical coordinates, it is seen that the integral

is ideally suited for asymptotic expansion by using a stationary phase approximation.

Bender & Orzag (1978) describe the evaluation of real and complex integrals using

asymptotic analysis by means of Laplace's method, the method of stationary phase, and the

method of steepest descents. The reader is referred to their text for a thorough

understanding of the subject; only a brief mathematical synopsis of the method of stationary

phase will be given here.

3.1 METHOD OF STATIONARY PHASE

The application of the method of stationary phase to obtain the far-field radiated

acoustic pressure from both an infinite beam and an infinite plate has been performed by

Junger & Feit (1986), and is well-documented. The formulation given by Junger & Feit is

for an unstiffened plate. However, note that the form of the plate's wavenumber response,

$\tilde{W}(k)$, ribbed or unribbed, is immaterial to the development of the expansion, provided that

the wavenumber response is well behaved at the point of stationary phase. In other words,

the point of stationary phase, denoted $\bar{k}$, is determined independently of the wavenumber

response. Hence, the formulation given by Junger & Feit (1986) is valid for the stiffened

plate and may be followed identically.

For convenience, equation (2.10a) is rewritten below. Note, the integral given by

equation (2.10b) is not in a form which can be expanded by the method of stationary phase

since the exponential argument is not pure imaginary. This is inconsequential since it is assumed the far-field radiation due to the integral given by equation (2.10b) is negligible. The far-field implies a large stand-off distance z, therefore the real-valued exponential term in equation (2.10b) is small.

$$P_a(x,z) = -\frac{1}{2\pi} \int_{|k| \leq k_0} \frac{i\rho_0 \omega^2 \tilde{w}(k)}{\sqrt{k_0^2 - k^2}} \, e^{i\sqrt{k_0^2 - k^2}\, z} \, e^{ikx} dk. \qquad (2.10a)$$

The following expressions are defined to clarify the evaluation of the above integral, equation (2.10a), by the method of stationary phase.

$$f(k) = -\frac{i\rho_0 \omega^2 \tilde{w}(k)}{2\pi \sqrt{k_0^2 - k^2}} \qquad (3.1a)$$

$$\Psi(k) = z\sqrt{k_0^2 - k^2} + kx. \qquad (3.1b)$$

Notice that equation (3.1b) is entirely real-valued for supersonic wavenumbers, which is necessary for the method of stationary phase. A change in variable from Cartesian coordinates (x,z) into polar coordinates (R,θ), is now introduced.

With the change in variables and with the substitution of equations (3.1a,b), the inversion integral becomes

$$P(R,\theta) = \int_{-\infty}^{\infty} f(k) \, e^{iR\Psi(k)} \, dk \qquad (3.2)$$

where $\Psi(k) = \cos(\theta)\sqrt{k_0^2 - k^2} + k \sin \theta$.

For the particular integral given by equation (3.2), the expansion is of second order, since $\frac{d^2\Psi(k)}{dk^2} \neq 0$, thus the asymptotic expansion is given (Bender) as

$$P(R,\theta) \sim \frac{f(\bar{k})\Gamma(\frac{1}{2})}{2} \left[\frac{2!}{R!\Psi''(\bar{k})!} \right]^{1/2} e^{iR\Psi(\bar{k})} \, e^{-i\,\pi/4} \quad R \rightarrow \infty. \tag{3.3}$$

The stationary phase value, $\bar{k}$, occurs when the first derivative of $\Psi(k)$ equals zero. This is the wavenumber for which the integrand is slowly varying over a small range of integration. Over other ranges of integration, the exponential term in the integrand oscillates between positive and negative values rapidly (for large values of R). Therefore, the contribution the integrand has over the latter domain of integration is negligible. The stationary phase value may be shown to be:

$$\bar{k} = k_0 \sin\theta.$$

Substituting the above stationary phase value into equation (3.3) and simplifying, the inversion integral, valid for large values of R and for an applied line force, may be expressed as

$$P(R,\theta) \sim -\frac{\rho_0 \omega^2 \tilde{w}(\bar{k})}{2\sqrt{Rk_0\pi}} \, e^{iRk_0(1+i)}. \tag{3.4}$$

3.2 VERIFICATION OF FAR-FIELD SOLUTION

Mace (1980a) presented results for the on-axis, far-field sound pressure level radiated from a fluid-loaded plate stiffened by identical and periodically spaced rib stiffeners for applied point force excitation. A distance of 1 meter, normal to the plate's surface, was chosen as an reference distance for the evaluation of the far-field pressure. Of course, this distance is strictly a reference value, and does not necessarily represent a valid far-field observation point. The value was chosen simply for convenience.

The methodology and the numerical examples given by Mace (1980a) have been used as a verification of the stiffened plate's wavenumber response, given by equation (2.26), and as a verification of the above asymptotic formula, equation (3.4).

Mace's formulation assumed point force excitation; however, for the particular far-field observation point chosen by Mace for numerical calculations, the point-forced and line-forced wavenumber responses are identical. However, the stationary phase expansions do differ. Therefore, for the comparisons shown in Figure 3.1 and Figure 3.2 only, the line-force expansion given above, equation (3.4), was changed to a point-force expansion, as described in the Appendix.

Figure 3.1 is a comparison of a numerical example given by Mace with the current analysis for the special case of a single set of identical rib-stiffeners. The excitation was a 1kN point force applied halfway between two adjacent ribs. The geometric and material values used to generate Figure 3.1 and Figure 3.2 are given in Mace.

In Figure 3.2, two different sets of rib stiffeners were considered and were positioned such that one set was offset by half the periodic spacing of the other set. In this manner, which corresponds to two bays between adjacent bulkheads in Mace's analysis, the offset, Δ, could be verified.

As can be seen in both figures, the agreement in far-field radiated sound pressure level is exact. Hence, at this point it can be confidently assumed that equation (2.26) and subsequently equation (3.4), are correct expressions for the computation of the far-field acoustic pressure radiated from a fluid-loaded, rib-stiffened plate of infinite extent.

3.3 PERIODIC FAR-FIELD RADIATION

Figure 3.3 compares the far-field sound pressure level radiated from the BASELINE and UNRIBBED plate at a distance of 1.0 meter normal to the plate's surface over the frequency range 100 Hertz to 10,000 Hertz. A line force of 1.0 kN is applied at the origin, $x_0=0$. Throughout this chapter, as well as in Chapter IV, the location and magnitude of the applied line force does not change.
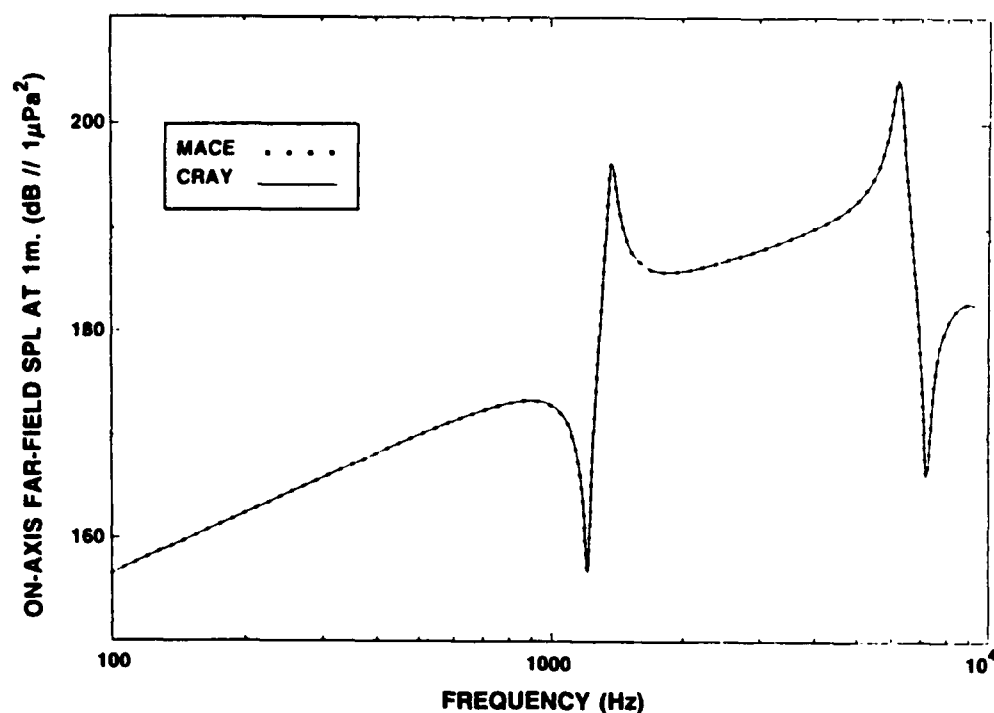
Figure 3.1. Comparison of a numerical result presented by Mace (1980a) with the current analysis for a single set of identical rib-stiffeners. The excitation here is a 1 kN point force applied halfway between two adjacent rib-stiffeners.
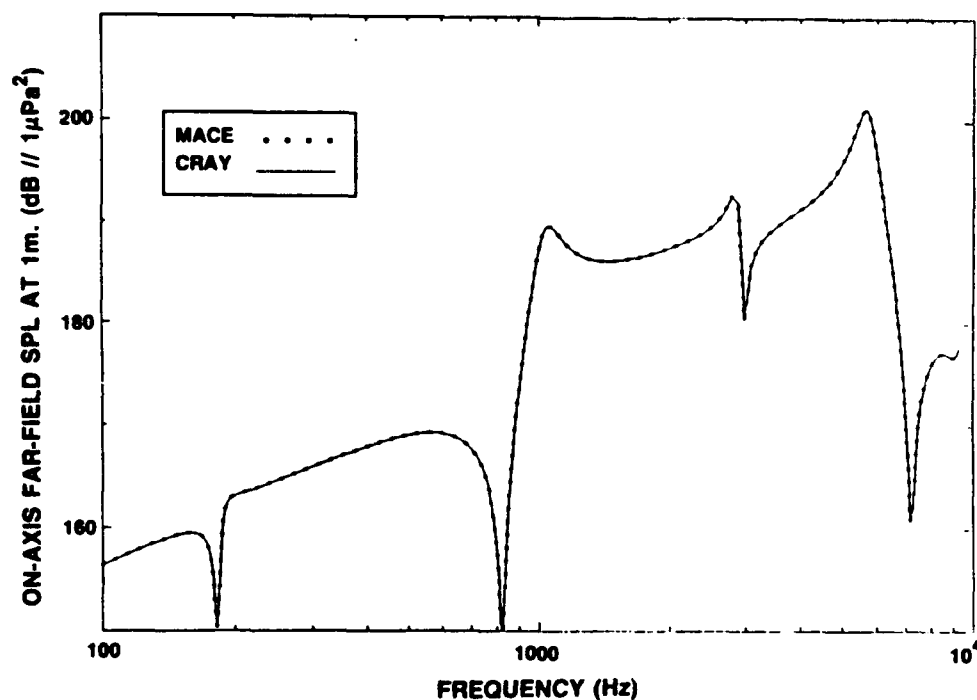

Figure 3.2. Comparison of results generated by the methodology of Mace (1980a) and the current analysis. Two different sets of rib stiffeners are positioned such that one set is offset by half of the periodic spacing of the other set.

Figure 3.3 indicates that the stiffeners have increased the radiated sound at certain frequencies of excitation. Elsewhere, the radiated sound from the ribbed BASELINE plate is *less*, substantially so at certain frequencies, than the UNRIBBED plate. At low frequencies, the sound pressure levels of both plates are equivalent. Before any conclusions may be drawn, however, it must be noted that the results shown in Figure 3.3, and in Figure 3.4, are for a fixed observation point, 1 meter normal to, and directly above, the excitation force. A change in the observation point may cause a dramatic change in the level of the radiated pressure from the BASELINE configuration.

Like Figure 3.3, Figure 3.4 compares the ALTERNATE and UNRIBBED plate radiated sound pressure level. It is seen, below 1000 Hertz, that the rib stiffeners have no apparent effect on the radiated pressure over that of the UNRIBBED plate. Beyond 1,000 Hertz, the trend of the variations of acoustic pressure with frequency is similar to that shown in Figure 3.3, with acoustic peaks followed by nulls.

For convenience, the frequency expressions which give the frequencies for maximum and minimum wavenumber response are written below

$$\omega_p = (p\pi)^2 \sqrt{\frac{D}{m\,\ell^4}} \qquad\qquad (2.40)$$

$$p = 2,3,4, \dots$$

$$\omega_p = (p\pi)^2 \sqrt{\frac{D}{\ell^4(m+(m_1'/\ell))}} \qquad\qquad (2.41)$$

The first four even index frequencies for minimum spectral response for the *light* fluid loaded BASELINE configuration, as given by equation (2.40) above, are 662, 2648, 5958, and 10,592 Hertz. For the maximum response, which is given by equation (2.41), the frequencies are 587, 2348, 5284 and 9395 Hertz. From Figure 3.3, the pressure nulls are located at frequencies 541, 2392, 5392, and 9092 Hertz, and the peaks in acoustic pressure occur at frequencies 467, 2092, 4792, and 8790 Hertz.

Figure 3.3. Comparison of the far-field on axis sound pressure level radiated from the BASELINE and UNRIBBED plate versus frequency at a distance of 1.0 m.

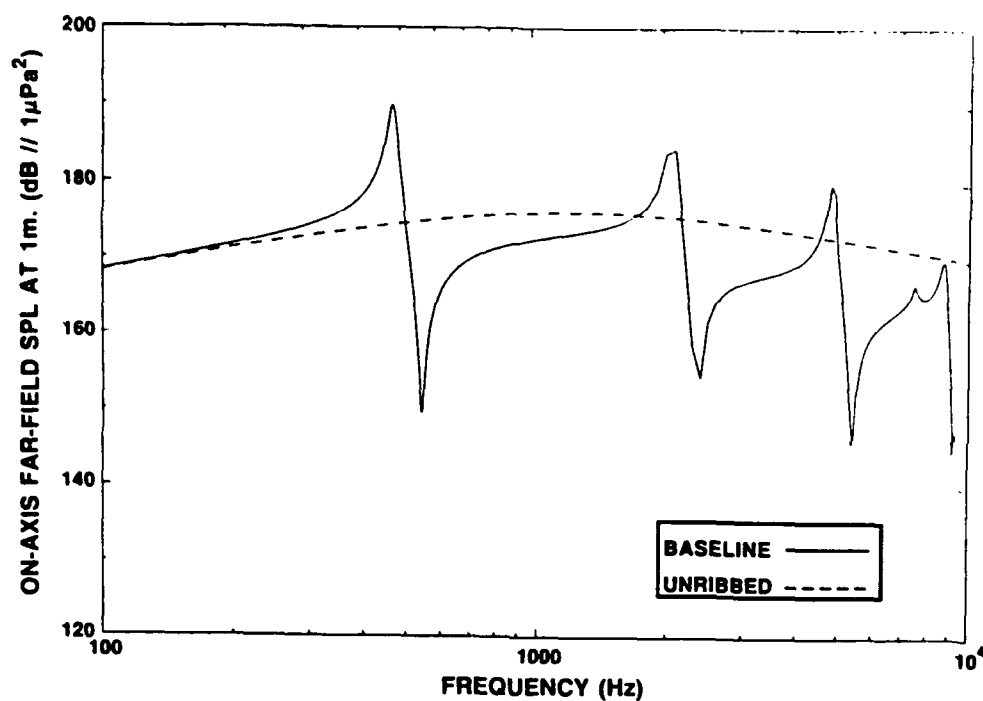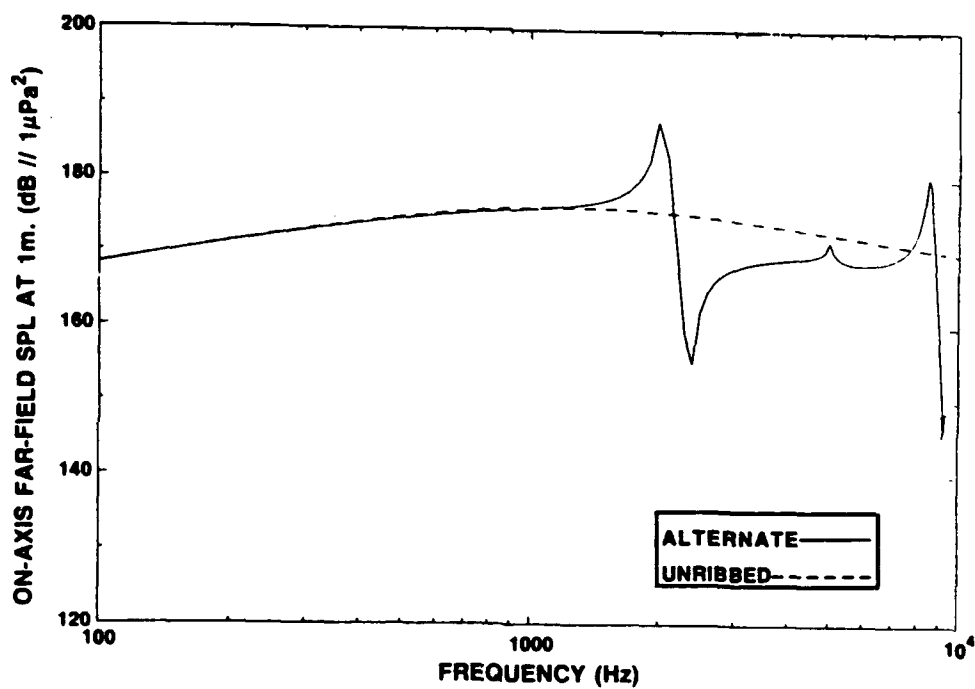
Figure 3.4. Comparison of the far-field on axis sound pressure level radiated from the ALTERNATE and UNRIBBED plate versus frequency at a distance of 1.0 m.

The difference between the frequencies which are predicted by equations (2.40) and (2.41), and those which are actually seen in Figure 3.3, are due to fluid-loading effects. For light fluid-loading (AIR), the frequencies match perfectly. These figures are not shown.

For the ALTERNATE configuration, which has a periodic spacing half that of the BASELINE configuration, equations (2.35) and (2.40) predict that there will be an upward shift in frequency of peak and null locations. The shift will be exactly four times above the location of the peaks and nulls given for the BASELINE plate. Figure 3.4 shows this frequency shift where, below approximately 1,000 Hertz, the radiated pressure from the ALTERNATE configuration differs little from the UNRIBBED sound pressure level.

Figure 3.3 and Figure 3.4 show results strictly for identical and periodically spaced rib stiffeners. The effect on far-field radiation of a change in offset, Δ, such that the stiffeners are no longer periodic, will be investigated in the next section.

3.4 VARIATION OF OFFSET Δ

Figure 3.5 is an illustration which conceptualizes the variation of one rib-stiffener set of offset Δ, along the plate between a fixed set of rib stiffeners positioned with periodic spacing ℓ. For the BASELINE design, the offset varies between $0 \leq \Delta \leq 0.6035$ meters and for the ALTERNATE design the offset varies as $0 \leq \Delta \leq 0.3175$ meters.

In Figure 3.6, the far-field sound pressure level versus changes in offset between fixed rib stiffeners is shown for frequencies of 250 and 500 Hertz. The stand-off distance is 1 meter perpendicular to the plate's surface above the origin. At 250 Hertz, the variation of the sound pressure level with offset is slight, no more than 1 dB. However, at 500 Hertz, large variations in radiated sound pressure level, as much as 20 dB, occur. Notice for all of the figures shown in this section, Figures 3.6 though 3.9, the far-field radiation characteristics are symmetric about an offset which is half the periodic spacing ℓ; that is, $\Delta = \ell/2$.
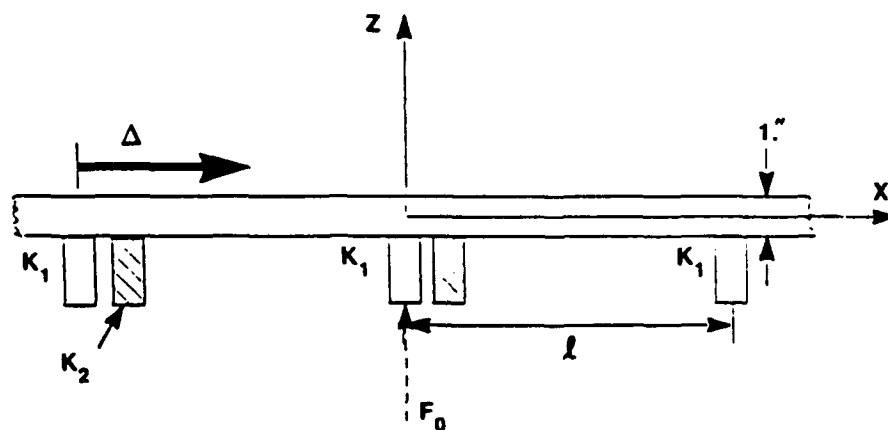
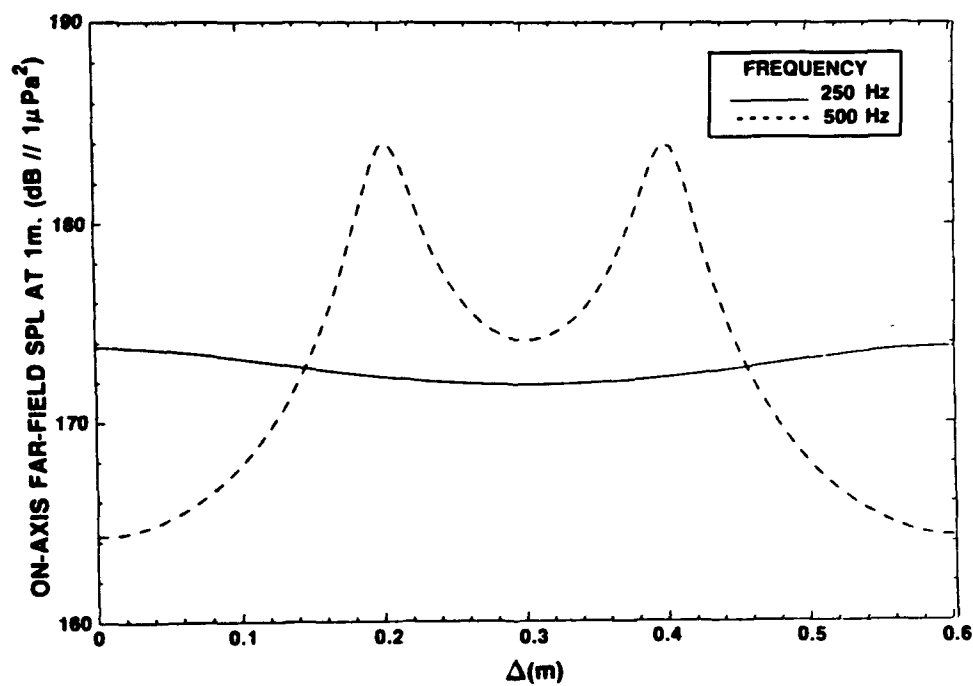Figure 3.5. Illustration showing the variation of offset, Δ, between a fixed set of stiffeners.

Figure 3.6. Far-field sound pressure level for the BASELINE configuration versus change in offset at frequencies 250 and 500 Hertz.

Figure 3.7 presents the far-field sound pressure level of the BASELINE configuration versus change in offset at 1,000 Hertz and at 2,000 Hertz. The overall variation at 1,000 Hertz is greater that that seen at 250 Hertz in Figure 3.6, but is much less than the dramatic change shown at 500 Hertz. At 2,000 Hertz, the BASELINE plates' radiated sound pressure level changes, with variations of approximately 12 dB, a number of times as the offset travels between the fixed set of rib stiffeners.

The far-field sound pressure level for the ALTERNATE design versus change in offset Δ, at frequencies of 250 and 500 Hertz, is given in Figure 3.8. In Figure 3.9, the radiated pressure from the ALTERNATE plate at 1,000 and 2,000 Hertz is shown.

As might be suggested by Figure 3.4, which indicated for frequencies below 1,000 Hertz the ALTERNATE plate behaved acoustically like the UNRIBBED plate, little variation in sound pressure level is seen in Figure 3.8 at 250 Hertz and at 500 Hertz. Even at 1,000 Hertz, the radiated far-field pressure from the ALTERNATE plate, illustrated in Figure 3.9, shows small variation, less than 1 dB, with change in offset. At a frequency of 2,000 Hertz, however, approximately 9 dB variations in the magnitude between maximum and minimum radiated pressure occur as the offset is swept along the plate.

The symmetry of the far-field pressure about the midpoint offset position in the above figures is reasonable. At the midpoint position, the stiffeners have periodic inter-rib spacing. Now consider the geometry of the stiffened plate and the location of the applied force. The stiffeners are symmetric about the applied line force for the variation of the offset between the fixed stiffeners up to the midpoint position and from the midpoint to the subsequent stiffener. Therefore, symmetry of the acoustic response about the midpoint offset position is expected.

The figures further indicate that at certain frequencies of excitation and offset positions, the stiffeners act as strong radiators of sound.
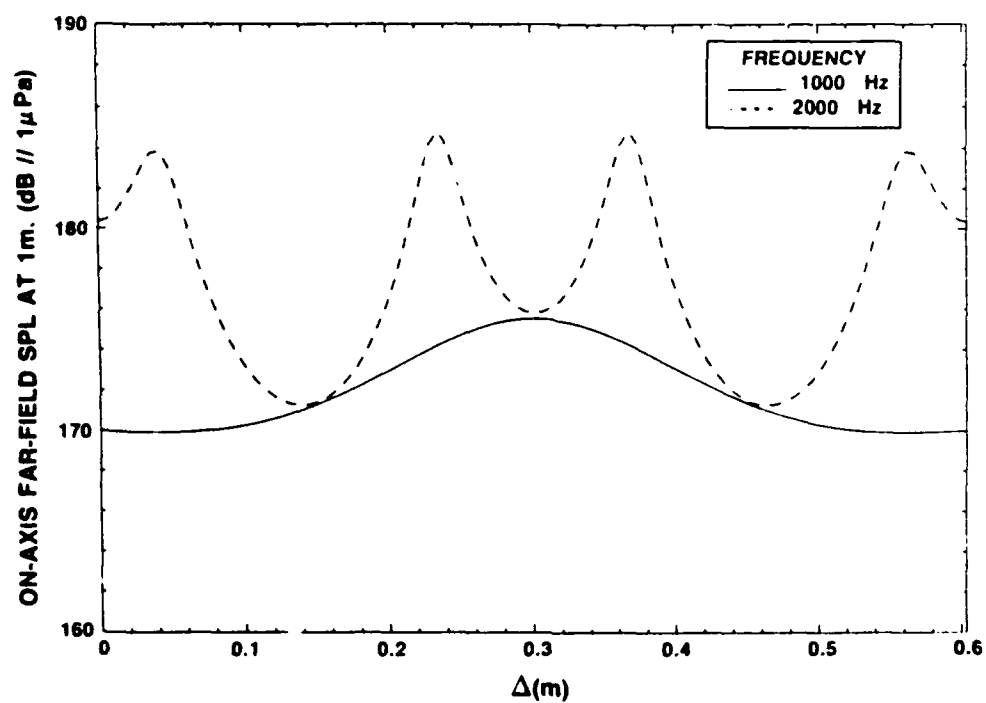
Figure 3.7. Far-field sound pressure level for the BASELINE configuration versus change in offset at frequencies 1000 and 2000 Hertz.
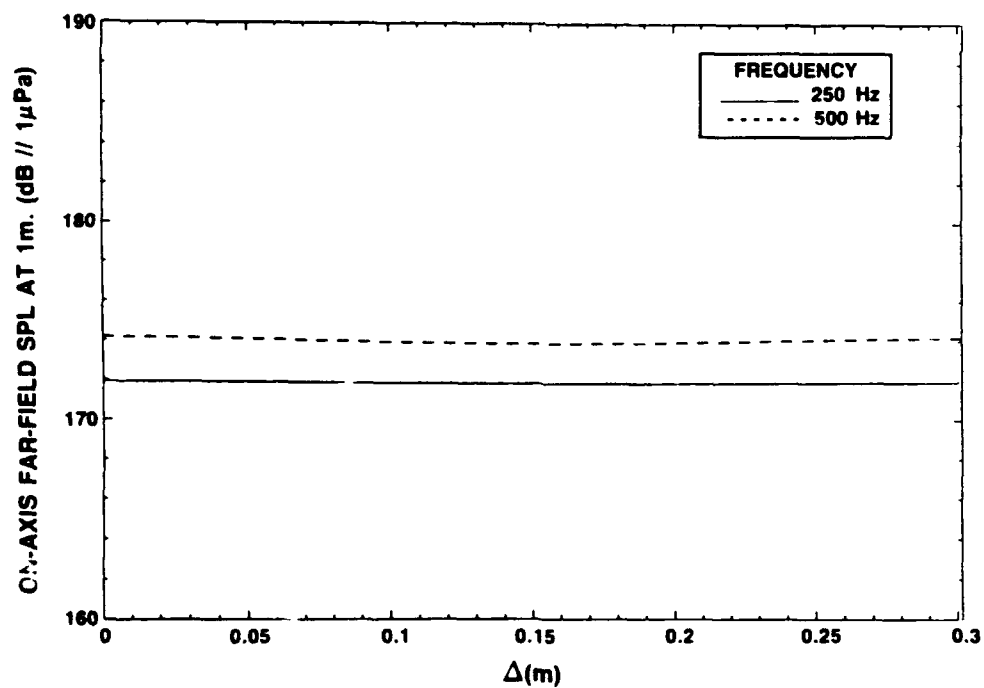
Figure 3.8. Far-field sound pressure level for the ALTERNATE configuration versus change in offset at frequencies 250 and 500 Hertz.
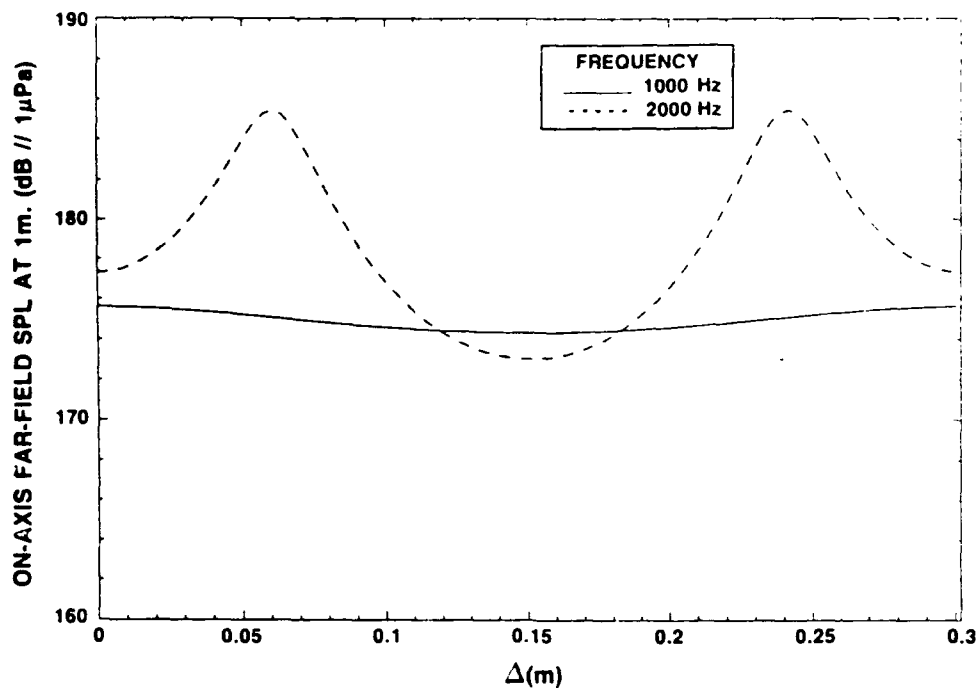
Figure 3.9. Far-field sound pressure level for the ALTERNATE configuration versus change in offset at frequencies 1000 and 2000 Hertz.

3.4.1 Periodic Directional Radiation Patterns

Figure 3.10 thru Figure 3.17, which will conclude the far-field analysis given in this chapter, are directionality patterns which show, in decibels, the difference in far-field sound pressure level of the the BASELINE and ALTERNATE plate configurations, with and without periodic offset, relative to the UNRIBBED plate. The directionality refers to the change in the magnitude of the radiated pressure with variation of polar angle, θ. The angle varies from -89 degrees to 89 degrees at a fixed radial distance, R, of 1 meter. For all of the figures, the applied line force is fixed at the plate's origin.

For the UNRIBBED plate, the radiation pattern is omni-directional, showing no preference for radiation at any angle, for frequencies less than the coincidence frequency. At coincidence, which for the UNRIBBED plate is approximately 9400 Hertz, the radiated

pressure becomes strongly directional, with the well-known result (Cremer) of radiation peaks at ±90 degrees.

Figure 3.10 illustrates the directionality pattern of the BASELINE plate relative to the UNRIBBED plate at a frequency of 250 Hertz. As might be expected, the low frequency radiation characteristics of the BASELINE and UNRIBBED plates are similar. Both configurations radiated pressure equally in all directions at low frequency, with the ribbed BASELINE being only a moderately stronger radiator than the UNRIBBED plate.

At 2,000 Hertz, the directionality pattern shown in Figure 3.11 shows a strong dependence of acoustic radiation on direction. The BASELINE design is no longer omni-directional. Radiation peaks are seen at approximately ±5 degrees; nulls occur at ±10 degrees. Notice, over much of the angular space, the BASELINE design radiates *less* acoustic pressure into the far-field than the UNRIBBED plate.

The ALTERNATE configuration radiation characteristics, given in Figure 3.12, Figure 3.13, and Figure 3.14 appear to be omni-directional below 1,000 Hertz. Again, this suggests that the ALTERNATE design behaves like an UNRIBBED plate for frequencies below 1,000 Hertz, that is, below the first peak frequency predicted by equation (2.40).

At 2,000 Hertz, as shown in Figure 3.14, the radiation pattern of the ALTERNATE plate relative to the UNRIBBED plate is strongly directional. The overall pattern shown, with a radiation peak at 0.0 degrees—or normal to the plate's surface—is similar to that shown at 500 Hertz for the BASELINE plate in Figure 3.15. Notice, in Figure 3.14, except for a narrow angular region centered about 0.0 degrees, the ALTERNATE plate radiates *less* sound than that which is radiated by the UNRIBBED plate for an excitation frequency of 2,000 Hertz.

72

Figure 3.10. Directionality pattern showing the difference in the far-field radiation of the BASELINE plate relative to the UNRIBBED plate at a frequency of 250 Hertz.

Figure 3.11. Directionality pattern showing the difference in the far-field radiation of the BASELINE plate relative to the UNRIBBED plate at a frequency of 2000 Hertz.

Figure 3.12. Directionality pattern showing the difference in the far-field radiation of the ALTERNATE plate relative to the UNRIBBED plate at a frequency of 250 Hertz.

Figure 3.13. Directionality pattern showing the difference in the far-field radiation of the ALTERNATE plate relative to the UNRIBBED plate at a frequency of 500 Hertz.
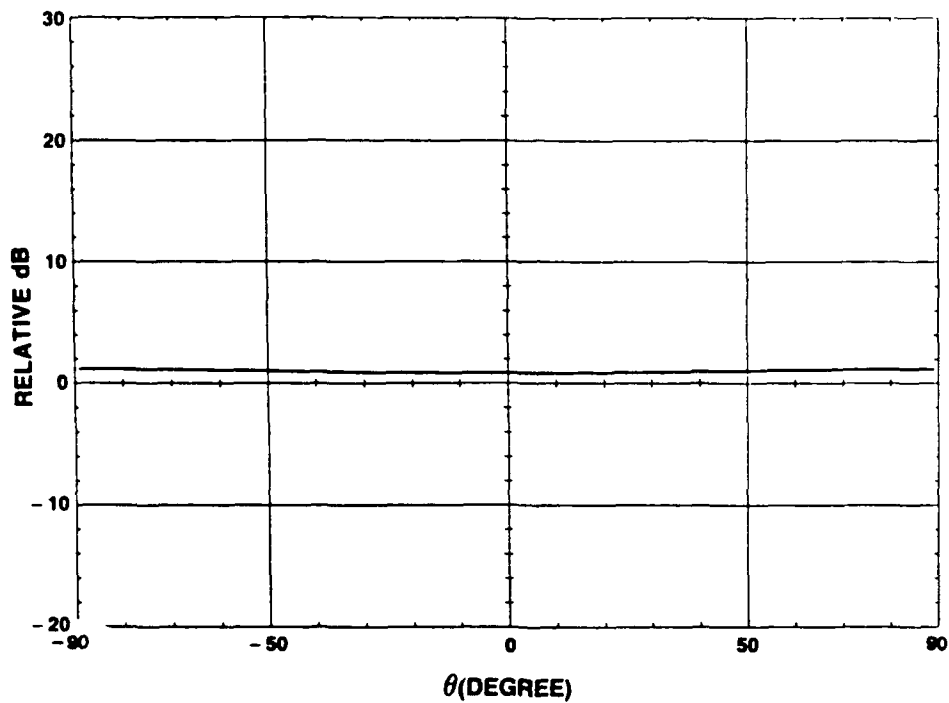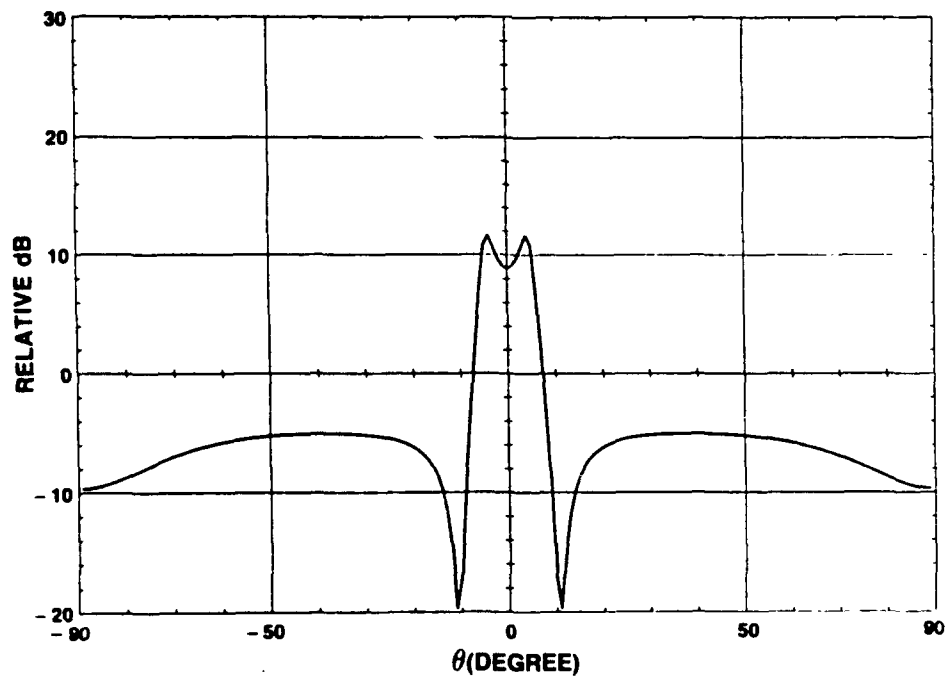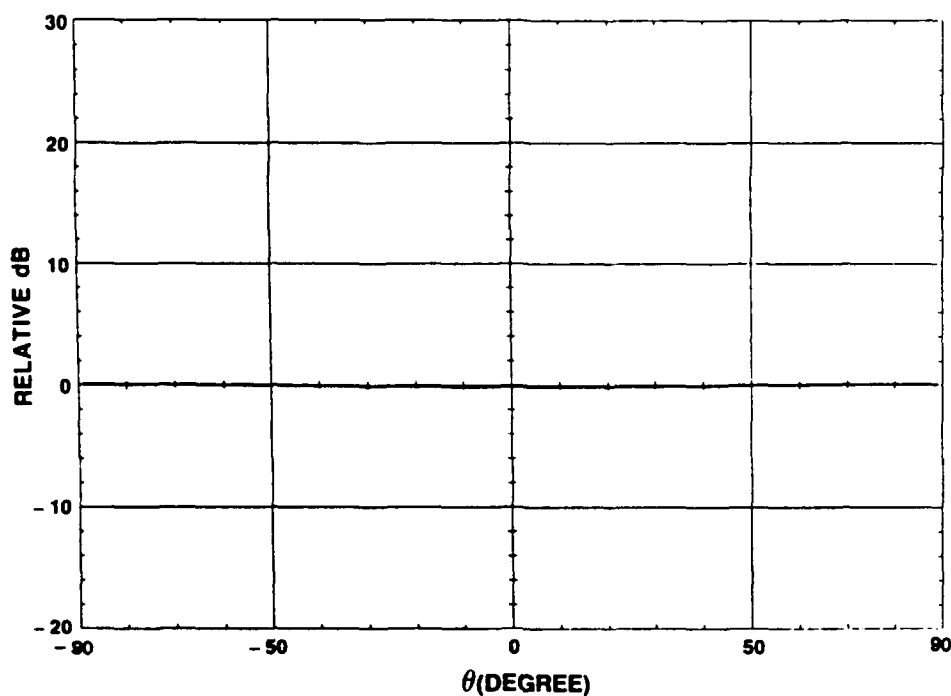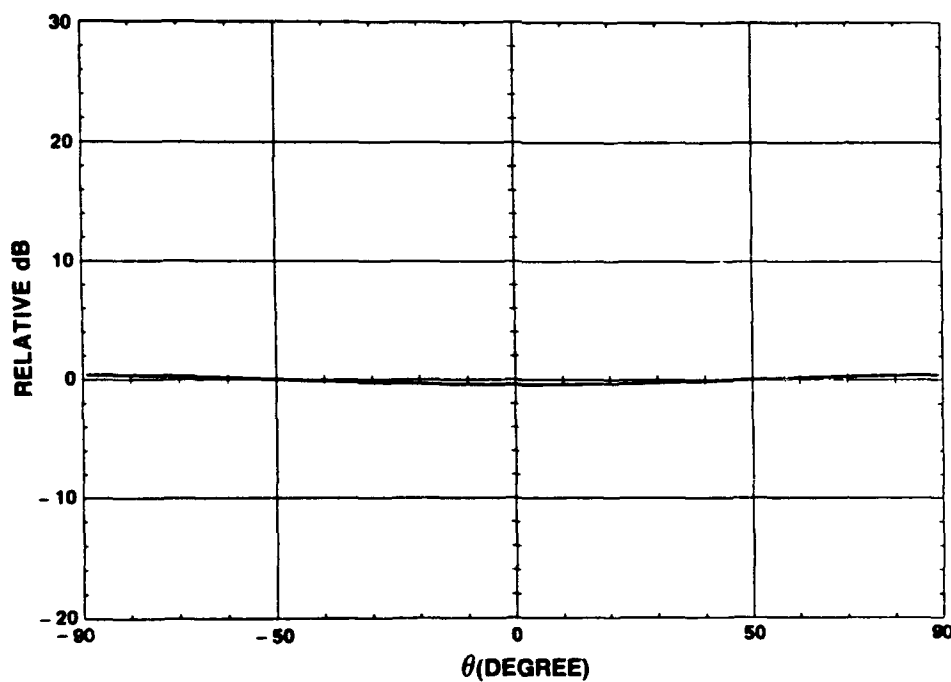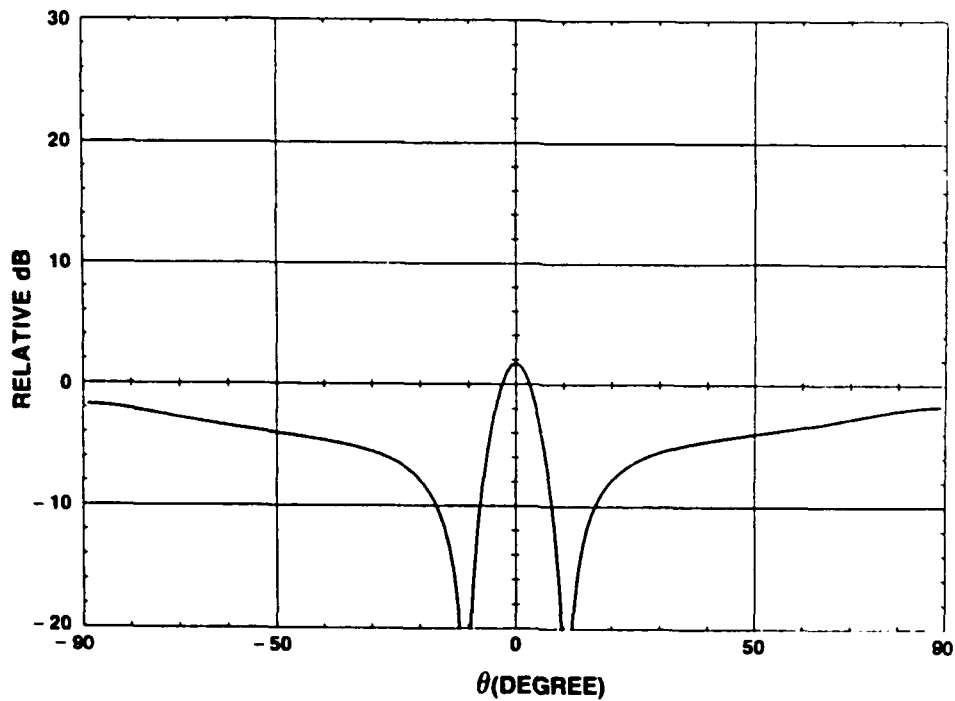
Figure 3.14. Directionality pattern showing the difference in the far-field radiation of the ALTERNATE plate relative to the UNRIBBED plate at a frequency of 2000 Hertz.

Figure 3.15. Comparison of the directionality patterns of the BASELINE plate and the *30% shifted* BASELINE plate at a frequency of 500 Hertz.

3.4.2 Non-Periodic Directional Radiation Patterns

Figure 3.15 compares the directionality patterns of the BASELINE plate and a *30% shifted* BASELINE plate, both relative to the UNRIBBED plate, at an excitation frequency of 500 Hertz. The *30 % shifted* BASELINE plate has an offset, $\Delta = 1.3(\mathfrak{L}/2)$, which produces overall non-periodic frame spacing.

The radiation patterns for the periodic rib spacing given by the BASELINE and ALTERNATE configurations all were symmetric in polar angle about the applied line force. It is apparent then, in Figure 3.15, that the *30% shifted* BASELINE configuration, which has non-periodic rib spacing, is slightly unsymmetrical at 500 Hertz with a narrow radiation peak which occurs at approximately 1 degree.

In Figure 3.16 a comparison is made between the directionality pattern of the BASELINE plate and a 10% shifted BASELINE plate, at an excitation frequency of 1,000 Hertz. The offset is, $\Delta = 1.1(\mathfrak{L}/2)$, which represents only a moderate change in the rib spacing from that of entirely periodic arrangement. Notice, however, that this slight change in offset, from periodic spacing to non-periodic spacing between the ribs, dramatically changes the plate's radiation characteristics.

The *10% shifted* BASELINE configuration is also seen to be entirely unsymmetrical, with a strong radiation peak, 26 dB greater than the UNRIBBED plate's level, occurring at approximately –70 degrees.

It is interesting to look at Figure 3.17, which is for a *–10% shifted* BASELINE design, as it compares with Figure 3.16. Figure 3.17 shows the directional radiation pattern of the BASELINE plate compared to a *–10% shifted* BASELINE plate, at a frequency of 1,000 Hertz. The offset for the *–10% shifted* BASELINE is $\Delta = 0.9(\mathfrak{L}/2)$. It is seen that Figure 3.17 is the mirror image of Figure 3.16 and this symmetry is readily understood if one considers the geometry of the *10% shifted* BASELINE and the *–10% shifted* BASELINE.
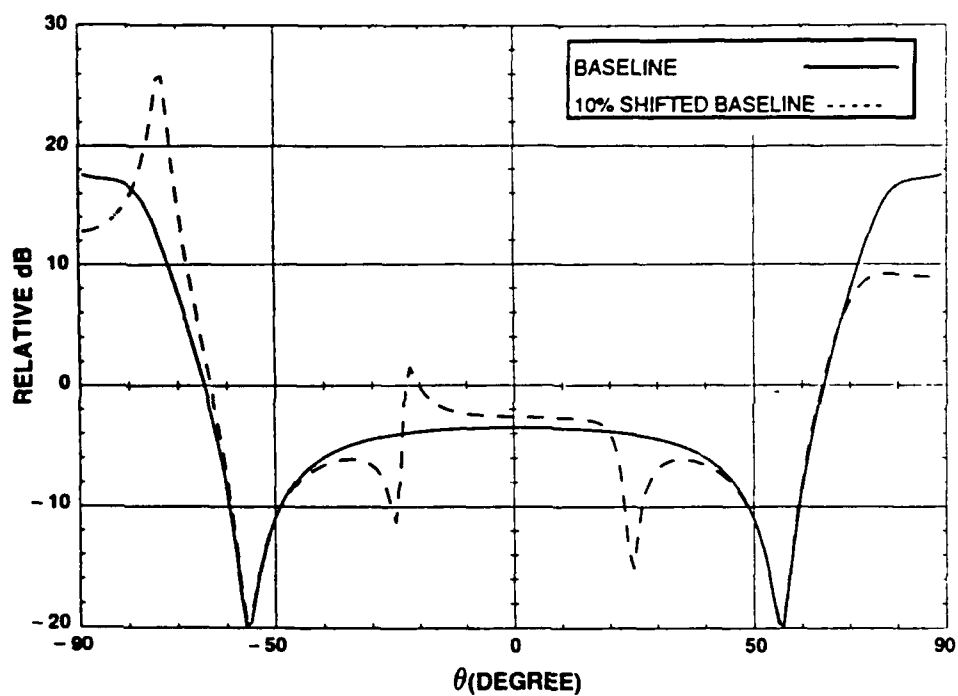
Figure 3.16. Comparison of the directionality patterns of the BASELINE plate and the *10% shifted* BASELINE plate at a frequency of 1000 Hertz.

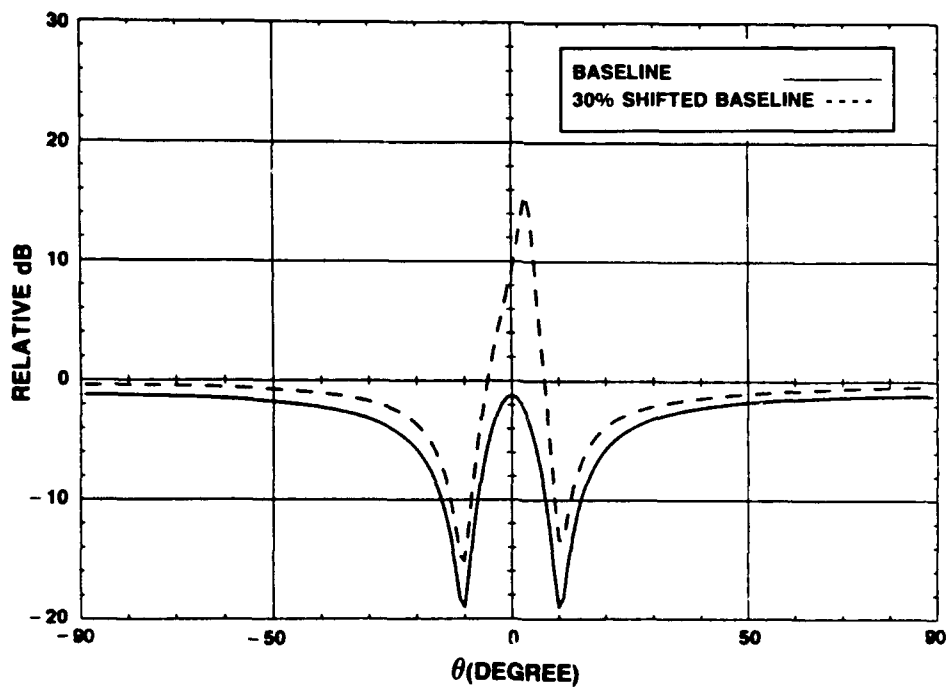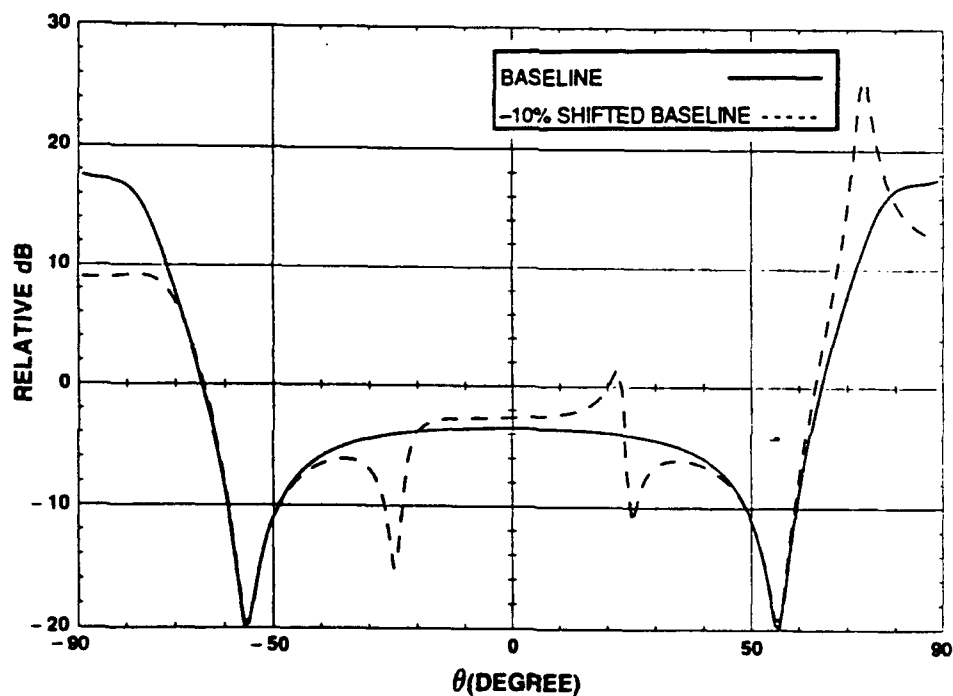Figure 3.17. Comparison of the directionality patterns of the BASELINE plate and the *−10% shifted* BASELINE plate at a frequency of 1000 Hertz

For the *10% shifted* BASELINE, the inter-rib spacing varies, from left to right, starting from the origin, as $1.1(\ell/2)$, $0.9(\ell/2)$, $1.1(\ell/2)$, and so on. However, for the *-10% shifted* BASELINE case, the spacing varies, left to right, as $0.9(\ell/2)$, $1.1(\ell/2)$, $0.9(\ell/2)$, and so on. Hence, the inter-rib spacing of the *-10% shifted* BASELINE design is the mirror image of the *10% shifted* BASELINE design.

From this section and from sections 3.4 and 3.4.1, it appears that the rib-stiffeners may act as an array of sources radiating pressures that constructively and destructively interfere in the far-field. The radiation characteristics of the stiffeners depend on the frequency of excitation and on the offset between one stiffener set and the other. Though no fundamental relationship between far-field directional radiation characteristics and offset has been found, many practical applications are suggested by the figures illustrated. A discussion of such applications is presented in Chapter 5.

Many investigators, such as Gorman (1974), Romonov (1971), and others, have recognized that the plate's internal structural damping alters the magnitude of the radiated acoustical pressure from a stiffened plate. Increasing the structural loss factor will decrease the magnitude of the radiation peaks, while decreasing damping will increase the magnitude of these radiation peaks. The effect is noted here, though, in typical engineering applications, a plate material is specified by other considerations and the structural damping factor is fixed. Hence, it is unlikely that this effect can be exploited.

In the next chapter the acoustic pressure near the surface of the stiffened plate will be investigated. This will require numerical integration of equations (2.10a) and (2.10b); no simplifying approximation of the radiated acoustic pressure, such as equation (3.4), is available.

4. NEAR-FIELD ACOUSTIC RADIATION OBTAINED BY NUMERICAL INTEGRATION

The near-field acoustic pressure radiated from the line-driven, fluid-loaded, rib-stiffened plate has been obtained using numerical integration techniques. As Chapter 1 indicated, there have been few investigations into the near-field behavior of stiffened structures. This lack of research is likely due to difficulty in an analytical evaluation of the inversion integral, equations (2.10a) and (2.10b), which determines the near-field radiated pressure.

For an unstiffened plate, contour integration has been used—for example, in Feit (1985) and Strawderman (1979)—to obtain expressions for the near-field acoustic pressure. The integration is accomplished by allowing the wavenumber, k, to be complex and defining a suitable contour of integration. The path of integration must encompass certain poles which satisfy physical radiation requirements. Such a procedure here would be quite cumbersome.

Inspection of the summation terms in equation (2.26) reveals that an infinite number of poles (separated by a distance nk_g, where n varies over all integers) and branch points exist and must be considered in defining a suitable contour of integration. Also, any additional poles associated with equation (2.26) must be considered. The location of these poles, their type, and, if required, their order must be determined. Hence, numerical integration was chosen as a means of evaluating the inversion integral.

Rewriting equations (2.10a) and (2.10b) here in terms of a positive integration interval yields

$$P(x,z) = \int_0^\infty A(\omega) \left\{ \frac{\tilde{w}(k)\, e^{i\sqrt{k_0^2 - k^2}\, z}}{\sqrt{k_0^2 - k^2}} e^{ikx} + \frac{\tilde{w}(-k)\, e^{i\sqrt{k_0^2 - k^2}\, z}}{\sqrt{k_0^2 - k^2}} e^{-ikx} \right\} dk$$

(4.1)

where

$$A(\omega) = -\frac{i\rho_0\omega^2}{2\pi}.$$

Note that the general wavenumber response given by equation (2.26) is not symmetric in wavenumber, and hence equation (4.1) does not collapse into an inverse Fourier Cosine transform.

For point force excitation, the integral given by equation (4.1) becomes a double integral, one which ranges over the wavenumber k_x, and the other over wavenumber k_y. The numerical calculations of the double integral are lengthy, with many thousands of integrand function evaluations required to obtain the acoustic pressure at a single (x,y) observation point.

4.1 NUMERICAL INTEGRATION

Many integration techniques were investigated for numerically computing equation (4.1). The focus was on reducing the total number of required evaluations of the integrand necessary for integral convergence.

Gaussian quadrature was tried; however, due to the oscillatory nature of the integrand, the method performed poorly. The upper limit of integration was fixed at a wavenumber two times the flexural wavenumber. Continuing to integrate beyond this value generates little contribution to the radiated acoustic pressure since the integrand decays very rapidly beyond the flexural wavenumber. Within the chosen range of integration then, both the real and imaginary parts of the integrand given in equation 4.1 oscillate through many zeros. For Gaussian quadrature, the integration interval should be broken into sub-intervals bounded by the integrand's zeros, and within each sub-interval a small point Gaussian formula should be used. On the other hand, a very large point formula could be used over

the entire range of integration. Either method, though, introduces a large number of integrand function evaluations, and for this reason, Gaussian quadrature was not used.

The general wavenumber response, $W(k)$, is independent of the coordinates normal to and along the plate's surface, the coordinates z and x respectively. Therefore, at a fixed frequency, it would seem redundant to continually compute $W(k)$ for a change in the x-coordinate or z-coordinate. It is specifically the wavenumber response, $W(k)$, which lengthens to the computational time necessary to evaluate the near-field acoustic pressure. Recall that the general spectral response, equation (2.26), involves five complex and slowly converging summations. Considering this, an investigation was made into computing the wavenumber response, $W(k)$, once, for a given frequency, storing the computed values, then linearly interpolating between the stored wavenumber values. In this way, changes in the x-coordinate or z-coordinate would not require recomputing the spectral response, $W(k)$. However, it was found that the response needed to be so finely sampled in wavenumber to obtain integral convergence, that little was gained in overall computational speed using linear interpolation.

A Romberg integration technique, Carnahan (1969), was finally chosen to perform the numerical integration. Romberg integration consists of repeated applications of low-order integration formulas, for example, the trapezoidal rule, until some initial integral convergence criterion is met. Then, without any further integrand function evaluations, a Richardson's extrapolation procedure is used to improve the estimate of the integral by reducing the approximation error.

Of the numerical integration techniques investigated, Romberg integration proved to be the simplest to implement and computationally faster than all other methods investigated. Regardless of chosen technique, the integral given by equation (4.1) becomes much more difficult to numerically integrate for large values of the x-coordinate or the z-coordinate.

4.2 NEAR-FIELD AND FAR-FIELD ACOUSTIC REGIONS

The demarcation of the acoustic near-field region and the onset of the far-field region depends on a number of parameters. The regions cannot be precisely specified at some fixed distance away from the stiffened plate's upper surface. The thickness of the plate, the given excitation frequency, and the acoustic medium all affect the region where the near-field acoustic components have decayed sufficiently so that a stationary phase far-field approximation becomes valid.

Figure 4.1 compares the near-field, obtained by numerically integrating equation (4.1), and the far-field approximation, equation (3.4), of the radiated sound pressure level from the BASELINE plate at 250 Hertz. The observation point moves perpendicularly away from the plate's surface. The far-field approximation, as expected, gives a poor estimate of the radiated pressure near—for stand-off distance of 1/3 meter or less—the stiffened plate's surface.

The comparison of the near-field and far-field calculations, at a frequency of 1,000 Hertz, for the BASELINE plate is given in Figure 4.2. Notice, as frequency increased, the stationary phase approximation becomes less accurate for greater stand-off distances. Beyond 1 1/2 meters, though, the magnitude of the acoustic pressure given by numerically integrating equation (4.2) and by the stationary phase approximation is essentially identical. However, caution is still warranted in assuming, at 1000 Hertz, the onset of the far-field region begins at 1 1/2 meters. Observation points other than directly above the excitation force, at a similar stand-off distance, may yield strong near-field pressures.

4.3 NEAR-FIELD PRESSURE VARIATION WITH FREQUENCY

Throughout this chapter, unless otherwise stated, the vertical stand-off distance, the z coordinate, is fixed at 1/3 meter. This value was chosen as typical to stand-off distances of passive sonar listening devices on Navy ships and submarines, Schloemer (1981).
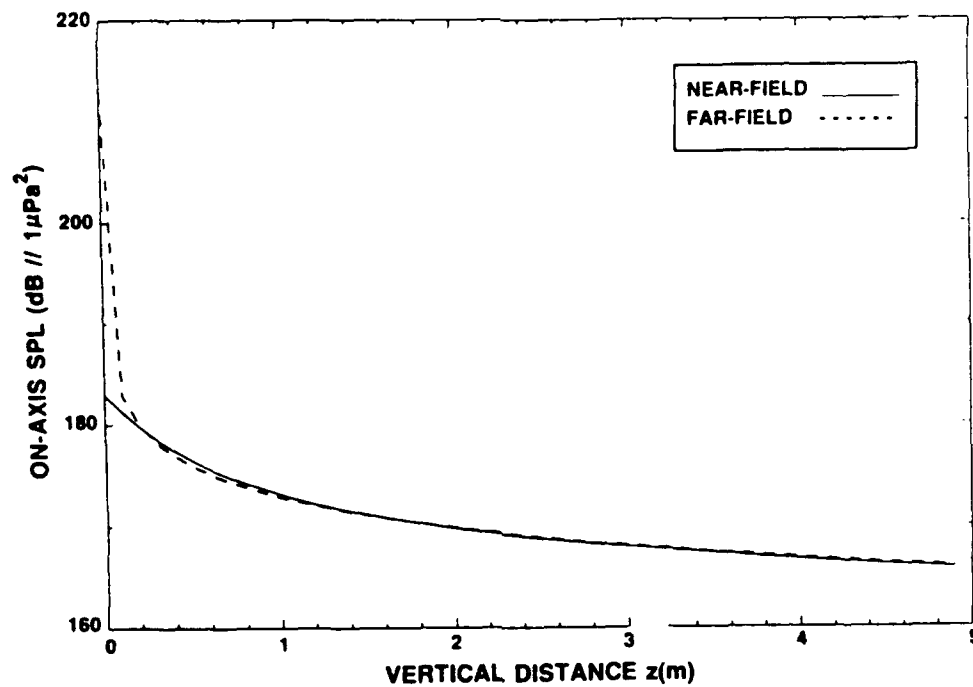
Figure 4.1. Comparison of the near-field and far-field radiated pressure from the BASELINE plate versus stand-off distance at 250 Hertz.
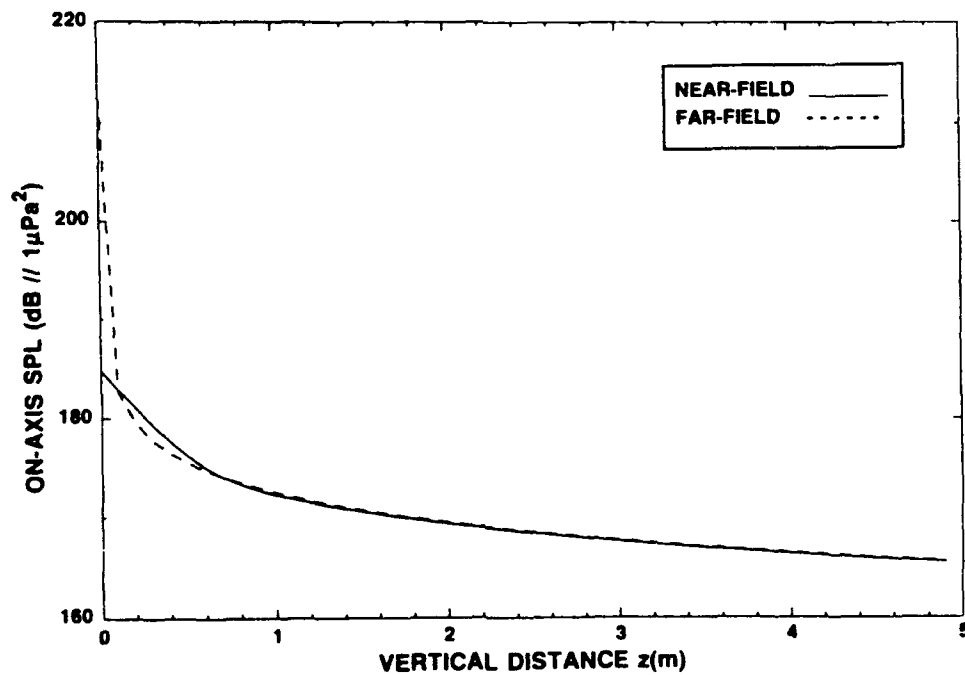

Figure 4.2. Comparison of the near-field and far-field radiated pressure from the BASELINE plate versus stand-off distance at 1000 Hertz.

Figure 4.3 and Figure 4.4 show the near-field sound pressure levels radiated from the BASELINE and ALTERNATE configuration, respectively, compared to the UNRIBBED plate over a frequency range of 100 Hertz to 10,000 Hertz. The figures are similar to those given by Figure 3.3 and Figure 3.4, which were in the far-field.

Figure 4.3 the BASELINE configuration, shows few well-defined radiation peaks, unlike that of the far-field results, and more nulls are given in the near-field calculations over that of the far-field. The sound pressure level over most of the frequency band is on the order of or less than the level radiated from the UNRIBBED plate. The nulls in acoustic pressure shown in Figure 4.3 do not directly match those given in Figure 3.3 for the far-field.

In Figure 4.4, the ALTERNATE plate's near-field radiated pressure is compared to the UNRIBBED plate's level over the same frequency band. Below 1,000 Hertz, the addition of rib-stiffeners seems to have little effect on the near-field sound pressure level. Beyond 1,000 Hertz, the stiffeners obviously do contribute. Notice that the far-field results shown in Figure 3.4 are much different than the near-field results illustrated in Figure 4.4. Again, as in Figure 4.3, the overall sound pressure level of the ALTERNATE configuration is equal or less than that of the UNRIBBED plate. However, it must be emphasized that the results shown are for a particular observation point; that is, a distance of 1/3 meter directly above the applied line force. For other observation points, the rib-stiffened plate's radiated acoustic pressure may be much greater than that radiated from the unstiffened plate.

The near-field region appears to be sensitive to changes in offset which yield non-periodic stiffener spacing. Figure 4.5 compares the near-field sound pressure level from a *50% shifted* BASELINE plate configuration to the UNRIBBED plate at a distance 1/3 meter above the plate's surface. The offset here is $\Delta = 1.5(\mathcal{Q}/2)$. Except for the pressure peak near 1000 Hertz, the location of pressure nulls and relative magnitude peaks have changed from those shown in Figure 4.3. The pronounced null at approximately 450

Hertz, seen in the BASELINE configuration, is no longer present in the *50% shifted* BASELINE configuration. The non-periodic inter-rib spacing has reduced the sound pressure level over most of the frequencies above 1,000 Hertz compared to the UNRIBBED plate and the BASELINE periodically ribbed plate.

4.3.1 Description of Near-Field Surface Pressure Variations

In the following section, a detailed analysis of the variation of near-field radiated pressure along the surface of the plate will be presented. Few papers have been published which have investigated the near-field pressure on the surface of a periodically stiffened structure. Hence, the following section should provide a beneficial addition to the field of structural acoustics. Certainly the investigation is warranted, and this section of the dissertation should eliminate the scarcity of knowledge of near-field sound radiation from periodic and non-periodic structures.

For all of the figures shown in the following section, the vertical stand-off distance is fixed at 1/3 meter. The observation point will move above the plate's surface, in the positive x-direction, from the origin to a distance of 10 or 20 meters away.

The results presented in this section are important in the design of passive sonar listening devices that are mounted on the external side of a ship or submarine hull. A sonar array designer seeks a way to reduce the structural radiation from a hull, since the radiation represents unwanted sound which contaminates an incoming signal. Hence, the interest here is to determine whether a selection of rib stiffeners—of proper size and inter-rib spacing—may reduce the radiated noise sensed by the passive sonar device.

Figure 4.6 shows a comparison of the near-field sound pressure level radiated from the BASELINE and the UNRIBBED plate versus horizontal distance at 1/3 meter above the plate's surface. The excitation frequency is 250 Hertz. The solid line denotes the BASELINE pressure and the dashed line is the UNRIBBED plate's radiated pressure.

Figure 4.3. Comparison of the near-field on axis sound pressure level radiated from the BASELINE and UNRIBBED plate versus frequency at a distance of 1/3 m.

Figure 4.4. Comparison of the near-field on axis sound pressure level radiated from the ALTERNATE and UNRIBBED plate versus frequency at a distance of 1/3 m.
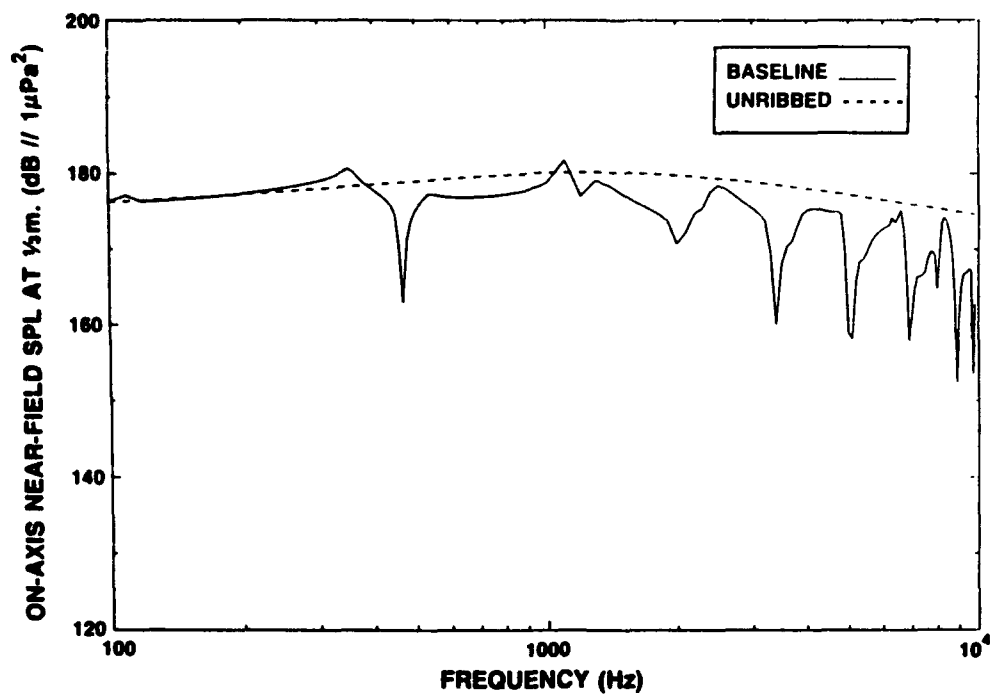
Figure 4.5. Comparison of the near-field on axis sound pressure level radiated from the *50% shifted* BASELINE and UNRIBBED plate versus frequency at a distance of 1/3 m.
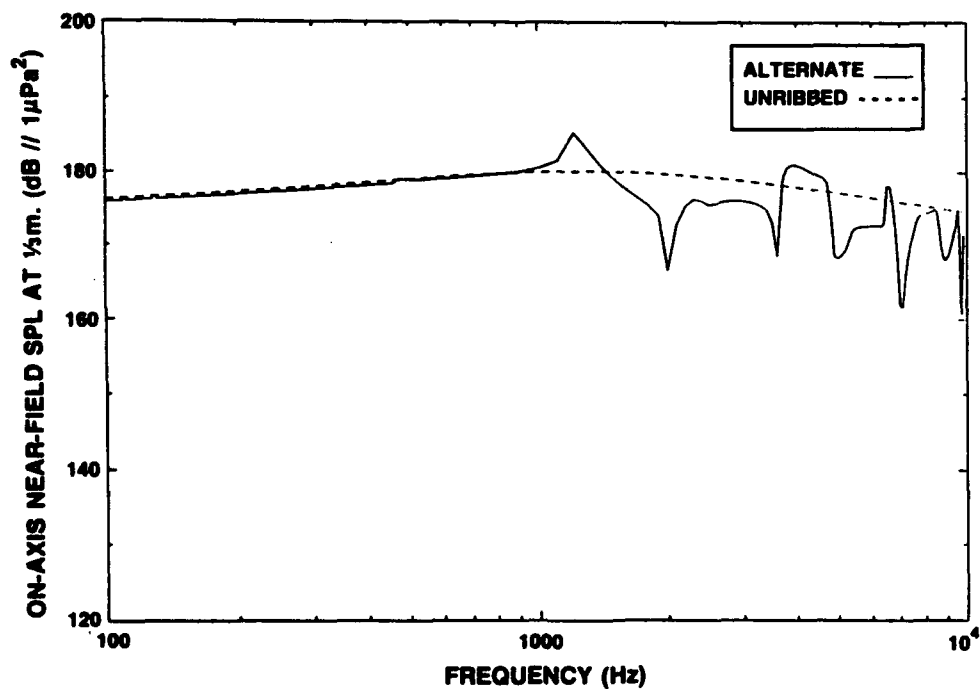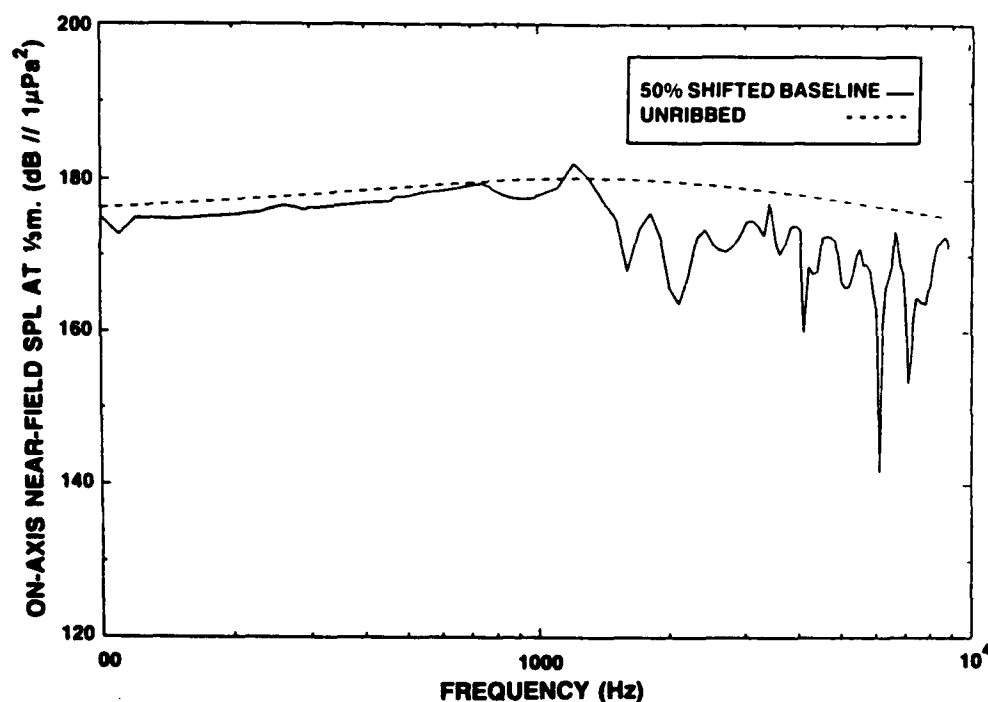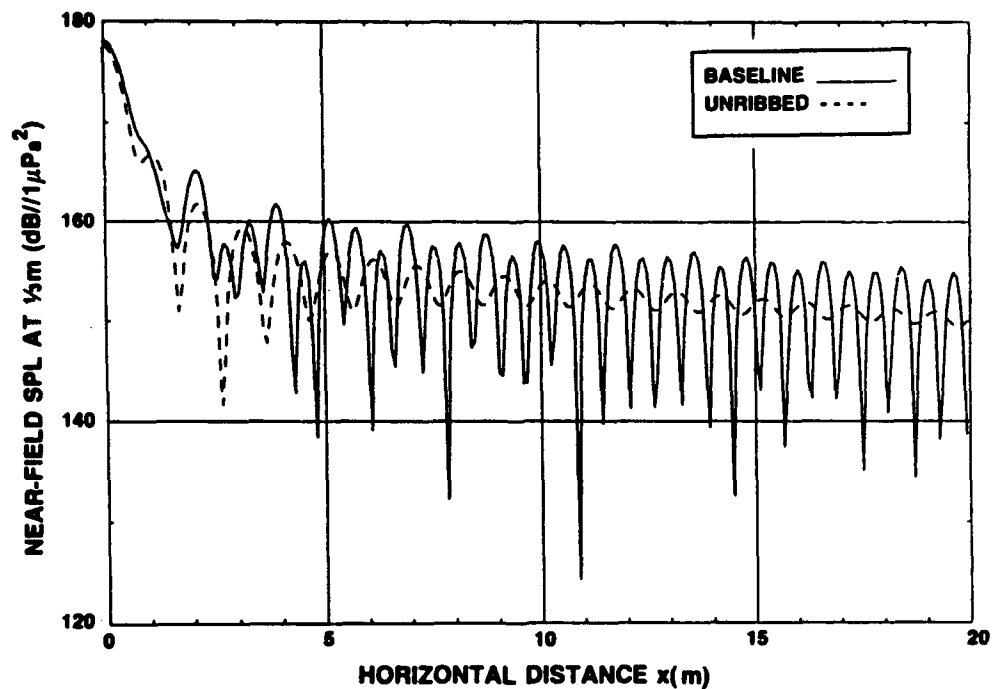

Figure 4.6. Near-field sound pressure level radiated from the surface of the BASELINE and UNRIBBED plate at 250 Hertz. The stand-off distance is 1/3 m.

Shown in Figure 4.6 are rapid oscillations in radiated pressure for both configurations. These oscillations are present in the acoustic near-field and quickly decay with distance away from the plate. The oscillations appear as a rectified sinewave close to the excitation force and become sinusoidal farther away. The spatial wavelength of the oscillations in the sinusoidal region is equal to the plate's bending wavelength, $\lambda_b = \frac{2\pi}{k_{fl}}$, at 250 Hertz. The phenomenon is well-documented, Fahy (1985), for acoustic radiation near the surface of an unstiffened infinite plate. Some authors have coined the phrase *evanescent field* to describe the region near the surface of the plate where the oscillations are observable. The amplitude of the oscillations decays exponentially with distance away from the plate, at a rate proportional to $e^{-k_{fl}z}$. The overall sound pressure levels, shown in Figure 4.6, of the BASELINE and UNRIBBED plate are similar.

Quite surprising is the result given in Figure 4.7, which compares the near-field sound pressure level along the plate's surface radiated from the BASELINE configuration and the UNRIBBED plate at an excitation frequency of 500 Hertz. Obviously, the oscillation of the BASELINE plate's radiated pressure is radically different than that of the UNRIBBED plate. Again, the wavelength of oscillation seen in the UNRIBBED plate corresponds to the free-bending wavelength. The BASELINE configuration, at 500 Hertz, shows an oscillation which has a wavelength much greater than that given by the stiffened plate's bending wavelength. The cause for this difference will be discussed shortly, after presenting Figure 4.9.

Figure 4.7 also shows a lower sound pressure level, for the BASELINE plate, for the first 1 1/2 meters along the plate's surface away from the excitation force. In this region and at this frequency, the rib-stiffened plate is quieter than the unstiffened plate. The rate of decay of sound pressure level along the BASELINE plate's surface is seen to be greater than the rate for the UNRIBBED plate.

Figure 4.8 is a comparison of the near-field radiated pressure from the BASELINE and UNRIBBED plate at a frequency of 1,000 Hertz. Unlike Figure 4.7 at 500 Hertz, the sinusoidal oscillations of the BASELINE configuration now have a wavelength equal to the flexural bending wavelength, and the wavelength is almost identical to that of the UNRIBBED plate.

However, the level of the radiated pressure of the two plates is very different, with the BASELINE configuration radiating sound at a level more than 20 dB higher than that of the UNRIBBED plate for distances beyond 6 meters. Also note, the near-field pressure in the BASELINE configuration does not decay monotonically away from the applied line force as has been seen in all previous results. Initially, for approximately the first meter, the BASELINE plate's near-field decays with distance from the origin. The radiated pressure then, surprisingly, begins to increase to a relative maximum at 6 meters, and then slowly tapers off. The rate of decay beyond 6 meters is much less than that shown for the UNRIBBED plate. It would appear that the *near-field* acoustic pressure has, at certain frequencies, directional radiation characteristics as was seen for far-field radiation. No effort was made to determine the source of this interesting near-field effect.

Figure 4.9 is a comparison of the near-field sound pressure level radiated from the ALTERNATE and the UNRIBBED plate at an excitation frequency of 1000 Hertz. The ALTERNATE configuration seems to have radiation features previously seen in the BASELINE configuration shown in Figure 4.6 and Figure 4.7, at 250 Hertz and 500 Hertz, respectively. The oscillations shown in Figure 4.9 have a wavelength corresponding to the flexural wavelength, though modulated by a much larger spatial wavelength.

The rate of decay in the magnitude of the radiated acoustic pressure for both configurations is comparable. However, though less dramatic, the ALTERNATE's near-field radiated pressure is seen to increase slightly from 8 meters to 10 meters; therefore, the pressure again does not decay monotonically away from the excitation source.

90
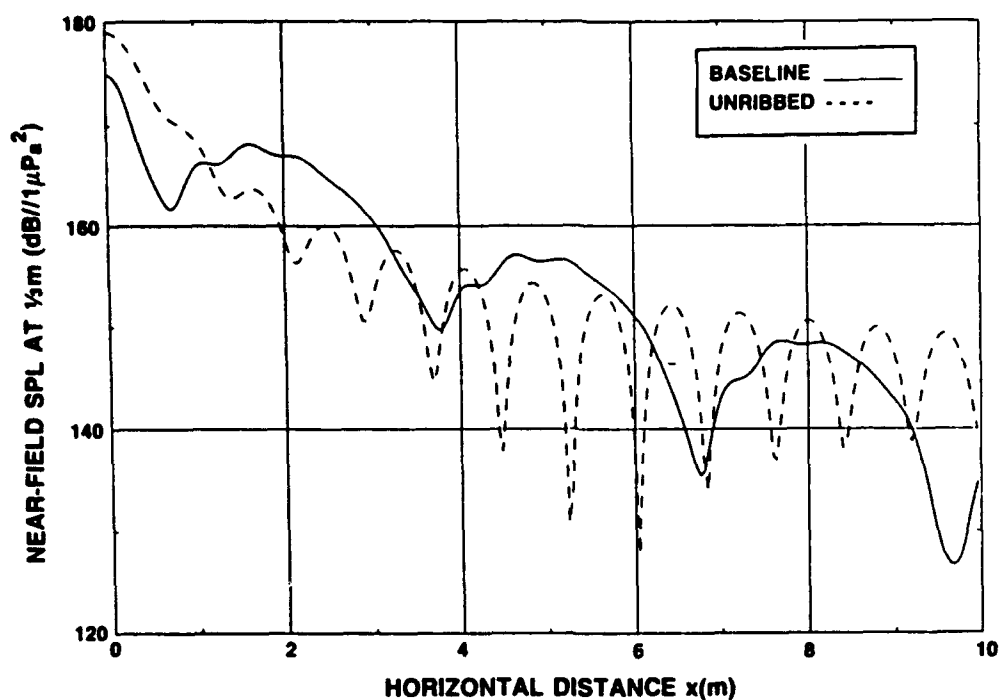
Figure 4.7. Near-field sound pressure level radiated from the surface of the BASELINE and UNRIBBED plate at 500 Hertz.
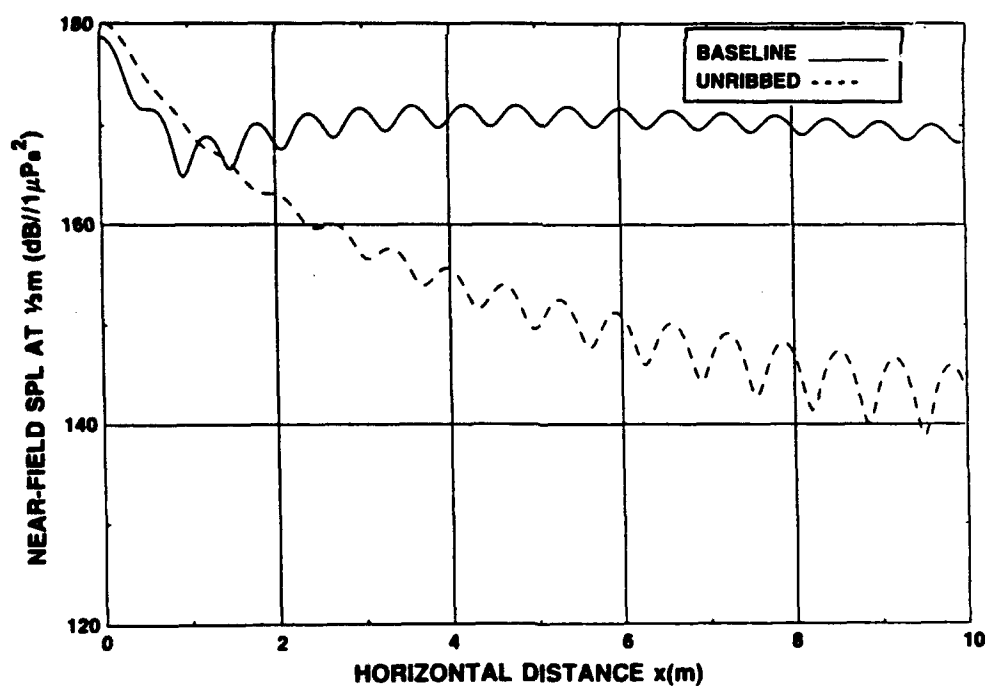
Figure 4.8. Near-field sound pressure level radiated from the surface of the BASELINE and UNRIBBED plate at 1000 Hertz.
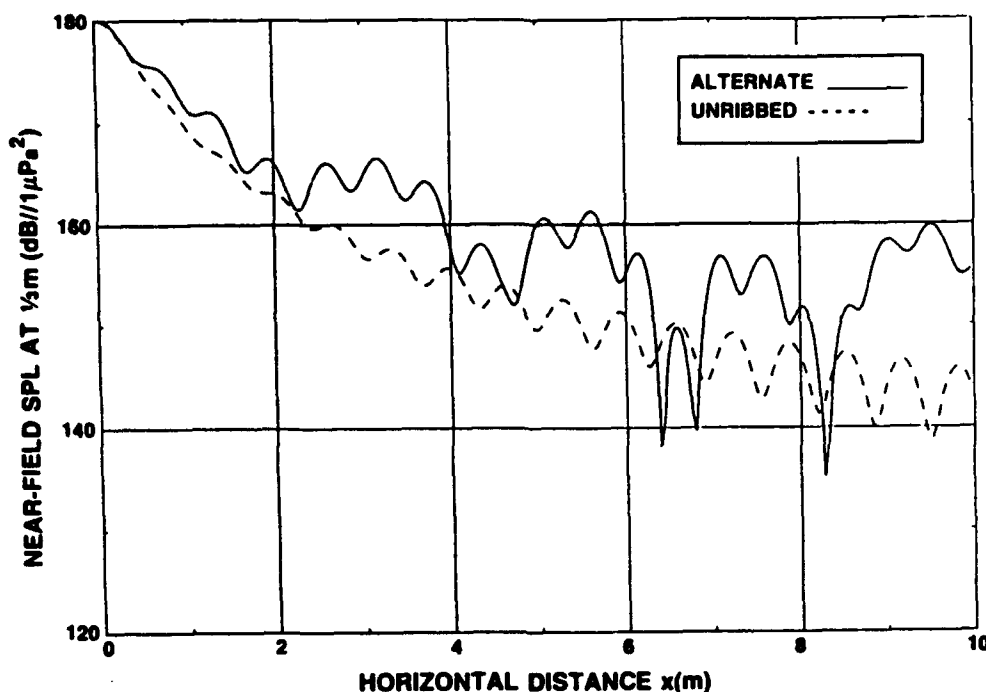
Figure 4.9. Near-field sound pressure level radiated from the surface of the ALTERNATE and UNRIBBED plate at 1000 Hertz.

Before continuing, the following is noted. The BASELINE configuration has a periodic rib spacing of 0.6035 meters and the ALTERNATE plate had a rib spacing of 0.30175 meters. Reviewing Figure 4.6 through Figure 4.9, it is apparent that no elementary geometrical correlation exists between the periodic rib spacing and the radiated acoustic pressure. That is, at a fixed frequency, as acoustic pressure is calculated along the plate, pressure maximums or minimums do not occur, in a simple manner, as the observation point slides over a rib-stiffener.

Romanov (1976) has advised that, "to preclude the influence of resonance of the spacings between beams," the acoustic pressure at each observation point along the plate, should be frequency-averaged over an interval which contains several span resonances. It is assumed the span resonances refer to the resonances of a finite plate simply supported at each end, and of length equal to the periodic spacing, ℓ. Romanov does present results

which show relative peaks in radiated pressure above rib-stiffeners. The peaks decay with distance along the plate.

4.3.2 Analysis of Near-Field Surface Pressure Variations: Periodic Configurations

In order to explain some of the phenomena illustrated in Figures 4.6 through 4.9, the integrand and the resulting integration, defined by equation (4.1), will be carefully considered. This analysis will explain the large wavelength pressure oscillations seen in Figure 4.7, for the BASELINE plate. The analysis also uncovers the reason for the much larger radiated pressure of the BASELINE configuration over that for the UNRIBBED plate at 1000 Hertz.

Figure 4.10 is a plot of the magnitude of the acoustic pressure integrand given in equation (4.1), showing both the periodic BASELINE configuration (the solid line) and the UNRIBBED plate (denoted by the dashed line). The stand-off distance was fixed at 1/3 meter, the x-coordinate was fixed at the origin, and the excitation frequency was 500 Hertz. As stated, the excitation force is applied at the plate's origin. The wavenumber ranges from $-20 \, m^{-1}$ to $20 \, m^{-1}$, which is a range that includes the flexural and acoustic wavenumber. For both configurations, BASELINE and UNRIBBED, the flexural wavenumber has an absolute value of approximately $10 \, m^{-1}$.

Notice the relative magnitude of the integrand at the flexural wavenumber for the BASELINE plate compared with the UNRIBBED plate. The integrand for the UNRIBBED plate has a flexural wavenumber response much greater than that shown for the BASELINE plate. Recall that Figure 4.7 illustrated interesting behavior of the BASELINE plate's radiated pressure along the surface of the plate. No oscillations corresponding the flexural wavelength were seen for the BASELINE plate at 500 Hertz. The reason is apparent from Figure 4.10; the BASELINE's integrand is quite diminished at this wavenumber and hence, this region contributes a negligible amount to the integration.

Another feature shown in Figure 4.10 is a prominent null in the BASELINE integrand at a wavenumber of ± 0.4 m^{-1}. It will be verified shortly that the wide peak in the BASELINE integrand seen after this null produces the large wavelength oscillations in the BASELINE radiated pressure seen in Figure 4.7.

Figure 4.11 is a comparison of the magnitude of the integrand given by equation (4.2) for the BASELINE and UNRIBBED plate at an excitation frequency of 1,000 Hertz. The ordinate scale has been changed in Figure 4.11, from that of Figure 4.10, to accommodate the very large wavenumber components, at wavenumbers ± 4.0 m^{-1}, present in the BASELINE integrand. Notice, that the relative magnitudes of the integrand given by the BASELINE and UNRIBBED plates at the flexural wavenumber, ± 14 m^{-1}, are comparable. Therefore, as Figure 4.8 illustrates, both configurations show oscillations in acoustic pressure with a spatial wavelength equal to the bending wavelength.

For the UNRIBBED plate, the characteristics of the magnitude of the integrand do not change with frequency. The integrand is symmetric and for, say, positive wavenumbers, increases steadily with wavenumber up to the acoustic wavenumber, k_0, where the response peaks. The magnitude rapidly decays beyond the acoustic wavenumber until the flexural wavenumber is reached, where the response again peaks. Beyond the flexural wavenumber, the magnitude decays very rapidly. Hence, it should be apparent that the significant contributions to the radiated pressure are generated by supersonic wavenumbers.

The large spike in the integrand for the BASELINE plate at 1000 Hertz, shown in Figure 4.11, is the component that generates the substantial increase in radiated pressure along the BASELINE plate's surface, as shown in Figure 4.8. The integrand for the stiffened plates is essentially determined by the spectral response, $W(k)$, and the spectral components of most importance are those which have wavenumbers less, in absolute value, than the acoustic wavenumber.
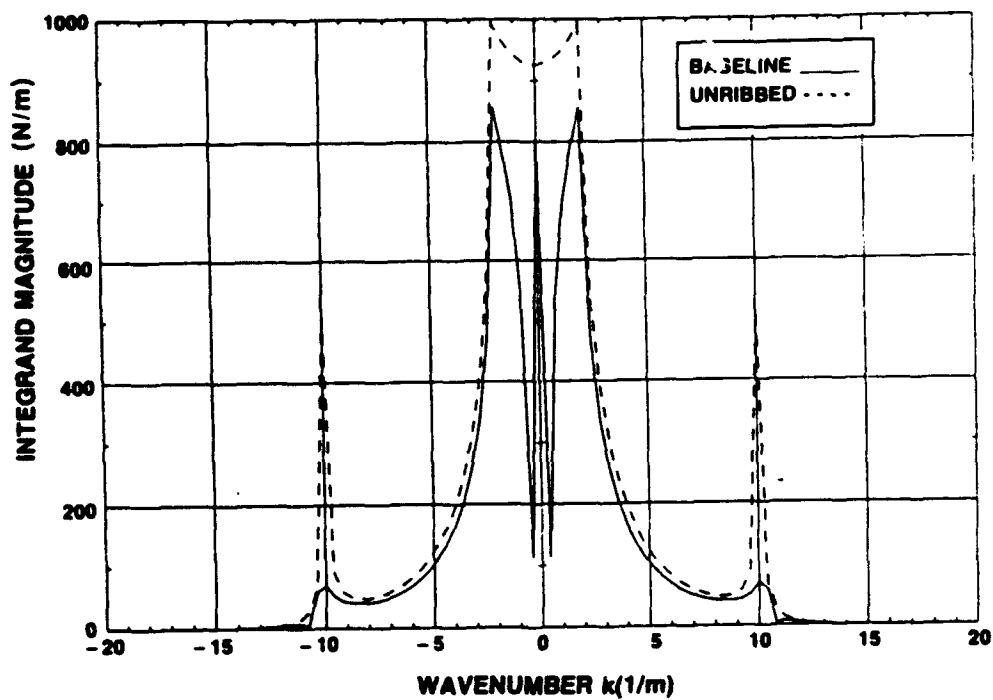
Figure 4.10. Comparison of the magnitude of the integrand, equation (4.1), of the BASELINE and UNRIBBED plate at 500 Hertz.
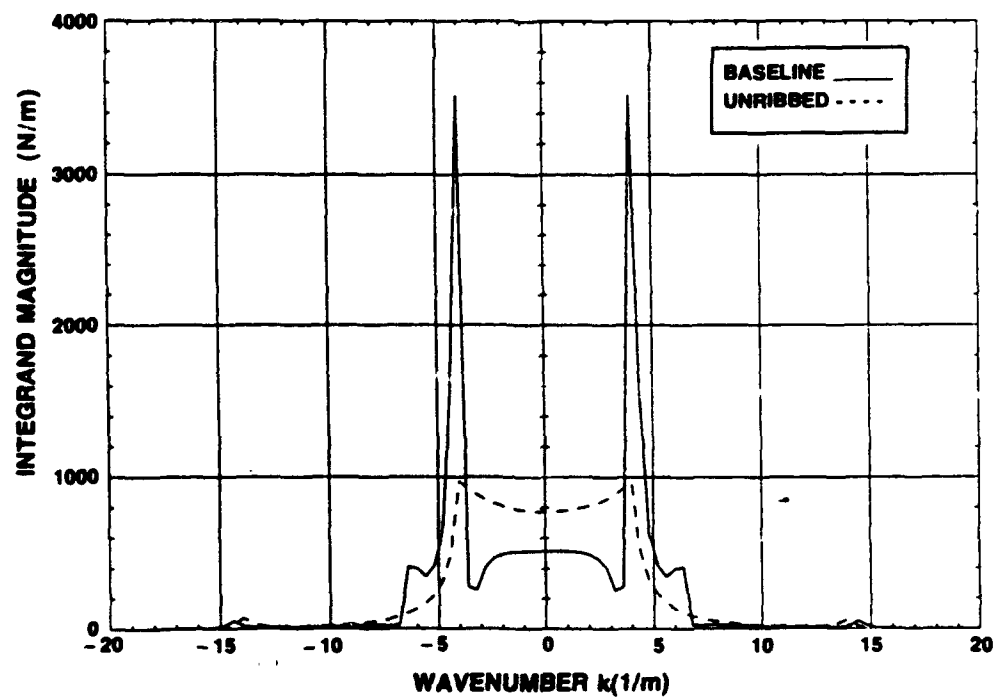

Figure 4.11. Comparison of the magnitude of the integrand, equation (4.1), of the BASELINE and UNRIBBED plate at 1000 Hertz.

Referring back to Chapter 2, a close look at Figure 2.5, for positive wavenumbers up to the acoustic wavenumber, $k_0 = 2.1$ m^{-1}, reveals that the magnitude of the integrand, shown in Figure 4.10, is determined by the BASELINE plate's wavenumber response. Similarly, Figure 2.6, an excitation frequency of 1000 Hertz, demonstrates the effect the wavenumber response has on the magnitude of the integrand given in Figure 4.11. Indeed, the large wavelength oscillations of the BASELINE plate's near-field radiated pressure, illustrated in Figure 4.10, are due to the small hump, between wavenumbers 0.4 m^{-1} and 2.0 m^{-1}, in the BASELINE plate's spectral response, $\mathcal{W}(k)$, shown in Figure 2.5.

As the observation point moves along the plate, the increasing value of the x-coordinate in the integrand in equation (4.1) causes increased oscillation of the exponential term, e^{ikx}. The rapid oscillation of this term, upon integration, tends to reduce spectral contributions which are slowly varying in slope. Other wavenumber components, such as spectral peaks, are sampled and retained. Hence, for this reason, the spectral hump shown in Figure 2.5 of the BASELINE wavenumber response at 500 Hertz, is seen to propagate along the plate's surface.

Referring to Figure 2.6 in Chapter 2, a maximum in wavenumber response occurs just below the acoustic wavenumber, $k_0 = 4.2$ m^{-1}. This represents the optimal situation for creating large radiated pressure levels. The integrand given in equation (4.1) shows that the wavenumber response, $\mathcal{W}(k)$, is divided by the term $\sqrt{k_0^2 - k^2}$. For wavenumbers near the acoustic wavenumber this term is small, and hence, upon division, the integrand will be large. The integrand will be even larger if a spectral peak in the wavenumber response, $\mathcal{W}(k)$, is located at the wavenumber near the acoustic wavenumber. This explains the large magnitude of the BASELINE plate's integrand at 1000 Hertz shown in Figure 4.11 and, therefore, the increase in radiated sound pressure level.

Figure 4.12 through Figure 4.15 are included to complete the examination of the inversion integral used to obtain the near-field radiated pressure. Figure 4.12 and Figure

4.13 show the magnitude of the BASELINE plate's sound pressure level, given by equation (4.1), over small finite intervals of integration in wavenumber. The interval is one-tenth of a unit wavenumber and the entire range of integration has been subdivided into 100 equal intervals.

For comparison, the magnitude of the acoustic pressure over each interval given by the UNRIBBED plate is shown by thin lines. In both figures, the location of the interval which contains the acoustic wavenumber is specified by a dashed line. Figure 4.12 is for an excitation frequency of 500 Hertz and Figure 4.13 is for an applied excitation at 1000 Hertz. Note that the figures do not give the actual radiated pressure levels since phase has not been retained from integration interval to interval.

Comparing the magnitudes of the UNRIBBED and BASELINE plate integrands, shown in Figure 4.10 and 4.11, it is not surprising that the magnitude of the acoustic pressure, over each small interval of integration, is of similar shape. At this point it should be very apparent that subsonic wavenumber components contribute an insignificant amount to structural radiation.

The dip in the magnitude of the sound pressure seen in Figure 4.12 at the fourth interval of integration corresponds to the null seen in the BASELINE plate's spectral response at a wavenumber of $0.4 \ m^{-1}$, Figure 2.5. The steady rise of the sound pressure level following the dip is predictable from the results shown in Figure 4.10. Notice, at the final integration interval, which is a interval over the flexural wavenumber, the UNRIBBED plate magnitude is approximately 12 dB greater than the BASELINE plate's magnitude. This agrees with the previous results presented in Figure 4.10. The figures imply that the magnitude of the flexural traveling wave of the BASELINE plate at 500 Hertz is greatly diminished.

Figure 4.12. Near-field integral contributions from the BASELINE and UNRIBBED plate over finite intervals of integration at a fixed frequency of 500 Hertz. The interval containing the acoustic wavenumber is denoted by the dashed line.

Figure 4.13. Near-field integral contributions from the BASELINE and UNRIBBED plate over finite intervals of integration at a fixed frequency of 1000 Hertz.

Figure 4.14. Near-field summed integral contributions from the BASELINE and UNRIBBED plate over finite intervals of integration at a fixed frequency of 500 Hertz.
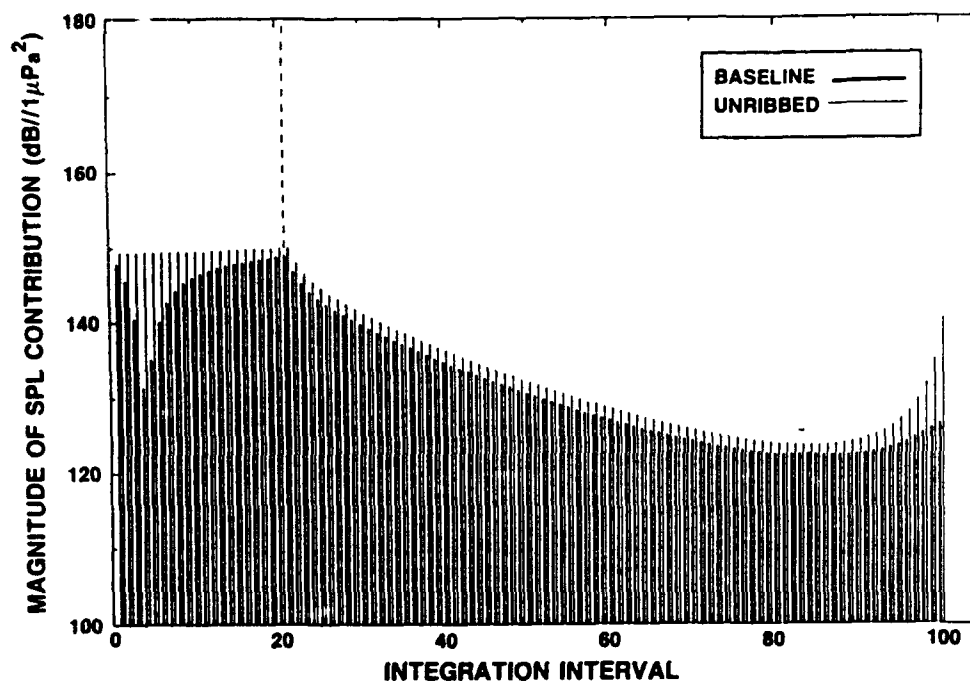

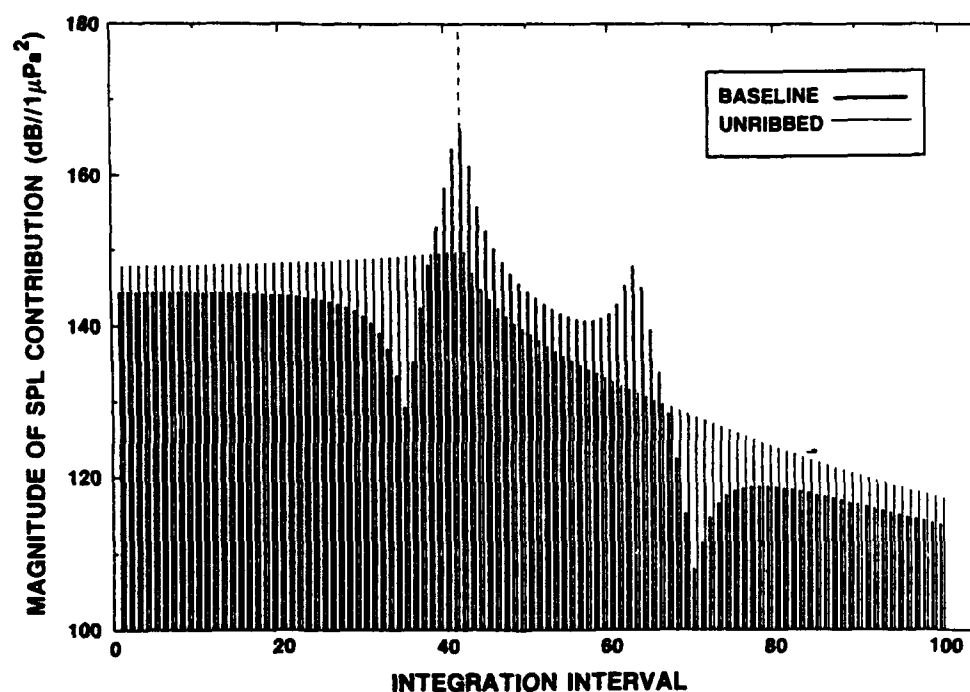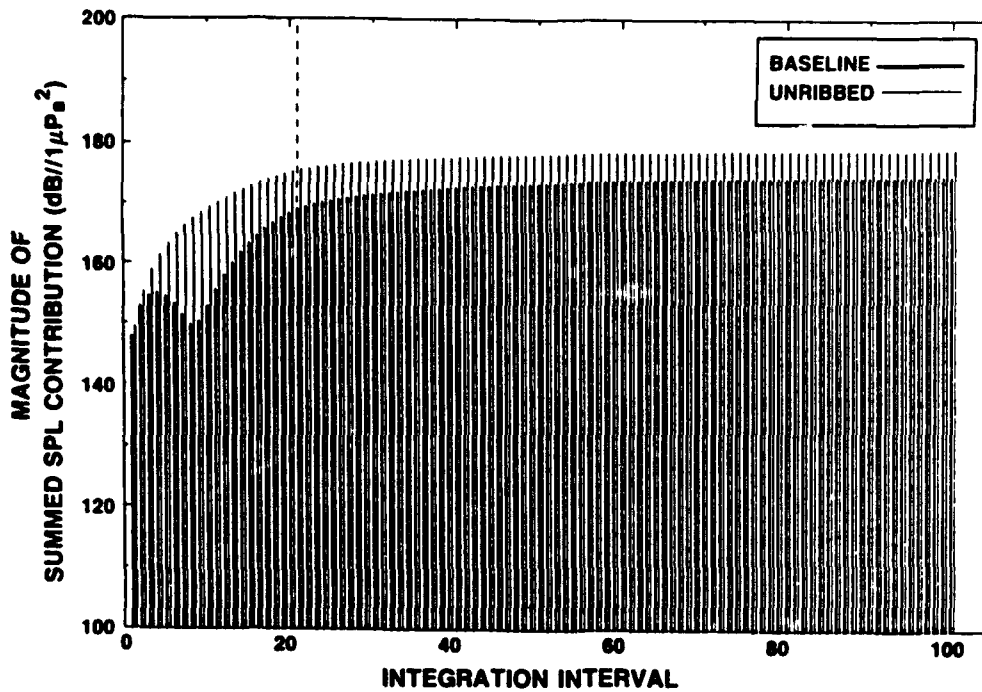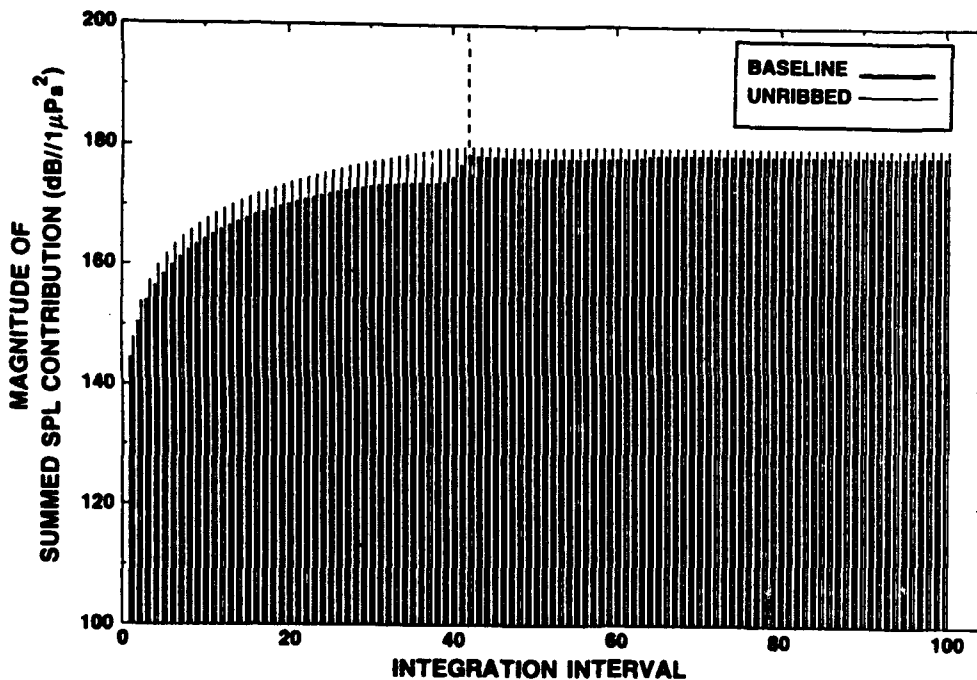Figure 4.15. Near-field summed integral contributions from the BASELINE and UNRIBBED plate over finite intervals of integration at a fixed frequency of 1000 Hertz.

Figure 4.13 illustrates the effect of the large wavenumber response of the BASELINE plate at a wavenumber of 4.0 m^{-1}. At the 40th interval of integration—the interval which contains the 4.0 m^{-1} wavenumber—the BASELINE configuration has a sound pressure level which is approximately 15 dB higher than that given by the UNRIBBED plate.

Shown in Figure 4.14 and Figure 4.15 are the summed acoustic pressure magnitudes of the near-field integral over the same interval of integration given in Figure 4.12 and Figure 4.13. These figures present a running sum of the integration—phase has been retained—and the sound pressure level given at the final interval of integration is the actual radiated sound pressure level. The figures show that the radiated sound pressure level for both the stiffened and unstiffened plate are generally determined by components having a wavenumber less than the acoustic wavenumber.

Recall that Figure 4.14 and Figure 4.15 are for an observation point directly above the excitation force. At the origin, Figure 4.7 and Figure 4.8 indicate that the near-field pressure radiated from the BASELINE configuration is less than that radiated from the UNRIBBED plate; this is confirmed in Figure 4.14 and Figure 4.15.

4.3.3 Analysis of Near-Field Surface Pressure Variations: Non-Periodic Configurations

The results just presented consider periodic rib spacing only. The following pages will present a single example which considers a change in the offset, Δ, such that the inter-rib spacing becomes non-periodic.

Figure 4.16 shows the normalized magnitude wavenumber response of a *20% shifted* BASELINE plate at an excitation frequency of 1000 Hertz. The offset here is $\Delta = 1.2\ (\mathcal{L}/2)$.
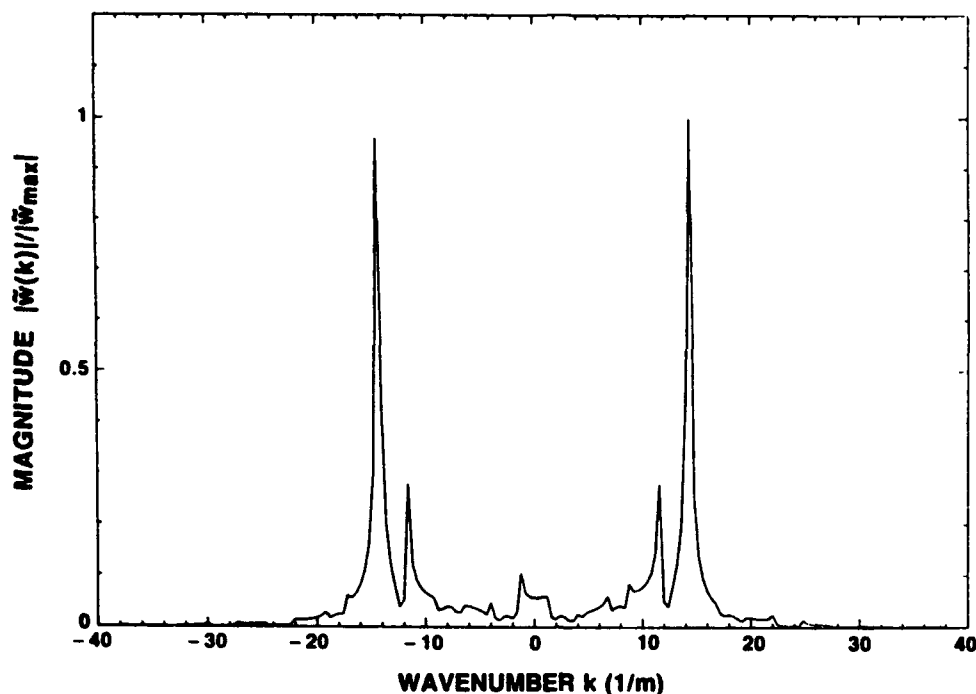
Figure 4.16. Normalized magnitude wavenumber response of the *20% shifted* BASELINE plate for a fixed frequency of 1000 Hertz.

As can be seen by comparing the Figure 4.16 with the periodic case given in Chapter 2, Figure 2.6, the new offset has disrupted and reduced the well defined peaks at $+$ 4.0 m^{-1}. Hence, it is expected that the new offset will reduce the radiated sound pressure level also.

The integrand resulting from the *20% shifted* BASELINE configuration, at an excitation frequency of 1000 Hertz, is shown in Figure 4.17. Observe that the large peaks shown in the BASELINE plate's integrand in Figure 4.11, have been reduced.

Figure 4.18 compares the near-field sound pressure level radiated from the BASELINE, *20% shifted* BASELINE, and from the UNRIBBED plate along the plate's surface at a frequency of 1000 Hertz. The radiated pressure from the BASELINE and UNRIBBED plate configurations has already been compared in Figure 4.8. These levels have been included in Figure 4.18 as reference for measuring the effect of the new offset.
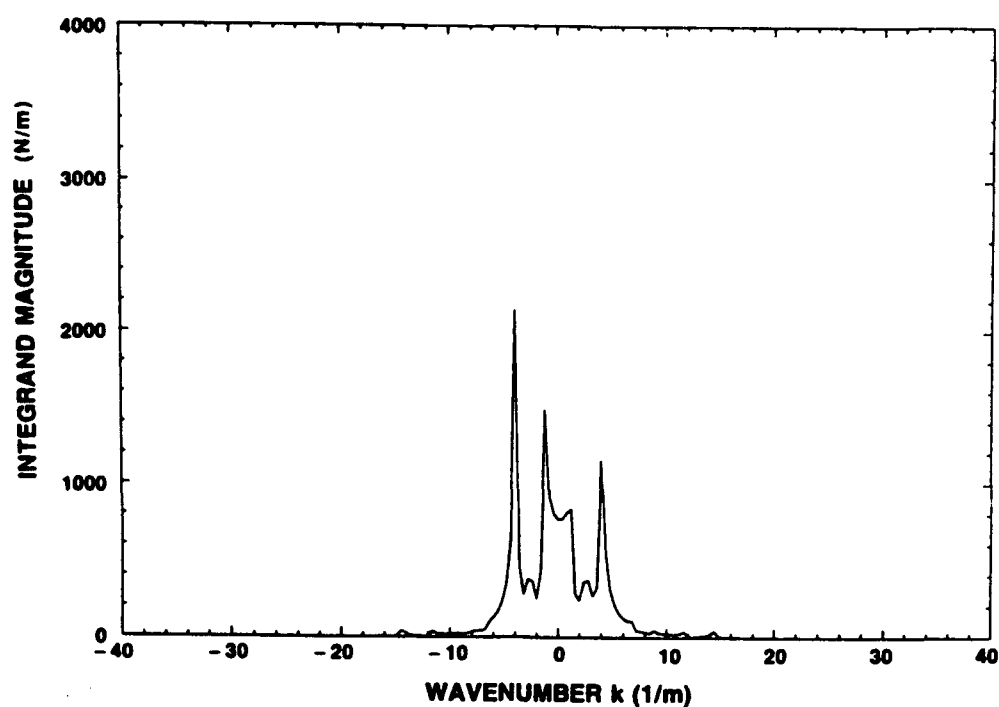
Figure 4.17. Magnitude of the integrand, equation (4.1), for the *20% shifted* BASELINE plate at 1000 Hertz.
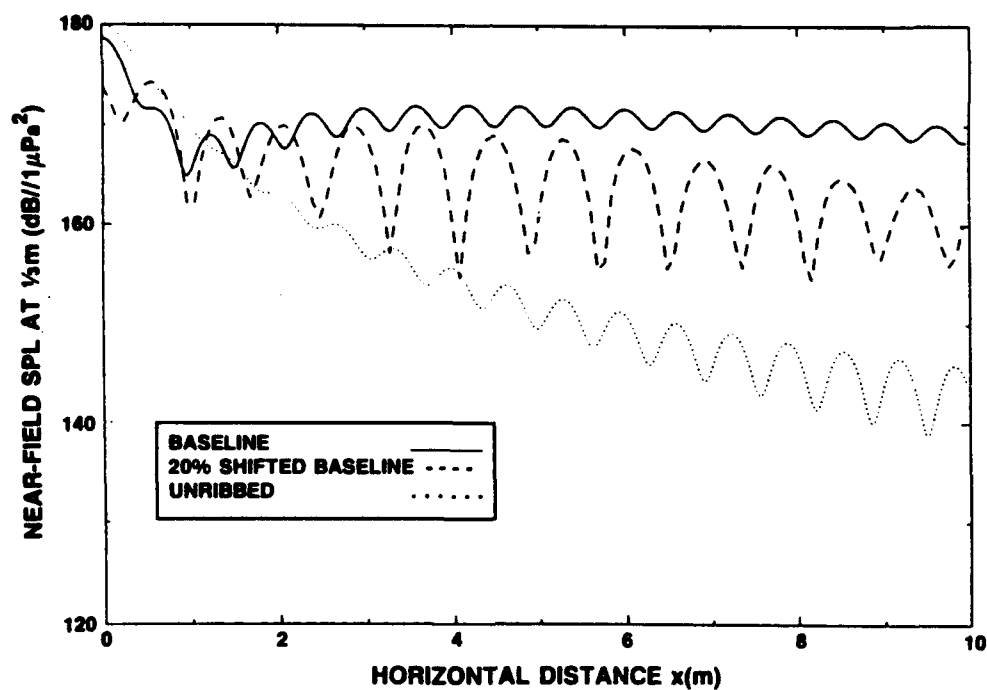
Figure 4.18. Near-field sound pressure level radiated from the surface of the BASELINE, *20% shifted* BASELINE, and the UNRIBBED plate at 1000 Hertz.

As predicted, the *20% shifted* BASELINE plate radiates less sound into the near-field than does the periodically ribbed BASELINE plate. The non-periodic spacing has reduced the large spectral components, near the acoustic wavenumber, seen in the periodic BASELINE configuration, at a frequency of 1000 Hertz. Reducing these components reduced the overall near-field radiated pressure.

4.4 SENSITIVITY OF NEAR-FIELD PRESSURE TO PERIODIC INTER-RIB SPACING

To conclude this chapter on near-field radiation, the following sequence of figures, Figure 4.19 through Figure 4.23, will be presented. This discussion will stress how sensitive the near-field pressure is to the periodic rib spacing, ℓ. The analysis will be similar to that given in the previous section, only here the real and imaginary parts of the integrand, rather than the magnitude, will be considered.

Two different periodic spacings of the rib-stiffeners are investigated, a spacing of 1.207 meters and 1.18 meters. The cross-sectional area of the stiffeners will be the same as that of the BASELINE configuration. All other parameters remain unchanged. The excitation frequency is fixed at 500 Hertz. Note that the two spacings differ from one another by 0.027 m, or approximately 1 inch.

Figure 4.19 shows the real and imaginary parts, solid and dashed line respectively, of the near-field pressure integrand for the periodic spacing of 1.207 meter. Figure 4.20 gives the real and imaginary parts of the near-field pressure integrand for a periodic spacing of 1.18 m.

Considering positive wavenumbers, Figure 4.19 indicates, starting from the zero wavenumber, that both integrand components, real and imaginary, have large negative values. With increasing wavenumbers, the components cross zero, at approximately 0.4 m^{-1}, and become positive. In Figure 4.20, a periodic spacing of 1.18 m, the real component of the integrand initially has a large negative value and crosses over, again at

approximately 0.4 m^{-1}, to a positive value. The imaginary term begins positive, crosses over to a negative value, at approximately 0.12 m^{-1}, and returns to a positive value at the wavenumber of 0.4 m^{-1}.

Figure 4.21 and Figure 4.22, similar to Figure 4.12, show the real and imaginary parts of the radiated pressure for a periodic spacing of 1.207 m and 1.18 m, respectively, over small finite intervals of integration. As before, the dashed line denotes the interval which contains the acoustic wavenumber.

Upon comparing Figure 4.21 with Figure 4.19, and Figure 4.22 with Figure 4.20, it is seen that the sound pressure level contributions from the real and imaginary components, per interval of integration, follow the shape of the components defined by the integrand.

The fundamental point to be made, though, is that the actual integration is the sum of the integration over each interval. It is apparent, then, that negative contributions will combine with positive contributions, which will reduce the overall summed radiated sound pressure level.

Hence, a method may exist for reducing the radiated sound pressure level of a periodically rib-stiffened plate, at a *fixed* frequency and a *fixed* observation point, by choosing a periodic spacing such that optimal cancelation of components will occur. A rib spacing would be chosen such that the integrand given by equation (4.1) would generate large negative spectral regions and positive regions of equivalent size. Upon summing the real and imaginary components over the entire range of integration, the negative areas would reduce the contributions from the positive areas, and the net radiated sound pressure level would be decreased.

Unfortunately, no formula was derived which gives an optimal periodic spacing for reducing the radiated sound pressure level at a fixed frequency and fixed observation point.
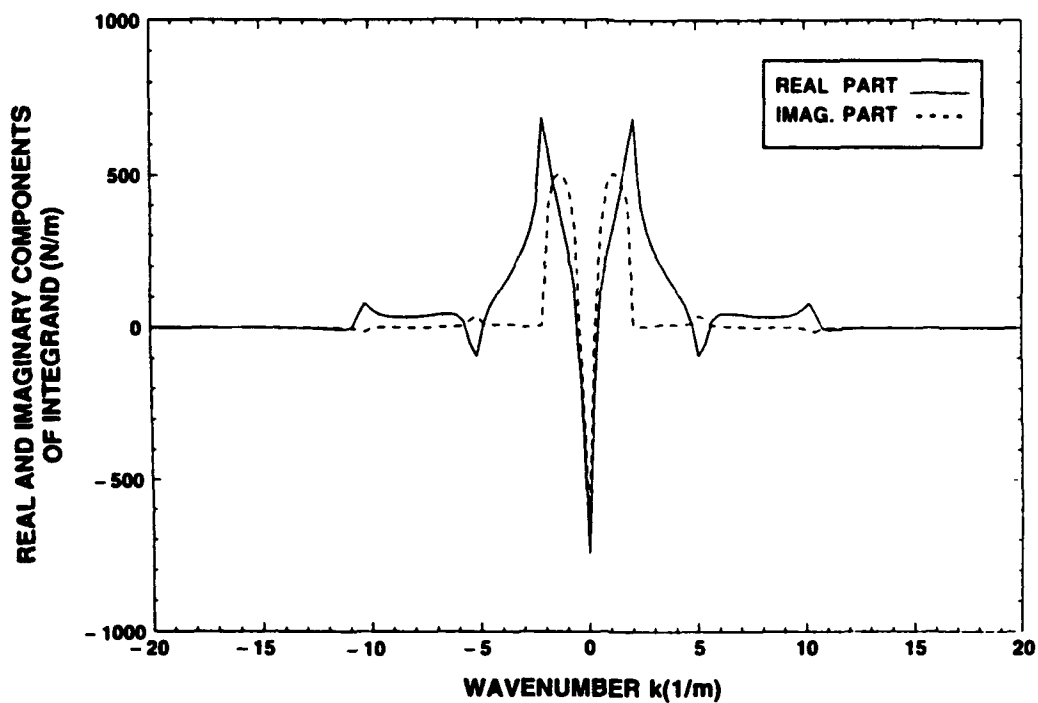
Figure 4.19. Real and Imaginary components of the integrand, equation (4.1), for a periodic rib spacing of 1.207 m. at 500 Hertz.
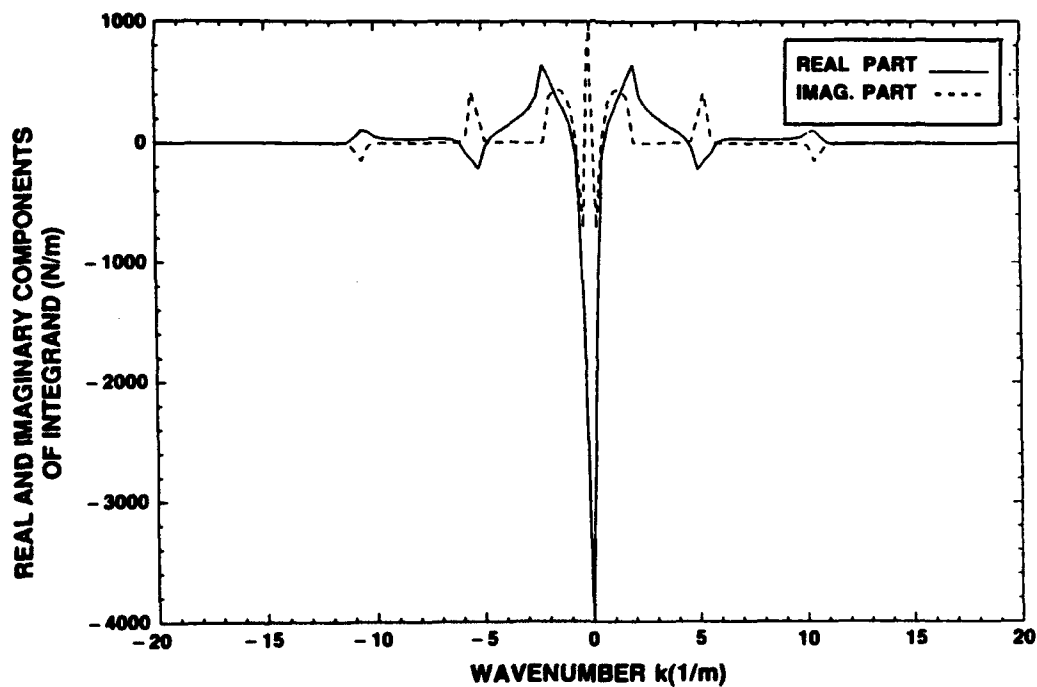
Figure 4.20. Real and Imaginary components of the integrand, equation (4.1), for a periodic rib spacing of 1.18 m. at 500 Hertz.
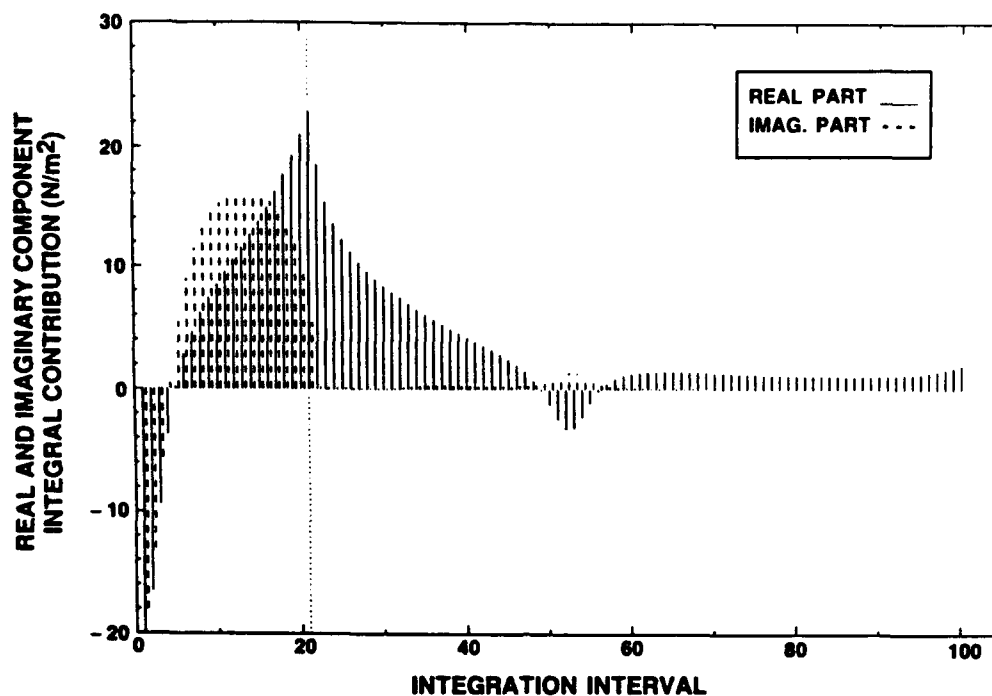
Figure 4.21. Real and Imaginary components of the integral contributions over finite intervals of integration for a periodic rib spacing of 1.207 m at 500 Hertz.
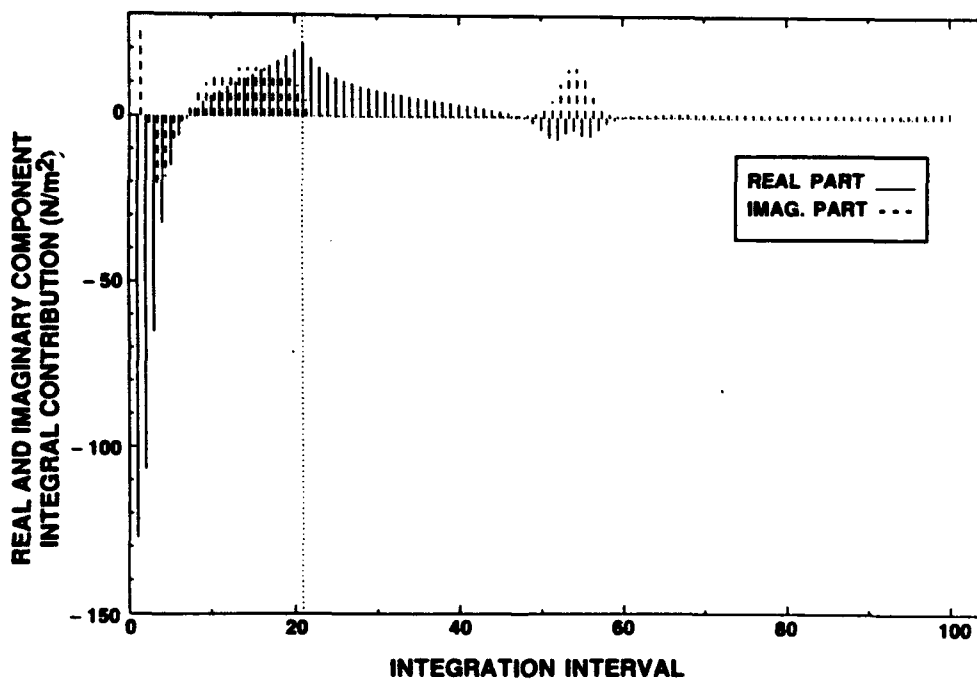
Figure 4.22. Real and Imaginary components of the integral contributions over finite intervals of integration for a periodic rib spacing of 1.18 m at 500 Hertz.

Figure 4.23 is a comparison of the summed magnitude of the near-field integral

contributions over each range of integration. The thick lines denote the summed pressure

level of the 1.207 rib spacing and the thin line denotes the 1.18 rib spacing. The actual

radiated sound pressure level, for the excitation frequency of 500 Hertz, is approximately

given by the level shown for the final interval of integration.
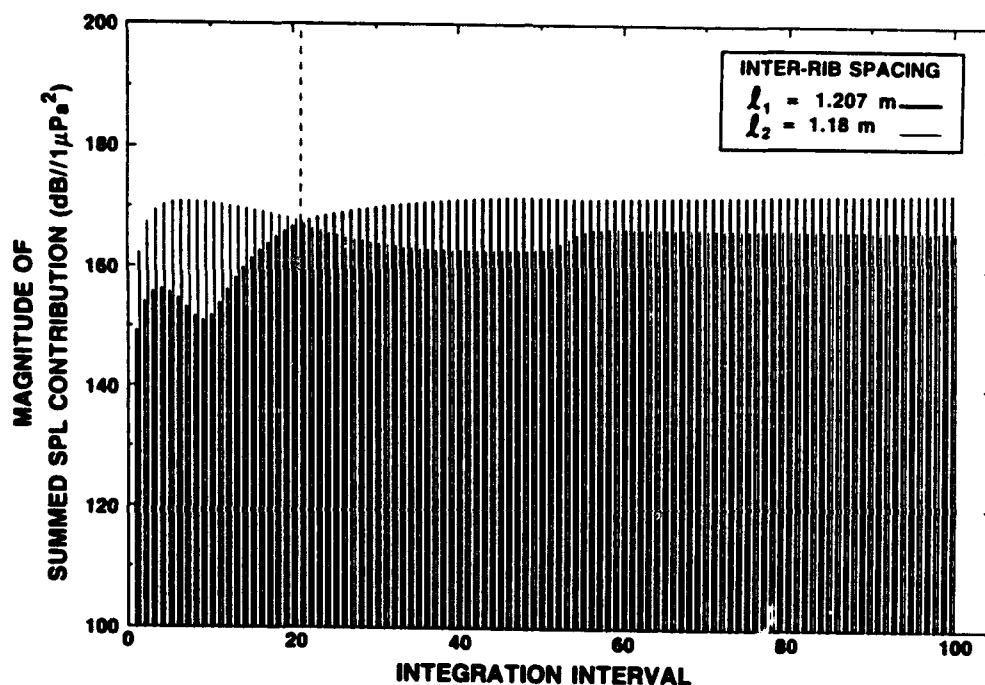
Figure 4.23. Comparison of the summed integral contributions over each
interval of integration for the periodic rib spacing of 1.207 m. and 1.18 m at a
requency of 500 Hertz.

For the periodic rib spacing of 1.207 m, the radiated sound pressure level is 174

dB, whereas the level given for the periodic rib spacing of 1.18 m, is 166 dB. Therefore, a

change of approximately 1 inch reduces the radiated sound pressure level by 8 dB at an

observation point 1/3 m above the applied force.

This chapter has presented, using numerical integration, the near-field acoustic

pressure radiation from periodic and non-periodic stiffened plates. In particular, the

radiated pressure along the surface of the stiffened plate has been analyzed. The stiffeners

can substantially alter the radiated pressure compared to that radiated from an unstiffened plate. The magnitude of the stiffened plates' radiated pressure may be greater than or less than that generated from an unstiffened plate. Obviously, there are a wide variety of phenomena associated with the attachment of rib-stiffeners to a fluid-loaded plate.

CHAPTER 5: SUMMARY AND CONCLUSION

The far-field and near-field structural radiation from a rib-stiffened plate of infinite extent has been examined. Two sets of stiffeners were considered, both having periodic inter-rib spacing, though one set was allowed to be arbitrarily offset from the other set. The formulation presented can be easily extended to include additional rib-stiffener sets, each possessing a different offset. By allowing the stiffeners to be arbitrarily shifted from one another, composite plate sections may be configured which have non-periodic spacing between the rib-stiffeners within a given section. Hence, a method now exists for analyzing the acoustic radiation from true non-periodic structures. Prior to this investigation, very little has been published on sound radiation from non-periodic structures. Therefore, this work represents a valuable contribution to the field of structural acoustics.

Past work has focused primarily on far-field radiation from periodic structures, with many authors idealizing a stiffened structure using a formulation based on propagation constants. These formulations typically consider an infinite structure which has rigid or flexible periodic supports. The displacement between a single set of supports is determined by classical means, and extended on to other regions of the plate by adopting propagation constants. These formulations do not lend themselves to non-periodic supported structures.

As an aid in interpreting the algebraic manipulations necessary to obtain an explicit expression for the stiffened plate's spectral response, certain simplifications were made. The rib-stiffeners were allowed to exert only reactive forces on the plate; angular moments were neglected. Further, an applied line force was chosen, eliminating any spatial dependence of sound radiation in a direction parallel to the stiffeners.

It was shown that each additional set of rib-stiffeners generates an additional equation in the wavenumber domain which must be solved simultaneously to obtain an

explicit form of the stiffened plate's wavenumber response. With many sets of stiffeners, the algebra would become cumbersome and would require assistance with a computer.

Two general configurations were investigated, denoted the BASELINE and ALTERNATE designs. Both had periodically positioned and identical rib-stiffeners. The ALTERNATE's rib spacing was half that of the BASELINE. Similarly, the mass of the ALTERNATE stiffeners was about half that of the BASELINE stiffeners. The near-field and far-field radiation from these structures was compared. The configurations were also compared to an UNRIBBED plate. Culminating the analysis, the offset of each configuration was allowed to deviate, and the radiation for non-periodic spacing was examined.

5.1 WAVENUMBER RESPONSE; PERIODIC CONFIGURATIONS

The special case of the wavenumber response for periodic rib spacing, equation (2.27), was mathematically examined in great detail. As equation (2.32) showed, the frequency of the free-traveling wave of the stiffened plate is less than that of the unstiffened plate, due to the additional mass of the rib-stiffeners. Therefore, both fluid-loading and stiffening change the frequency at which a flexural wave propagates.

It was also shown that the wavenumber response of the periodically stiffened plate goes to zero for the wavenumbers

$$k_n = \pm k_b \pm k_q n \qquad n = 1,2,3,... \qquad (2.34)$$

Similar relationships were derived for wavenumbers at which the spectral response has relative maximums; these wavenumbers are given by

$$k_m = \pm \left(k_b^4 + k_r^4\right)^{1/4} \pm mk_q \quad m = 1,2,3,...$$

The above relationships were verified, for light fluid-loading (AIR), in Figure 2.13 through Figure 2.18.

The spectral components of most interest were those which coupled with the acoustic medium and radiate sound. Therefore, of particular interest were components which have wavenumbers which are less than, in absolute value, the acoustic wavenumber. These components are vividly shown in Figure 2.4, Figure 2.8, Figure 2.19, and Figure 2.20.

Also notable were the frequencies at which the wavenumber nulls given by equation (2.35a) intersected with equation (2.35b), and the frequencies for the intersecting maximas given by equation (2.38a) and equation (2.38b). The former circular frequencies are

$$\omega_p = (p\pi)^2 \sqrt{\frac{D}{m\,\ell^4}} \quad p = 2,3,4,\ldots \tag{2.40}$$

The circular frequencies which yield the largest supersonic spectral components, below coincidence, are

$$\omega_p = (p\pi)^2 \sqrt{\frac{D}{\ell^4(m+(m_i'/\lambda))}} \qquad p = 2,3,4,\ldots,P \tag{2.41}$$

The form of both of the above frequency equations is similar to that given by classical resonant frequency analysis, Meirovitch (1967), of a simply-supported strip plate.

The above equations are valid for periodic inter-rib spacing and become invalid for non-periodic spacing. Qualitative examination of equation (2.26), the general wavenumber response, was only possible, with the conclusion that even a small change from periodic spacing disrupts the spectral peaks and nulls, as derived above. The non-periodic spacing introduces additional nulls and peaks in the spectral response, though the location of these spectral components, at this point, is not predictable.

Finally it was shown that the cross-sectional area of the rib-stiffeners, for the plate geometry and material properties used during the investigation, had only a small effect on the location of the spectral nulls and peaks. The stiffeners' structural mass does affect the magnitude of the spectral peaks, though not in a dramatic fashion.

5.2 FAR-FIELD ACOUSTIC RADIATION

Using the method of stationary phase, an analytical expression was derived giving the far-field radiation from a fluid-loaded, stiffened plate driven by a harmonic line force.

For light fluid-loading, it was shown that the even index frequencies, given by equation (2.40) and equation (2.41), predict acoustic nulls and peaks in the radiated far-field. The observation point, however, was fixed and it was not determined whether the peaks or nulls varied with observation position.

Large variations in far-field pressure—20 dB at 500 Hertz—were illustrated in Figure 3.6 for a change in offset. Here the offset was allowed to vary, from one end to the other, between a fixed set of stiffeners. It was shown, at certain frequencies of excitation and offset position, that the stiffeners were strong radiators of sound. However, other frequencies and offset positions lessened the radiated pressure.

In Figures 3.10 through Figure 3.17, the directional radiation characteristics of the stiffened plate were shown. Figure 3.14, the ALTERNATE configuration at 2000 Hertz, indicated that *less* far-field sound is radiated from the stiffened plate than from the unstiffened plate over most of the angular radiation space. All of the directional radiation patterns of the periodic stiffened plate were symmetric in polar angle. For an offset which introduced non-periodic spacing, the directionality patterns were no longer symmetric. The stiffeners exhibited radiation characteristics not unlike that which would be seen from an array of sources radiating pressures which constructively and destructively interfere in the far-field. A recommendation for future work would be to determine whether an equivalent source strength for a rib-stiffener could be obtained and used as an acoustical source in an

array of sources. The directionality patterns given here could then be compared to those generated from an array of equivalent sources.

Another feature of the radiation characteristics of periodic and non-periodic stiffened plates, amplified by Figure 3.11, Figure 3.15, and Figure 3.16, is the plate's ability to focus acoustic radiation within a fairly narrow direction. This may be beneficial in the design of active sonar devices. Surface ship and submarine silencing may also benefit from the research presented in Chapter 3. Provided the inter-rib spacing may be modified, a change in periodic spacing may improve, that is reduce, the far-field radiation from a surface ship or submarine.

5.3 NEAR-FIELD ACOUSTIC RADIATION

Numerical integration techniques were necessary to obtain the near-field acoustic radiation. The chosen method was a Romberg integration technique using a simple trapezoidal rule; Gaussian integration methods performed poorly.

It was shown, in Figure 4.1 and Figure 4.2, that the near-field acoustic pressure components decay rapidly with distance away from the plate. It was noted, however, that the demarcation of the near-field and far-field depended on many parameters, and cannot be specified precisely.

Near-field acoustic pressure versus frequency at a fixed observation point was shown in Figure 4.3, Figure 4.4, and Figure 4.5. Prominent nulls in acoustic pressure were illustrated in each figure. The nulls, though, did not match up with those shown for the far-field radiated pressure. Further, additional nulls were present within the near-field region than in the far-field. The relative magnitudes of the difference in peak and null pressures were less in the near-field than in the far-field.

The variation of near-field radiated pressure over the surface was also calculated. The vertical stand-off distance was fixed and the observation point moved along the surface of the plate. Clearly shown in all the figures of surface pressure were fairly rapid acoustic

oscillations due to a propagating flexural wave. The amplitude of these oscillations decayed quickly with vertical distance away from the plate.

At certain frequencies, the stiffened plate's near-field pressure differed greatly from that of the unstiffened plate. An example is shown in Figure 4.7 for the BASELINE configuration at 500 Hertz, where the wavelength of the acoustic oscillations is much larger than that of the unstiffened plate. The difference may be due to the presence of a spatial 'beating' phenomenon. The phenomenon is implied by examining Figure 2.5, the BASELINE plate's wavenumber response. The figure depicts the flexural response being split into two components (though one component is of less magnitude than the other) which are close together in wavenumber. Hence, the wavelength of oscillation seen in Figure 4.7 may result from taking the difference of the wavenumbers of the two spectral components shown in Figure 2.5. This conclusion is supported by the work of Keltie (1991). Keltie examined the near-field radiation from a fluid-loaded, rib-stiffened finite flat plate. In particular, Keltie analyzed in detail, a *beating* phenomenon which arised due to the presence of rib-stiffeners.

A situation which resulted in very large near-field radiated pressures along the surface of the plate was observed in the BASELINE configuration at 1000 Hertz. As was shown in Figure 2.6, the BASELINE plate's wavenumber response at 1000 Hertz, a large spectral peak existed at a wavenumber just less than the acoustic wavenumber. The magnitude of the integrand of the inversion integral, equation (4.1), was shown in Figure 4.11 for the BASELINE design at 1000 Hertz. The magnitude was shown to have a spectral peak 3.5 times greater than that of the UNRIBBED integrand. Therefore, as Figure 4.8 illustrated, the radiated surface pressure of the BASELINE design was, at 1000 Hertz, much greater than the radiated pressure from the unstiffened plate.

A change in offset, which made the BASELINE plate non-periodic, was also examined, and was shown to reduce the spectral peaks at 1000 Hertz, seen in Figure 2.6,

for the periodic BASELINE wavenumber response. Consequently, the surface radiated pressure was reduced, as indicated in Figure 4.18.

5.4 RECOMMENDATIONS FOR FUTURE ANALYSIS

An immediate recommendation for future investigations would be to consider broad-band excitation. Romanov (1971) has discussed the need for averaging the near-field over frequency to illuminate the spatial variation of radiated pressure over the rib-stiffeners. The calculations would be computer intensive, though not difficult to formulate mathematically.

The radiation due to a point force needs to be examined in more detail. Incorporating bending stiffness of the rib-stiffeners would permit a more realistic model. An ideal investigation would be to analyze the near-field acoustic radiation over an entire two-dimensional region of the plate's surface for broad-band frequency excitation. The focus would be to determine a set of stiffener sizes, and attachment positions, such that the overall radiated pressure, within a selected frequency band, would be less than that for an unstiffened plate.

The model presented here may also be improved by including the effects of beam and plate rotary inertia, and, if necessary, shear deformation. Also, bending moments exerted by the rib-stiffeners onto the plate may be incorporated in to the mathematical model.

Another recommendation would be to extend the formulation from an infinite rib-stiffened flat plate to an infinite stiffened cylindrical shell. The formulation would likely follow the work of Burroughs (1984). Again, the numerical calculations would become more involved, though the formulation seems tractable.

This study has examined the near-field and far-field sound radiation from periodic and non-periodic rib-stiffened plates of infinite extent. For the far-field region, an

analytical solution was obtained by means of a stationary phase approximation. In the near-field, it was necessary to use numerical integration. For both regions, it has been shown, that a judicious selection of the attachment location of the rib-stiffeners may *reduce*, remarkably at certain frequencies, the radiated sound compared to that generated by an unstiffened plate.

6. REFERENCES

Bansal, A. S. (1979). "Flexural wave motion in beam-type disordered periodic systems: coincidence phenomenon and sound radiation." J. Sound Vib. 62(1), 39-49.

Bender, C. M., Orszag, S.A. (1978). Advanced mathematical methods for scientists and engineers. (McGraw-Hill, New York). p. 247-302.

Burroughs, C. B. (1984). "Acoustic radiation from fluid-loaded infinite circular cylinders with doubly periodic ring supports." J. Acoust. Soc. Am. 75(3), 715-722.

Carnahan, B., Luther, H., and Wilkes, J. (1969). Applied Numerical Methods. (John Wiley & Sons, New York). p. 69-131.

Cremer, L., Heckl, M. (1988). Structure-Borne Sound. (Springer-Verlag, New York). p. 502-505.

Crighton, D. G., Maidanik, G. (1981). "Acoustic and vibration fields generated by ribs on a fluid-loaded panel, I: Plane-wave problems for a single rib." J. Sound Vib. 75(3), 437-452.

Eatwell, G. P. (1982). "The response of a fluid-loaded, beam stiffened plate." J. Sound Vib. 84(3), 371-388.

Evseev, V. N. (1973). "Sound radiation from an infinite plate with periodic inhomogeneities." Sov. Phys. Acoust. 57, 370-373.

Fahy, F. (1985). Sound and Structural Vibrations. (Academic Press, New York), p. 72.

Feit, D. and Liu, Y. N. (1985). "The nearfield response of a line-driven fluid-loaded plate." J. Acoust. Soc. Am. 78(2), 763-66.

Garrelick, J. M., Gaw-Feng Lin (1975). "Effect of the number of frames on the sound radiation by fluid-loaded, frame-stiffened plates." J. Acoust. Soc. Am. 58(2), 499-500.

Gorman, R. M. (1974). "Vibrations of and acoustic radiation from line-excited rib-stiffened damped plates in water." Ph.D. dissertation, the Pennsylvania State University.

Heckl, M. (1961). "Wave propagation on beam-plate systems." J. Acoust. Soc. Am. 33, 640-651.

Hodges, C. H. (1982). "Confinement of vibration by structural irregularity." J. Sound Vib. 82(3), 411-424.

Hodges, C. H., Woodhouse, J. (1983). "Vibration isolation from irregularity in a nearly periodic structure: Theory and measurements." J. Acoust. Soc. Am. 74(3), 894-905.

Junger, M. C., Feit, D. (1986). Sound, structures, and their interaction. (MIT Press, Cambridge, MA.) p. 112-119.

Keltie, R. F. (1991). "The effects of rib stiffeners on the structural and acoustic response of fluid loaded finite flat plates." IPA Activity Report. (Naval Underwater Systems Center, New London, CT.)

118

Lamb, G. L. (1961). "Input impedance of a beam coupled to a plate." J. Acoust. Soc. Am. 33, 628-633.

Mace, B. R. (1980a). "Sound radiation from a plate reinforced by two sets of parallel stiffeners." J. Sound Vib. 71(3), 435-441.

Mace, B. R. (1980b). "Periodically stiffened fluid-loaded plates, I: Response to convected harmonic pressure and free wave propagation." J. Sound Vib. 73(4), 473-486.

Mace, B. R. (1980c). "Periodically stiffened fluid-loaded plates, II: Response to line and point forces." J. Sound Vib. 73(4), 487-504.

Maidanik, G., Tucker, A. J., Vogel, W. H. (1976). "Transmission of free waves across a rib on a panel." J. Sound Vib. 49(4), 445-452.

Mead, D. J. (1970). "Free wave propagation in periodically supported, infinite beams." J. Sound Vib. 11(2), 181-197.

Mead, D. J., Pujara, K. K. (1971). "Space-harmonic analysis of periodically supported beams: Response to convected random loading." J. Sound Vib. 14(4), 525-541.

Mead, D. J. (1978). "An approximate theory for the sound radiated from a periodic line-supported plate." J. Sound Vib. 61(3), 315-326.

Mead, D. J. (1990). "Plates with regular stiffening in acoustic media: Vibration and radiation." J. Acoust. Soc. Am. 88(1), 391-401.

Meirovitch, L. M. (1967). Analytical methods in vibrations. (Macmillan Publishing Co., New York). p. 179-185.

Mindlin, R. D. (1951). "Influence of rotatory inertia and shear on flexural motions of isotropic elastic plates." J. Appl. Mech., March, 31-38.

Nuttall, A. H. (1992). "Explicit solution of the wavenumber response of a fluid-loaded stiffened plate," NUWC-NL TR 10,015, February 1992, Naval Undersea Warfare Center Detachment, New London, CT.

Romanov, V. N. (1971). "Radiation of sound by an infinite plate with reinforcing beams." Sov. Phys. Acoust. 17, 92-96.

Rummerman, M. L. (1975). "Vibration and wave propagation in ribbed plates." J. Acoust. Soc. Am. 57(2), 370-373.

Stakgold, I. (1979). Green's functions and boundary value problems. (John Wiley & Sons, Inc., New York). p. 138-140.

Strawderman, W. A., Ko, S. H., and Nuttall, A. H. (1979). "The real roots of the fluid-loaded plate." J. Acoust. Soc. Am. 66(2), 579-85.

Schloemer, H. H., (1981). Submarine design notes. Harry A. Jackson, Capt. USN(Ret.). Summer at Massachusetts Institute of Technology, Cambridge, MA, p. 96.

Timoshenko, S. (1955). Vibration Problems in Engineering (Van Nostrand, Princeton, NJ).

Ungar, E. E. (1961). "Transmission of plate flexural waves through reinforcing beams; dynamic stress concentrations." J. Acoust. Soc. Am. 33, 633-639.

7. APPENDIX

POINT FORCE EXCITATION OF A FLUID-LOADED INFINITE PLATE HAVING TWO SETS OF ATTACHED RIB-STIFFENERS

For an applied point force, the formulation presented in Chapter 2 for line force excitation differs only slightly. Equation (2.1) is rewritten below for two sets of attached rib-stiffeners:

$$D(\frac{\partial^2}{\partial x^2} + \frac{\partial^2}{\partial y^2})^2 \, w(x,y) - m\omega^2 w(x,y) =$$

$$P_e(x,y) - P_a(x,y) - \{P_1(x,y) + P_2(x,y)\}. \tag{A.1}$$

The Fourier transform of equation (A.1), adopting the same notation as in Chapter 2, is

$$\left\{ D(k_x^2 + k_y^2)^2 - m\omega^2 \right\} \tilde{w}(k_x,k_y) =$$

$$\tilde{P}_e(k_x,k_y) - \tilde{P}_a(k_x,k_y) - \left\{ \tilde{P}_1(k_x,k_y) + \tilde{P}_2(k_x,k_y) \right\} \tag{A.2}$$

where k_x and k_y denote the wavenumbers in, respectively, the x and y direction.

The transforms of the applied pressures, $\tilde{P}_e(k_x,k_y)$, $\tilde{P}_a(k_x,k_y)$, $\tilde{P}_1(k_x,k_y)$, and $\tilde{P}_2(k_x,k_y)$, are obtained in a manner identical to that given in Chapter 2. For a point force, the Fourier transform becomes

$$\tilde{P}_e(k_x,k_y) = F_0 \, e^{-ik_x x_0} \, e^{-ik_y y_0}. \tag{A.3}$$

The transform of the acoustic pressure, $\tilde{P}_a(k_x,k_y)$, acting on the surface of the plate, is simply

120

$$\tilde{P}_a(0;k_x,k_y) = \frac{i\rho_0\omega^2\tilde{w}(k_x,k_y)}{\sqrt{k_0^2 - (k_x^2+k_y^2)}} \qquad \sqrt{k_x^2+k_y^2} \leq k_0, \qquad \text{(A.4a)}$$

$$\tilde{P}_a(0;k_x,k_y) = \frac{-\rho_0\omega^2\tilde{w}(k_x,k_y)}{\sqrt{(k_x^2+k_y^2)-k_0^2}} \qquad \sqrt{k_x^2+k_y^2} \geq k_0. \qquad \text{(A.4b)}$$

The analysis for obtaining the transformed applied pressure due to both sets of rib-stiffeners differs little from that given in Chapter 2. For a point force acting on the plate, however, the bending stiffness of the ribs must be retained. Hence, the spectral dynamic stiffness, K_1 and K_2, now becomes

$$K_1 = \frac{E_1 I_1 k_y^4 - m_1'\omega^2}{\ell}$$

$$K_2 = \frac{E_2 I_2 k_y^4 - m_2'\omega^2}{\ell} .$$

The above expressions are substituted back into equation (A.2), as done in Chapter 2, which yields

$$\tilde{w}(k_x,k_y) = F(k_x,k_y) - K_1 Y(k_x,k_y) \sum_{n=-\infty}^{\infty} \tilde{w}(k_x + nk_\ell,k_y)$$

$$- K_2 Y(k_x,k_y) \sum_{n=-\infty}^{\infty} \tilde{w}(k_x + nk_\ell,k_y)e^{ik_\ell n\Delta} \qquad \text{(A-5)}$$

where

$$F(k_x,k_y) = \frac{F_0\,e^{-ik_x x_0}\,e^{-ik_y y_0}}{S(k_x,k_y)}$$

and

$$Y(k_x,k_y) = \frac{1}{S(k_x,k_y)} .$$

$$S(k_x,k_y) = \begin{cases} D(k_x^2 + k_y^2)^2 - m\omega^2 - \dfrac{i\rho_0\omega^2}{\sqrt{k_0^2-(k_x^2+k_y^2)}} & \sqrt{k_x^2+k_y^2} \leq k_0, \\[4ex] D(k_x^2 + k_y^2)^2 - m\omega^2 - \dfrac{\rho_0\omega^2}{\sqrt{(k_x^2+k_y^2)-k_0^2}} & \sqrt{k_x^2+k_y^2} \geq k_0. \end{cases}$$

To obtain an explicit form for the wavenumber response, $\widetilde{w}(k_x,k_y)$, the identical manipulations given in section 2.3 of Chapter 2 are used. The wavenumber, k_y, is treated simply as a parameter.

The far-field radiated pressure, due to an applied point force, can be obtained by asymptotically approximating the Fourier inversion integral using the method of stationary phase.
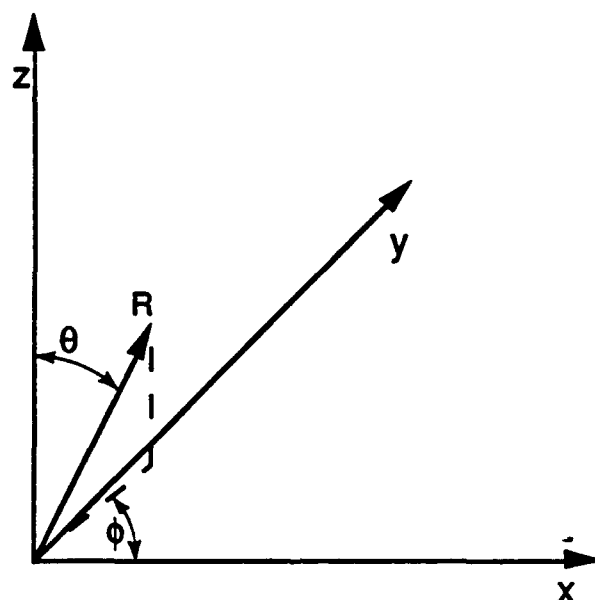
With the above coordinate transformation, the stationary phase integral approximation becomes

$$P_a(R,\theta,\phi) \sim \frac{-\rho_0\omega^2\widetilde{w}(\bar{k}_1,\bar{k}_2)\, e^{-ik_0R}}{2\pi R} \qquad (A.6)$$

The stationary phase values, $\bar{k}_1$, $\bar{k}_2$, given above are

$$\bar{k}_1 = k_0 \sin\theta_0 \cos\phi_0,$$

and

$$\bar{k}_2 = k_0 \sin\theta_0 \sin\phi_0.$$

INITIAL DISTRIBUTION LIST

Addressee	No. of Copies
NAVSEA (Code O6URB, Code O6UR4)	2
NSWC, Carderock Division (Dr. D. Feit, Code 1902; Dr. M. Sevik, Code 1900; Dr. W. K. Blake, Code 1905 Dr. Y. F. Hwang, Code 1942; Dr. P. Shang, Code 1942; Dr. G. Maidanik, Code 1902; Dr. W. Vogel, Code 1902; Dr. Y. Liu)	8
NRL/Washington (Douglas M. Photiadis)	1
NRL/Orlando (Dr. J. Blue, Dr. B. Montgomery)	2
ONR (Dr. A. J. Tucker, Code 122; Dr. P. B. Abraham, Code 1132)	2
DARPA	1
ARL/Penn. State (Courtney Burroughs)	1
URI (Prof. Peter Stephanishen)	1
Cambridge Acoustical Associates (Dr. M. Junger)	1
BBN (Dr. R. Huberman)	1
Yale University (Dr. Keyes)	1
Iowa State university (A. B. Flatau)	1
University of Washington (Dr. G. Reinhall)	1
Georgia Inst. of Technology (Dr. J. Ginsberg)	1
DTIC	2